Norwegian University
of Life Sciences

Master's Thesis 2020   60 ECTS
Faculty of Chemistry, Biotechnology and Food Science

The Establishment of a CRISPR-Cas13a Diagnostic Assay for SARS-CoV-2 Detection

Charlotte Solum Krog
Master of Science, Chemistry and Biotechnology

I

The Establishment of a CRISPR-Cas13a Diagnostic Assay for SARS-CoV-2 Detection

Department of Microbiology,
Oslo University Hospital

And

The Norwegian University of Life Science
Faculty of Chemistry, Biotechnology and Food Science
© Charlotte Solum Krog 2020

Acknowledgements

Abstract

The scarcity of fast and reliable tests in diagnostic laboratories for detection of pathogens with high sensitivity is a significant disadvantage particularly for critically ill patients. Given the global health crisis caused by the ongoing pandemic of Severe Acute Respiratory Syndrome 2 (SARS-CoV-2) that pervades today's society, rapid and robust infection detection is important in reducing virus spread. Novel technology based on CRISPR-Cas proteins has demonstrated improved diagnostic turnaround time whilst maintaining high specificity and sensitivity for viral and bacterial detection. The innovative platform called Specific, High sensitivity Enzymatic Reporter unLOCKing system (SHERLOCK) allows ultra-sensitive nucleic acid detection down to attomolar sensitivity and even single molecules in less than one hour. SHERLOCK combines an isothermal pre-amplification step to increase the amount of DNA or RNA with Cas13/Cas12 orthologues exhibiting high levels of collateral RNase activity upon recognition of a specific target sequence.

In this thesis, the aim was to establish a rapid and sensitive CRISPR-Cas13 diagnostic assay using a fluorescence-based SHERLOCK platform with reverse transcription (RT)-Recombinase polymerase amplification (RPA) for sequence-amplification and the Cas13a orthologue from *Leptotrichia wadei* (Lwa)Cas13a for detection of SARS-CoV-2. We aimed for fast SARS-CoV-2 detection with comparable sensitivity to the gold standard diagnostic method RT-qPCR. To establish a high sensitivity SHERLOCK assay, we focused on instrumentation, reaction components, and target optimization. Synthetic targets were used for the initial assay optimization and clinical SARS-CoV-2 samples to evaluate assay sensitivity and specificity. Targets included a region within the SARS-CoV-2 *orf1ab-* and *orf1b-* genes used in recent studies and two highly conserved regions within the N-gene identified by sequence alignment analysis.

Results in this work show that SHERLOCK maintained high specificity (95%) and a sensitivity of 86% for the detection of *orf1ab*, compared to RT-qPCR analysis of the SARS-CoV-2 *E-gene*. Within one hour, a significant ($p \leq 0.001$) signal from SARS-CoV-2 samples equal to a Ct value of 33,2 was obtained using, the novel target, MSA_T1, in SARS-CoV-2. The results demonstrate that correct instrument optimization is crucial in order to achieve high sensitivity as well as careful target sequence selection and iterative crRNA guide design. Results also

reveal that the primary limitation on assay sensitivity is unspecific noise from the RPA reaction, suggesting that choice of primers play a critical role in assay optimization. The SHERLOCK platform has great potential in clinical diagnostics for rapid detection of pathogens, though sensitivity must be increased to obtain that achieved by RT-qPCR.

Sammendrag

Knappheten på raske og pålitelige diagnostiske tester for påvisning av patogene bakterier og virus med høy følsomhet er en betydelig ulempe, spesielt for intensivavdelinger. På grunn av det globale helseproblemet forårsaket av alvorlig akutt luftveissyndrom corona 2 virus (SARS-CoV-2) er rask infeksjon-påvisning viktig for å redusere spredning av virus. Et stort press er satt på det norske helsevesenet, og testkapasiteten i landet. Ettersom viruset kan gi et spekter av symptomer, kan det ikke påvises basert på sykdomstegn. Ny teknologi basert på CRISPR-Cas har vist sitt potensiale til rask og sensitiv påvisning av virus og bakterier. Den innovative plattformen kalt Specific, High-sensitivity Enzymatic Reporter unLOCKing system (SHERLOCK) tillater sensitiv nukleinsyre-deteksjon ned til attomolar følsomhet på under en time. SHERLOCK kombinerer et isotermisk pre-amplifikasjonstrinn for å øke mengden nukleinsyrer i en prøve, med Cas13 / Cas12-ortologer som har en sekvens-uspesifikk trans-RNase-aktivitet ved gjenkjenning av en målsekvens. En vellykket etablering av en slik plattform kan redusere diagnostisk behandlingstid og samtidig opprettholde høy spesifisitet og følsomhet.

I denne oppgaven var målet å etablere en rask og sensitiv CRISPR-Cas13 diagnostisk plattform ved bruk av et fluorescens-basert SHERLOCK system for påvisning av SARS-CoV-2. Revers transkripsjon (RT)- Rekombinase Polymerase Amplifikasjon (RPA) ble brukt til pre-amplifisering, mens Cas13 fra *Leptotrichia wadei* (Lwa)Cas13a og assosierte crRNAer ble brukt til virus deteksjon. Vi ønsket en rask SARS-CoV-2 deteksjon med samme følsomhet som dagens diagnostiske gullstandard, RT-qPCR. For å etablere en SHERLOCK-plattform med høy følsomhet fokuserte vi på instrument-, reaksjons- og målsekvens optimalisering. Syntetiske mål-sekvenser ble brukt for analyseoptimalisering, og kliniske SARS-CoV-2 prøver ble brukt for evaluering av analysens følsomhet og spesifisitet. Målsekvensene inkluderte en region i SARS-CoV-2 *orf1ab*- og i *orf1b*-genet. To svært konserverte regioner i N-genet hentet fra en sekvensanalyse av SARS-CoV-2 genomet ble også brukt til SARS-CoV-2 deteksjon.

Resultatene viser at SHERLOCK hadde høy spesifisitet (95%) og en sensitivitet på 86% for påvisning av *orf1ab*. Høyest signifikans ble oppnådd ved bruk av en ny mål-sekvens, MSA_T1 hentet fra sekvensanalysen. Dette tilsvarte en RT-qPCR Ct-verdi på 33,2 av E-genet. Data fra denne oppgaven demonstrerte viktigheten av riktig instrumentoptimalisering og utstyr for å oppnå høy følsomhet i metoden. Resultatet fastslår også at den primære faktoren som begrenser

analyse-sensitiviteten, er uspesifikt støy fra RPA-reaksjonen. Funnene tyder på at valg av RPA primere spiller den viktigste rollen i analyse optimalisering sammen med guide-RNA-design. SHERLOCK-plattformen har stort potensiale i klinisk diagnostikk, selv om sensitiviteten må økes for å oppnå tilsvarende nivå som RT-qPCR (95%).

Table of contents

Abbreviations

AMR	Antimicrobial resistance
Bp	Base-pair
Cas	CRISPR associated protein
crRNA	CRISPR-RNA
Ct	Cyclic threshold
DNA	Deoxyribonucleic acid
dNTP	Deoxynucleotide phosphate
dsDNA	Double stranded DNA
E. coli	*Escherichia coli*
EDTA	Ethylenediaminetetraacetic acid
FPLC	Fast Protein Liquid Chromatography
g	Gravity (g-force)
HEPES	S4-(2-hydroxyethyl)-1-piperazineethanesulfonic acid
i.e	id est
IPTG	Isopropyl beta-D-1-thiogalactopyranoside
KDa	Kilo Dalton
LB	Luria-Bertani
LwaCas13a	*Leptotrichia wadei* Cas13a orthologue
M	Molar
MES	2-(N-morpholino) ethanesulfonic acid
Nt	Nucleotide
ONC	Overnight culture
OUH	Oslo University Hospital
PAM	Protospacer adjacent motif
PCR	Polymerase chain reaction
PFS	Protospacer flanking sequence
RNA	Ribonucleic acid
RNase	Ribonuclease
rNTPs	Ribonucleotide phosphate
RPA	Recombinase Polymerase Amplification
RT-qPCR	Quantitative real time-polymerase chain reaction
RT-RPA	Reverse Transcription - Recombinase Polymerase Amplification
SARS-CoV-2	Severe Acute respiratory syndrome coronavirus 2
SDS-PAGE	Sodium dodecyl sulfate polyacrylamide gel electrophoresis
sgRNA	Single guided RNA
SHERLOCK	Specific High-sensitive Enzymatic Reporter unlocking
ssDNA	Single stranded DNA
TAE	Tris acetate buffer
TAPS	Tris(hydroxymethyl) methylamino propane-sulfonic acid
TE	Tris-HCl and ethylenediaminetetraacetic acid
Tris	Tris(hydroxymethyl)aminomethane

1 Introduction

1.1 Current state-of-the-art in diagnostics

Upon hospital admission patients, particularly those in a critical state, are treated empirically, according to observed symptoms and local experience and practice. Diagnostics attempts to clarify the medical situation and focus treatments to tackle the underlying cause of the observed morbidity. In the case of suspected bacterial infection, the primary approach is based on blood cultivation. Traditionally, blood samples are identified as bacteria-positive or negative through aerobic or anaerobic growth in specific media. If positive blood-cultures are detected, additional steps for microbial identification start with morphological characterization, through gram staining and microscopy to confirm the actual presence of microbes and phenotypic characteristics (1,2). Next, the positive cultures are plated on solid media for isolation of single pure colonies that can be further characterized and classified through 1) conventional biochemical screens (3), 2) sequence analysis and nucleic acid amplification such as polymerase chain reaction (PCR) (4), or 3) mass spectrometry like matrix assisted laser desorption ionization – time of flight mass spectrometry (MALDI-TOF) (5).

The long turn-around time from sampling to identification is a major limitation when using blood culture-based methods, considering patients having acute infections like sepsis with high mortality outcomes (6,7). In scenarios when sepsis is suspected, broad-spectrum antibiotics or a combination of several antibiotics are used in fear of the patient's health. This empirical treatment strategy has side effects for both the patient and society. This includes exposure of the patient the unnecessary antibiotics and the development of anti-microbial resistance (AMR) (8) making subsequential treatments less efficient. Currently this drawback does not overcome the grave risk of not treating the patient with sepsis.

Blood culture-based methods lack sensitivity as not all infective agents are cultivable, like virus, or the causative agents are not systematically present and not present at the site of sampling (9). This leads to negative blood cultures despite the patient presenting signs of infection (10,11). Further, the method is prone to false positives where the identified microbes do not always represent the true infectious agent and thus cannot directly determine the site of infection (3,7).

Rapid identification of the pathogenic agent and site of infection is desirable, to ensure proper treatment and minimize the use of broad-spectrum antibiotic when acute bacterial infections. Traditional blood-culture based diagnostic methods are time consuming which leads to negative effects on both health services and patient well-being (7). Numerous molecular methods for detection of viral or bacterial infections have been developed beside antigen identification (ongoing active viral infection) and serology testing (post viral infection) using antibodies (12). There are both advantages and disadvantages for each of these methods. The problem with antibody testing is that it cannot be used for severe sick patients as it only detects previous infections at the time of testing (12). Antigen test have been optimized for fast detection of pathogens, but they are less sensitive than molecular approaches (12).

The lack of fast and reliable diagnostic tests with high sensitivity and specificity to detect viral as well as bacterial infections is a significant disadvantage, especially for intensive care units (2). The development of new diagnostic tests and platform to overcome the use of empirical treatment strategies is necessary for personal diagnostics, but also strengthen society's health care system. Future solutions point to methods such as rapid sequencing of sample material, including algorithms that can provide information about content and quantity of pathogens, replacing the empiric diagnostic approach.

1.2   SARS-CoV-2 Pandemic

Severe Acute Respiratory Syndrome Coronavirus 2 (SARS-CoV-2) has for almost a year been at the center of attention in global news. Since the first outbreak was officially reported in Wuhan China on the 31 December 2019, the virus has spread across all continents, resulting in a global pandemic causing millions of deaths (13). A prominent problem that has arisen during the SARS-CoV-2 (Covid-19) outbreak, is limited testing capacity (14). The health service system is under great pressure, and well-established diagnostic tools are being put to the test (14). Symptoms of a SARS-CoV-2 infected person vary greatly, as such it is impossible to identify infection based only on signs of illness (15). Giving the lack of efficient treatments, rapid disease monitoring using reliable tests becomes essential to prevent the spread of infection and ensure prompt treatment in severe cases.

1.3   Characteristics of SARS-CoV-2

SARS-CoV-2 virus belong to the *Coronaviridae* family, characterized by its distinctive morphology of each particle surrounded by a "corona" or fringe which is formed due to an envelope embedded by glycoproteins (16). Similar to SARS-CoV and Middle East respiratory syndrome-related Coronavirus (MERS-CoV), the human SARS-CoV-2 (HCoVs) virus cause humans respiratory diseases and have emerged from zoonotic events (17–20). Several circulating human infectant coronaviruses exist including HCoV-NL63, HCoV-229E, HCoV-HKU1 and HCoV-OC43, known to cause common cold (21,22). Through mutations, recombination events and positive selection, the human SARS-CoV-2 has become much more deadly and viable to human host, as in case of MERS-CoV and SARS-CoV with occasional transmission between human and animals (21,23,24). The SARS-CoV-2 virus encodes several open reading frames, including genes resulting in four main conserved structural proteins: S (spike)-E(envelope)-M(membrane)-N(nucleocapsid) from 5' to 3' end, respectively (Figure 1.1) (25).
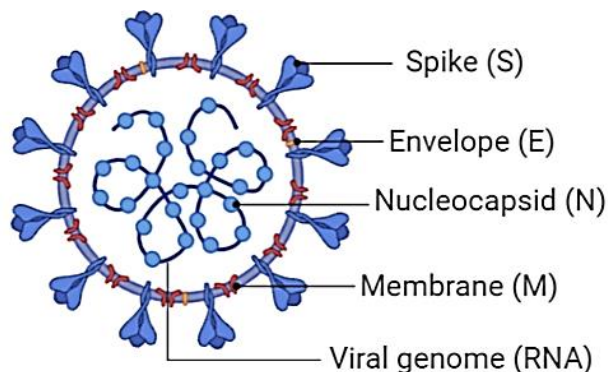
Figure 1.1 The SARS-CoV-2 virion structure, including structural proteins; spike (S), membrane (M), envelope (E), nucleocapsid (N), and the vial RNA genome. The figure is created with Biorender (https://biorender.com/).

1.4   Detection of SARS-CoV-2

Reverse transcription quantitative polymerase chain reaction (RT-qPCR) has become the primary molecular platform for genomic detection of active SARS-CoV-2 infections and is considered as the "gold standard" for SARS-CoV-2 diagnostics (26,27). The RT-qPCR method was developed from the original PCR technique (4) and monitors the deoxyribonucleic acid (DNA) amplification process in real time by the inclusion of fluorescence dyes or probes. The

generated signal correlate with the amount of target and are visualized by measurement of fluorescence intensity (4,28). The amplified target of interest is detected when the fluorescence intensity is significantly greater than a defined cyclic threshold (Ct) defined by background fluorescence (28). RT-qPCR is highly accurate and a sensitive tool (95%) to detect and track bacteria or viruses such as SARS-CoV-2 (29–31). Numerous RT-qPCR protocols have been developed for quantification of SARS-CoV-2 ribonucleic acid (RNA), mainly targeting the spike, nucleocapsid or envelope proteins or the RdRp gene in ORF1ab (32). The RT-qPCR process takes about 1,5 hours excluding the reaction assembly and RNA extraction (29,32).

Although many RT-qPCR platforms have been developed to efficiently detect active SARS-CoV-2 infections (31–33). Current bottlenecks like laboratory capacity, availability of reagents, suppliers and equipment impact the turnaround time for RT-qPCR diagnostic testing of SARS-CoV-2 and the number of samples to be tested each day (14,34).

Other technologies have been exploited to improve sensitivity and reduce test-time in a point of care diagnostic perspective. Especially one technology has the potential to significantly simplify the viral or bacterial nucleic acid detection, and is based on the Clustered Regularly Interspaced Short Palindromic Repeats (CRISPR-Cas) system (35–37). Discovery of the CRISPR-Cas platform by Emmanuelle Charpentier and Jennifer Doudna was awarded the 2020 Nobel prize in Chemistry based on the precise CRISPR/Cas9 genomic editing tool (38,39). In addition to being a powerful gene editing tool, novel CRISPR-Cas diagnostic platforms have proved to be powerful nucleic acid detection tools by reprogramming a different CRISPR/Cas system with crRNAs specifically designed for desirable target sequences (36,40–42).

1.5   The CRISPR-Cas systems

A novel distinct class of direct repeats called Clustered Regularly Interspaced Short Palindromic Repeats (CRISPR) (43) was originally discovered in *Escherichia coli* (44), and later found to be present in many other bacteria and archaea genomes (43,45–50). The CRISPR loci is characterized as structural motifs including multiple short direct repeats, separated by non-repetitive sequences called spacers, a common leader sequence and the presence of Cas genes (43,51). CRISPR genes span over the genome in a noncontiguous manner, as several direct repeats separated by variable "spacer" sequences which mostly represent captured

segments of viral or plasmid sequences (48,51–53). CRISPR associated proteins were first characterized as protein coding genes with high sequence similarity found close in sequence to the CRISPR clusters (43,49,54). Later researchers realized these proteins have an important function linked to CRISPR genes, and that a coordination of these elements resulted in an immunity protective system named the CRISPR-Cas system to protect against foreign genetic elements (55–59).

Naturally CRISPR/CAS systems function as defense mechanisms, protecting prokaryotes against attack from mobile genetic elements, plasmids, or bacteriophages (60). Foreign nucleic acids (DNA or RNA) from the intruders can be incorporated into spacer regions on to the CRISPR array, functioning as a genomic memory bank of former infections (Figure 1.2 (1)) (56–58,60,61). Upon subsequent invasion, the CRISPR loci is transcribed to precursor crRNAs (pre-crRNAs) (Figure 1.2 (2)) that are further recognized and processed by ribonucleases (RNases) to single stranded guide CRISPR-RNAs (sgRNAs) (Figure 1.2 (3)) (59). The sgRNA structures consist of a 25-50 nucleotides (nt) complementary sequence (spacer) needed to detect the invasive elements and a part of the repeat sometimes referred to the trans-activating crRNA (tracrRNA) represented as a secondary structure for interaction with Cas (48,52,59,62,63).

Together, a repertoire of sgRNAs complex with CRISPR-associated enzymes (Figure 1.2 (4)) and scan through cellular nucleic acids in the search for complementary sequences, called protospacers. Recognition and/or destruction of invasive elements is activated in a sequence specific manner (39,57). That is, that the occurrence of complementary base-pairing between invasive genetic sequences and crRNA protospacer can stimulate a nuclease activation of Cas enzymes, which leads to cleavage of invasive sequences (Figure 1.2 (5)). The system work as a robust protection mechanism to virulent attacks, making organisms more viable in the battle against competing or hostile organisms (47,64).
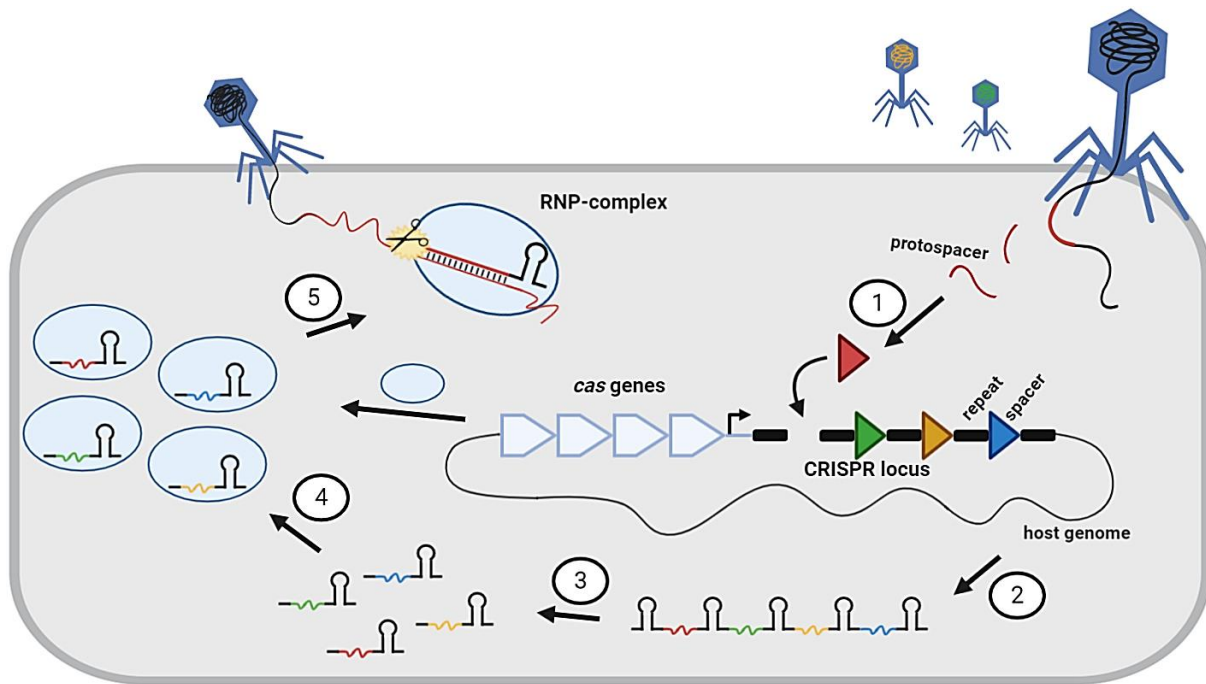
Figure 1.2 A simplified example mechanism representing a CRISPR-Cas system in bacteria. (1) Integration of invasive DNA sequences (protospacer) to the host genome from an initial viral infection. **(2)** Expression of CRISPR-RNAs (crRNA) and **(3)** processing of pre-crRNAs to mature sgRNAs. **(4)** Formation of a ribonucleoprotein (RNP) complex of sgRNA interaction with Cas enzymes. **(5)** RNA guided sequence specific nuclease activation upon recognition and pairing between crRNA -spacer and target sequence. Cas9 degrades genomic DNA. The figure is created with Biorender https://biorender.com/ and adapted from Doudna lab (65).

A great diversity of known CRISPR-Cas systems exists and extensive bioinformatic analysis has allowed researchers to classify CRISPR systems into two classes, types; I, II, III, IV and V, and subtypes (66–70) . In class 1 systems, a team of Cas proteins form a surveillance complex with an associated crRNA while a class 2 includes single multidomain Cas protein (69). Further classification is based on the variety of reaction mechanisms, enzymes and their characteristics, thus the involvement of Cas proteins in the different steps (69–71). In some CRISPR/Cas systems, a nuclease activation and destruction of foreign nucleic acids is dependent on the vicinity of a short protospacer adjacent motif (PAM) typically comprised of 1-3 nts (64), or a protospacer flanking sequence (PFS) upstream of the protospacer (Figure 1.3) (72–74).
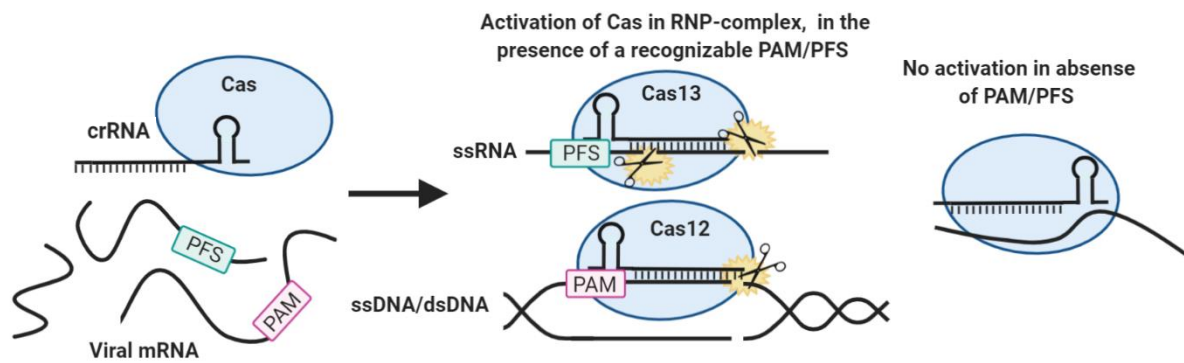
Figure 1.3 RNP activation dependency of PAM or PFS. Activation of ribonucleotide-protein (RNP)- complex is dependent on the presence of a PAM or PFS flanking the target sequence complementary to the crRNA (spacer) sequence. The Cas12 enzyme target single or double stranded DNA at a specific cite, and the Cas13 enzyme restrictively target single stranded RNA with multiple cleavage sites. The figure is created with https://biorender.com/ and adapted from Kellner et al., (36).

1.6   Class 2 Cas proteins

Class 2 CRISPR/Cas systems includes three types: type II, V and VI single protein moldules which have further been charatetized and classified. The type II protein module includes among others the widely used genome editing enzyme Cas9 which cleaves genomic double stranded DNA (dsDNA) complementary to a guide-RNA consiting of a tracrRNA and crRNA (39). Type V proteins including Cas12 (formally known as Cpf1) exhibit a spesific DNase activity, similar to the type II proteins (75). However the nuclease activity of proteins in type V are only dependent on the crRNA sequence (70). The proteins from both type II and V systems have a PAM dependent nuclease activity (75,76). The third and recently discovered system, VI can be divided into four subtypes (A-D) and consist of a single nuclease known for exclusively targeting single stranded RNA (ssRNA), called C2c2 or Cas13 (72,77).

1.7   Cas13

Cas13 target specificity is encoded by a ~64 nt crRNA including a 28-30 nt spacer sequence and a secondary hair-loop structure for interaction between the protein and the crRNA. (72). The RNase activity of Cas13 is highly independent of the presence of a PAM sequence (74), but some Cas13 orthologues requires the presence of a PFS site preferring single nts of 3'A,U or C (40,72). It was further discovered that Cas13 enzymes possess a collateral activity by trans-cleaving nearby non-target ssRNA molecules upon target recognition (40,72,78,79). This

feature is also observed in some Cas12a orthologues, but in a non-target single or double stranded DNA dependent matter (41,80). The non-specific RNA degradation of Cas13 and Cas12 orthologues has been exploited by researchers to create novel platforms for nucleic acid detection (36,40,42,81).

1.8   SHERLOCK

The specific high-sensitivity enzymatic reporter unlocking (SHERLOCK) platform was first developed by the Zhang Lab (82), and refers to the novel nucleic acid detection using Cas13 or Cas12 nucleases paired with an isothermal pre-amplification step (36). Kellner *et al.,* (36) recently published a protocol for SHERLOCK nucleic acid detection using Cas13a from *Leptotrichia wadei* (LwaCas13a). The SHERLOCK platform including Cas13 consist of three main steps: 1) the isothermal pre-amplification, which generates many copies of a given RNA or DNA template using specific primers 2) T7 transcription to convert dsDNA amplicons from 1) to ssRNA targets for LwaCas13a and 3) fluorescence based nucleic acid detection with LwaCas13a by including a fluorescence probe that emits detectable signal (Figure 1.4). The fluorescence signal is monitored by a plate reader over time.
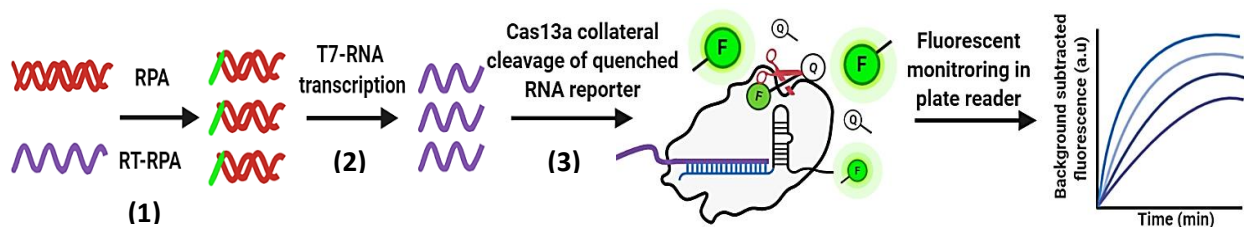
Figure 1.4 Simplified illustration of the fluorescence-based SHERLOCK nucleic acid detection assay flow. A sequence from a target genome is amplified by recombinase polymerase amplification (RPA) or reverse transcription-RPA (RT-RPA) if the initial sequence is RNA and converted to short amplicons using specific RPA primers. The forward primer contains a T7 promoter overhang integrated into the amplicons during the RPA reaction (green sequence). In the LwaCas13a reaction, the amplicons are converted to ssRNA by T7 RNA transcription from the T7 promoter to provide targets for the LwaCas13-crRNA complex. Recognition and base pairing between crRNA (spacer sequence, blue) and the target sequence, activates the LwaCas13a collateral activity leading to sequence-unspecific degradation of adjacent quenched-RNA reporters. The degraded RNA reporter emits a detectable fluorescence signal which determines the presence of virus or bacteria. The figure is created with Biorender (https://biorender.com/) and adapted from Kellner et al., (36).

1.8.1 Isothermal amplification of nucleic acids

The isothermal pre-amplification step of RNA or DNA extracted from clinical samples is responsible for the high SHERLOCK platform sensitivity (36). The recombinase polymerase amplification (RPA) was initially developed for the detection of DNA molecules (83), and is commonly used as a pre-amplification step in SHEROCK (82). The isothermal RPA reaction is a driven by a recombinase that targets specifically designed primers to a DNA sequence of interest (84). Together with the recombinase and RPA primers, a DNA polymerase and single stranded binding (SSB) proteins are needed to facilitate the RPA reaction (84).

The mechanism starts with a hybridization step facilitated by the recombinase that complexes with and guides the oligonucleotide primers to their homologous sequences found in a dsDNA template by scanning through the genome sequence (Figure 1.5, 1). SSB-proteins stabilize the reaction as they bind to open single stranded DNA (ssDNA) regions forming a D-loop (Figure 1.5, 2). Once base pairing is induced between the primers and their binding site in the DNA template, open single stranded regions enable the polymerase to bind and amplify the sequence (Figure 1.5, 3-4). The highly specific amplification proceeds rapidly after initiation from the primers, making a few initial copies to detectable amounts within a short time (Figure 1.5, 5) (84). If the target of interest is a single stranded RNA, a reverse transcription step is required by inclusions of reverse transcriptase in the RPA reaction (RT-RPA).

RPA can be performed within 30- minutes, either separate from the LwaCas13a nucleic acid detection (two-pot SHERLOCK assay) or within the same reaction (termed one-pot SHERLOCK) (36). RPA kits are currently available from TwistDx, including RPA reagents lyophilized together in reaction pellets that are stable for several months at room temperature (84). The user-friendly reaction setup makes RPA suitable for field diagnostics and the technique can be performed in different environments outside laboratory by non-trained lab personnel. The RPA reaction is optimal at 37°C, and 40-42°C if a reverse transcription is performed simultaneously (RT-RPA) but can also proceed at temperatures down to 25 degrees, which makes this amplification technique particularly attractive in the context of low-resource areas (84).
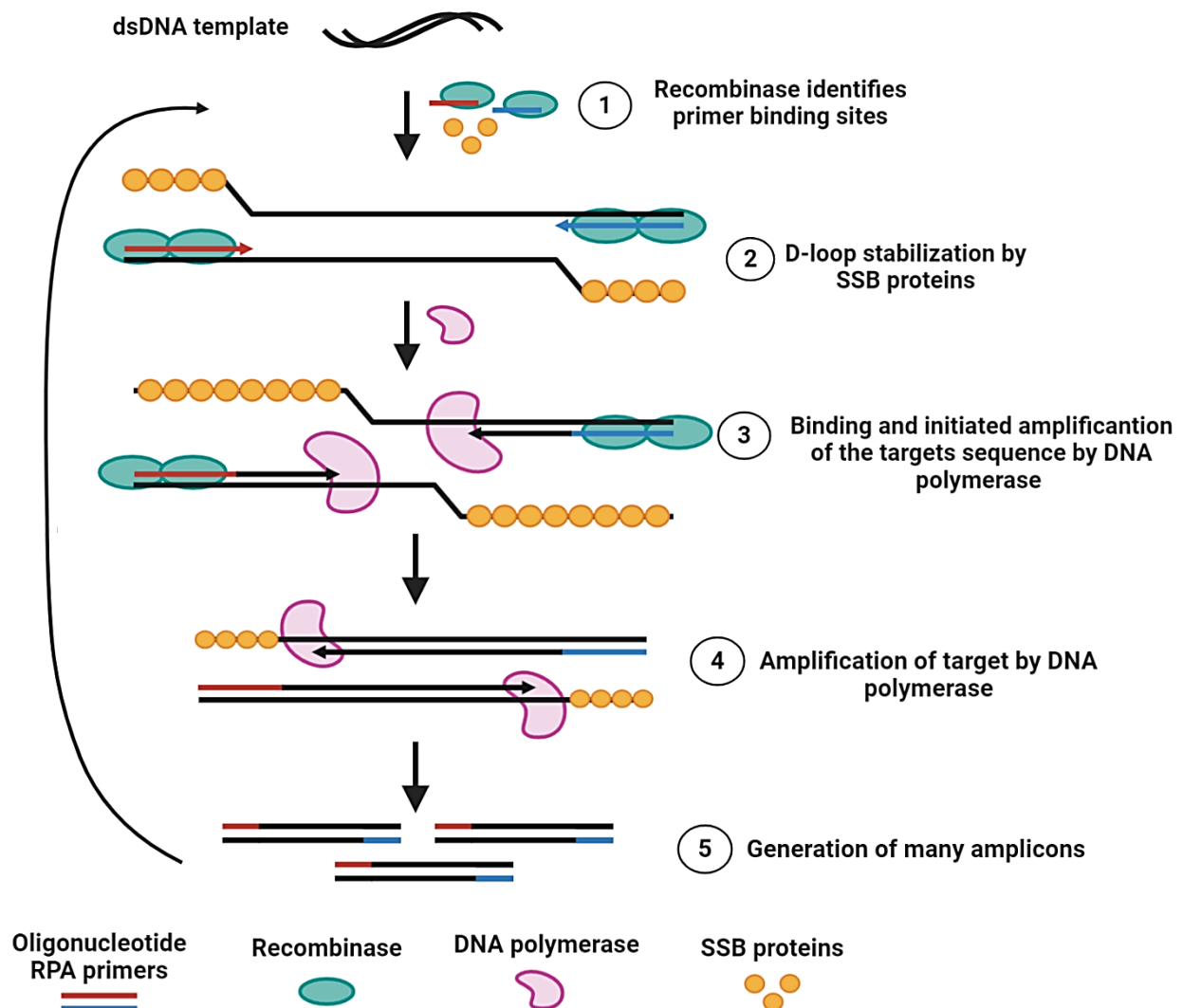
Figure 1.5 Simplified illustration of the RPA reaction cycle mechanism; 1) Recombinase interacts with the RPA primers and searches for a complementary primer binding site in the target sequence. 2) SSB proteins stabilize the open ssDNA areas in the reaction under D-loop formation. 3) Strand synthesis by DNA-polymerase is activated upon complementary base pairing between the primer and primer binding site. 4) DNA-polymerase amplifies the target region and 5) generated amplicons including primers and the target of interest. The cycle is repeated many times, and rapidly amplifies viral or bacterial sequences. The figure is created with Biorender (https://biorender.com/) and adapted from TwistDx™ (84).

1.8.2 RPA primer design

The RPA reaction requires specific primers for proper interaction with the recombinase that directs them to correct primer binding site in the target sequence. Generally, primers should be between 30-35 nt in length, with a GC content between 20-70% and the final amplicon length usually represent a 80-140 base pair (bp) long sequence (83,85). Each primer pair should be designed to minimize repeating mononucleotides and avoid primer-dimer propagation or the

formation of secondary structures. To obtain high assay sensitivity, primer screens are often necessary (85). Unlike PCR primers, melting temperatures of RPA primer are not as important because of the isothermal nature of the recombinase (85).

In a two-pot SHERLOCK assay the dsDNA amplicon generated by RPA serves as the input for the Cas13 nucleic acid detection reaction. Since LwaCas13 exclusively detects RNA molecules, the amplicons must be converted to RNA substrates for LwaCas13 detection (36). The inclusion of a T7-RNA polymerase is therefore necessary for the LwaCas13 nucleic acid detection reaction (36,40,81). A 5' T7-promoter overhang (Figure 1.5, green sequence) is added to the forward RPA primers to enable T7 transcription of amplicons simultaneously as LwaCas13 nucleic acid detection using a T7- RNA polymerase. (Figure 1.5, green sequence).
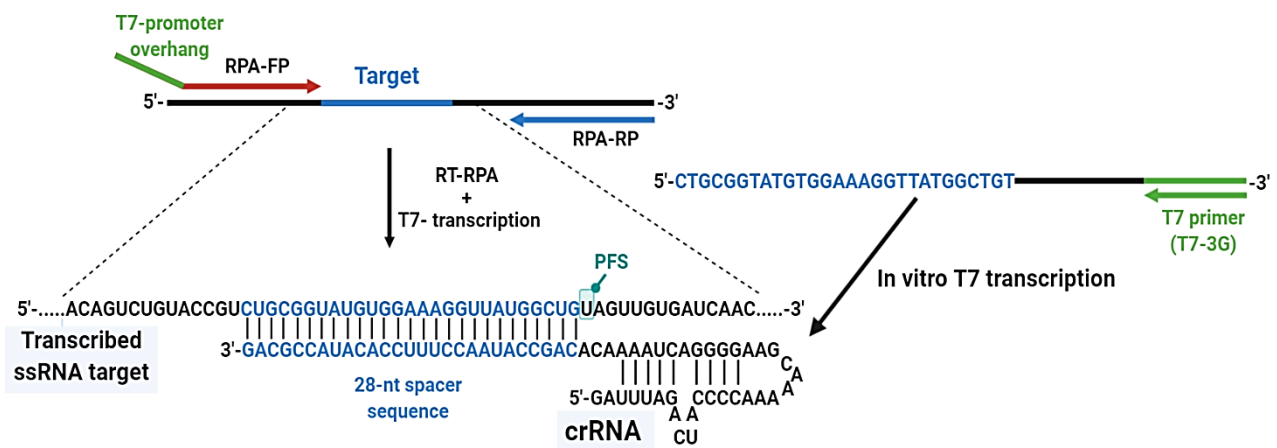
Figure 1.5. crRNA and RPA-primer design. Schematic illustration of the crRNA and RPA primer design for the SARS-CoV-2 *orf1ab* target used in this thesis. (RT-)RPA forward (FP) and reverse (RP) primers are designed to flank the target sequence of interest with lengths of 30-35 nt. The forward primer also contains a T7-promoter overhang for subsequent T7-transcription of the RNA amplicon generated from RT-RPA. The crRNA is transcribed from a ssDNA oligo *in vitro* containing the reverse complement sequence of the target site in the 3' end. A direct repeat followed by an additional T7 promoter sequence are added to the 5' and of the ssDNA oligo. The 28-nt spacer sequence of the mature crRNA base-pairs with the target of interest with a given protospacer flanking site (PFS). The figure is created with Biorender (https://biorender.com/) and adapted from Kellner et al., (36) and Zhang Lab- Cas13 (82).

1.8.3 Cas13 nucleic acid detection

The single RNA guided RNase Cas13a (known also as C2c2) exhibits a promiscuous RNase activity upon target recognition by complementary base pairing with an associated crRNA (72). The enzyme can be programmed to target any ssRNA sequence, by designing crRNAs complementary to the target of interest. The collateral activity is the key to detect the presence of a specific sequence (82,86). In a fluorescence-based detection assay, fluorescence signals

can be detected by the inclusion of a Cas13a sequence specific quenched fluorophore RNA reporter in the reaction. In a non-cleaved state, the quencher will absorb the energy emitted from the fluorophore upon illumination. Once the trans-cleavage of Cas13 is activated, the reporter is degraded, and the fluorophore emits a detectable signal. Some Cas enzymes have a motif specific cleavage preference, which can be included in the reporters to ensure efficient cleavage (42). LwaCas13a used in Kellner et al., (36). has a poly U/AU specific motif preference (Figure 1.6) (36,42). The quenched RNA reporter therefore consists of a fluorophore in the 5', a poly AU stretch and a quencher in the 3'.
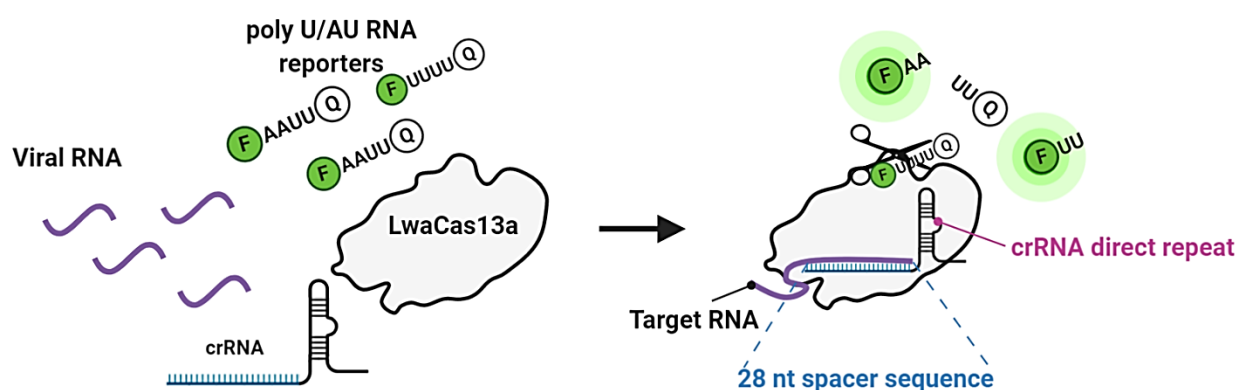
Figure 1.6: Promiscuous nuclease activity of LwaCas13a. LwaCas13a recognizes and interacts with a direct repeat (DR) in the associated crRNA and forms a ribonucleotide-protein complex (70,72,74). The nuclease activity of LwaCas13a is activated when its associated crRNA complementary pairs with a target sequence encoded by a 28 nt spacer sequence. LwaCas13a undergoes a configurational change and exhibits a collateral degradation of adjacent poly U/AU reporter RNA creating a detectable signal. The figure is created with Biorender (https://biorender.com/) and adapted from Gootenberg et al., (42).

1.8.3.1 Other SHERLOCK variants

Additional features of the SHERLOCK exist (SHERLOCKv2), including multiplex fluorescence based detection with several Cas enzymes and visual readouts with colorimetric-based lateral-flow detection are included (36,42,81). Similar nucleic acid detection platforms with Cas12 (CRISPR-Dx) have been developed including DNA Endonuclease Targeted CRISPR Trans Reporter (DETECTR) referring to a combination of Cas12a (formally known as Cpf1) ssDNase activation with RPA as isothermal pre-amplification (41). The one-HOur Low-cost Multipurpose highly Efficient System (HOLMES) also utilize the Cas12a for rapid detection of target DNA as well as RNA using PCR as pre amplification (87). Another amplification technique termed Loop-Mediated Isothermal Amplification (LAMP) has also been coupled with Cas detection of nucleic acids in SHERLOCK, HOLMES (HOLMESv2)

and DETECTR (37,88–90). LAMP operates at a 60-65°C temperature range and includes a unique set of primers for amplification of several targets in the DNA or RNA template (36,88,91). The modified version of HOLMES, termed HOLMESv2 is an one-pot detection using a thermophilic Cas12b with LAMP (92).

1.8.4 crRNA design

Correct crRNA design is one of the most important aspects in the SHERLOCK assay. The LwaCas13a associated RNA guide secondary structure consists of a 28-nt spacer region complementary to the target sequence of interest, and a stem-loop structure from a 36-nt direct repeat in the 5´end (Figure 1.6) (36,79). Guides should be constructed to minimize off-target events on genes that resemble the target sequence, to maintain the high specificity (36,93). Overlap between primers and guides may lead to a false detection of the primer sequence instead of viral RNA, and increase background noise in the fluorescence reaction (36,85). To ensure specific and sensitive nucleic acid detection, the crRNAs are designed to target conserved areas within the bacterial or viral genome of interest (36).

LwaCas13 detection is very specific, and alterations within the crRNA sequence can make single-nt distinction in the target site possible (36,82). Introduction of a single-base mismatch ("a synthetic mismatch") in the crRNA (36,82) allows LwaCas13a to further discriminate between pathogenic target sequences that differs in only a single base, making the assay capable of strain discrimination (36,40,82). This adjustment can also be useful to identify anti-microbial resistance (AMR) in bacteria.

The most common approach when considering crRNA design, is to construct ssDNA oligonucleotides which can be transcribed *in vitro* to ssRNA (36,42,82). The RNA transcription is then induced by an appended T7 promoter in the 3' end of the oligomer (Figure 1.6). Alternatively, synthetic crRNAs can be custom ordered from a selection of companies (36,82).

1.9 Research aims and objectives

Novel diagnostic approaches such as the SHERLOCK assay, have demonstrated equal or even higher sensitivity, compared to RT-qPCR (92,94). SHERLOCK has a low dependence on instruments, contains easy handling steps and promotes faster nucleic acid detection, a potensially advantage over RT-qPCR (36). The platform has potential as a SARS-CoV-2 detection tool, capable of rapid identification of infected individuals which is crucial for disease monitoring, thus increase the daily test-capacity. A successful establishment of the Cas13 nucleic acid detection tool could have a large impact on both sensitivity and accuracy within diagnostic testing. In addition, as a tool for rapid alternative SARS-CoV-2 testing, the platform can be adjusted to identify any nucleic acid sequence of interest including other pathogens and identify drug resistant genes.

In this thesis, the main aim was to establish a CRISPR-Cas13 based nucleic acid detection tool at Oslo University Hospital as a faster alternative to the gold standard RT-qPCR diagnostic method maintaining specificity and sensitivity. For this we adapted the SHERLOCK platform to create a rapid diagnostic tool for SARS-CoV-2 detection (36). We used a fluorescence-based detection assay of SARS-CoV-2 with RT-RPA as a pre-amplification step and LwaCas13a for the nucleic acid detection. The thesis is divided into four main parts **I)** Preparation of SHERLOCK components, **II)** SHERLOCK assay optimization, **III)** SHERLOCK on clinical SARS-CoV-2 samples and **IV)** final validation of the SHERLOCK platform. In part I-II, goals included successful design of crRNAs and RPA primer, finding optimal targets for SARS-CoV-2 detection and to achieve best possible fluorescence monitoring. To establish a fast and high sensitivity SHERLOCK platform, assay optimization was done with focus on instrumentation, reaction components, and target optimization. Variables in the (RT-)RPA and LwaCas13a reaction were examined using synthetic sequences. In part III, the goal was to detect clinical SARS-CoV-2 samples and in part IV, we evaluated the SHERLOCK sensitivity and specificity. The flow chart below describes an overall overview of the content of the thesis with the steps in SHERLOCK, focus, main experiments, and the most important findings (Figure 1.7)
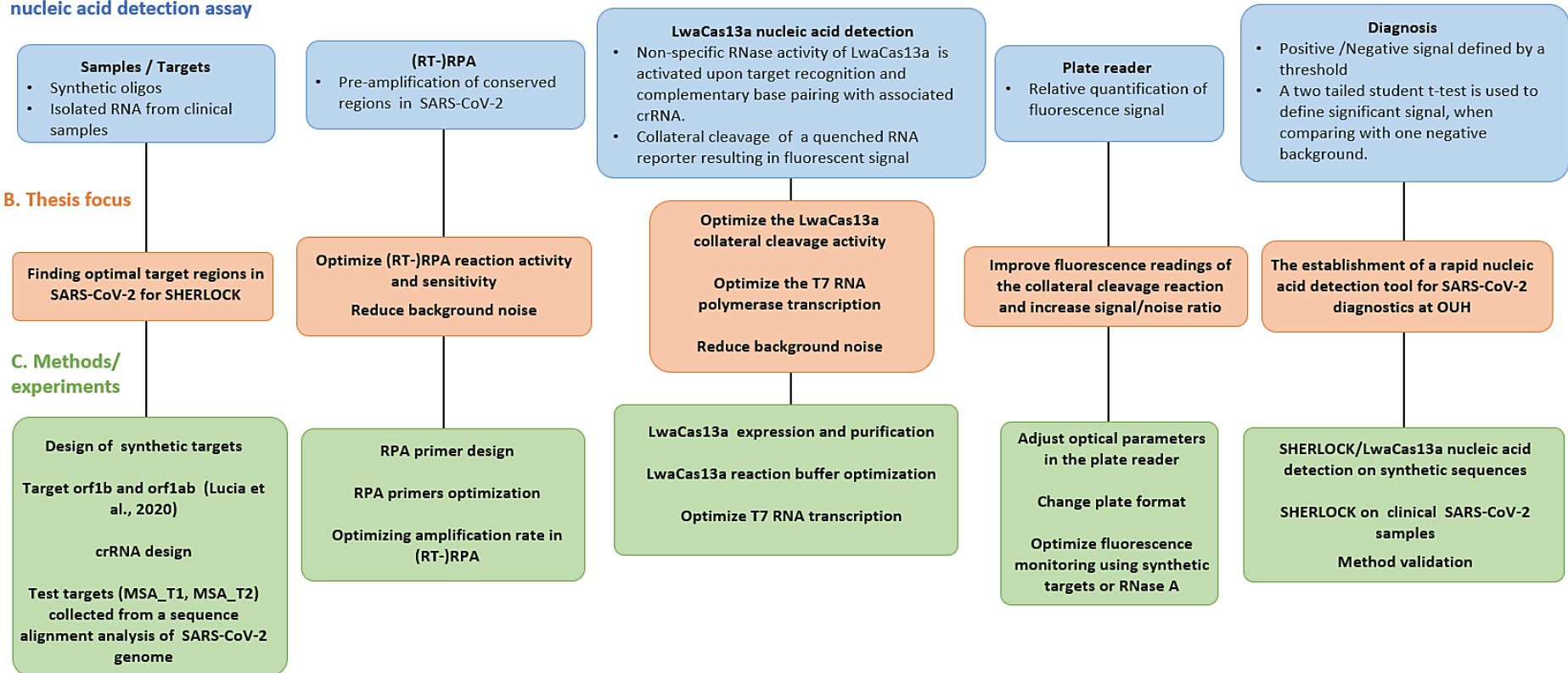
Figure 1.7 An overall overview of the content of this thesis as a flow diagram. A) Workflow for a two-pot SHERLOCK nucleic acid detection using a plate reader for fluorescence monitoring. B) A workflow of focus in the thesis, and C) experiments executed to reach main goals.

2 Materials & Methods

All materials are given in appendix A besides plasmids noted below.

2.1 Plasmids

Pre transformed Rosetta™ 2(DE3)pLysS Singles™ Competent Cells (Novagen® Sigma-Aldrich ,71401-M) containing the pC023-Twinstrep-SUMO-huLwCas13a (Addgene, plasmid no.90097) plasmid was used to express LwaCas13a in this study. The plasmid map can be found in Appendix C.

2.2 Statistical methods

Statistical calculations were done in Microsoft excel. All technical replicates are represented as n, and biological replicates are noted as m. When using more than two technical replicates for a series tested in the LwaCas13a collateral cleavage reaction, an average of each series in calculated and represented as mean ± SD. Statistically significant was determined by student two tailed, unpaired t-tests (assumed unequal variance), and are represented with the following significant levels in the results; ns $\geq$ 0.05, *P < 0.05, **P < 0.01, ***P < 0.001, **** P <0.0001.

PART I Preparing SHERLOCK components

2.3 LwaCas13a protein expression and purification

Protein expression and purification was done according to Kellner et al. with some modifications detailed below (36). The Cas13a orthologue LwaCas13a, was used for the CRISPR Cas- nucleic acid detection, in the SHERLOCK assays. To create mature LwaCas13a protein for SHERLOCK, a twinstrep-SUMO-huLwCas13a plasmid (Figure S1) pre-transformed in *E.coli* cells were expressed and purified. In addition to the LwaCas13a gene, the plasmid contains ampicillin resistance and a T7 promoter for Isopropyl beta-D-1-thiogalactopyranoside (IPTG) induction of LwaCas13a expression in recombinant *E.coli* cells . The expressed protein includes on the N-terminal a SUMO-tag which is cleavable by SUMO protease, and a twin-Strep-tag which is two linked modified "Strep-Tags" used in subsequent

protein purification of LwaCas13a. The Strep tag is used for isolation of LwaCas13a from other proteins by binding to a Strep-Tactin resin. During purification, aliquots were collected for SDS-PAGE to validate protein purification (Figure S2). Procedures for expression and purification are described below.
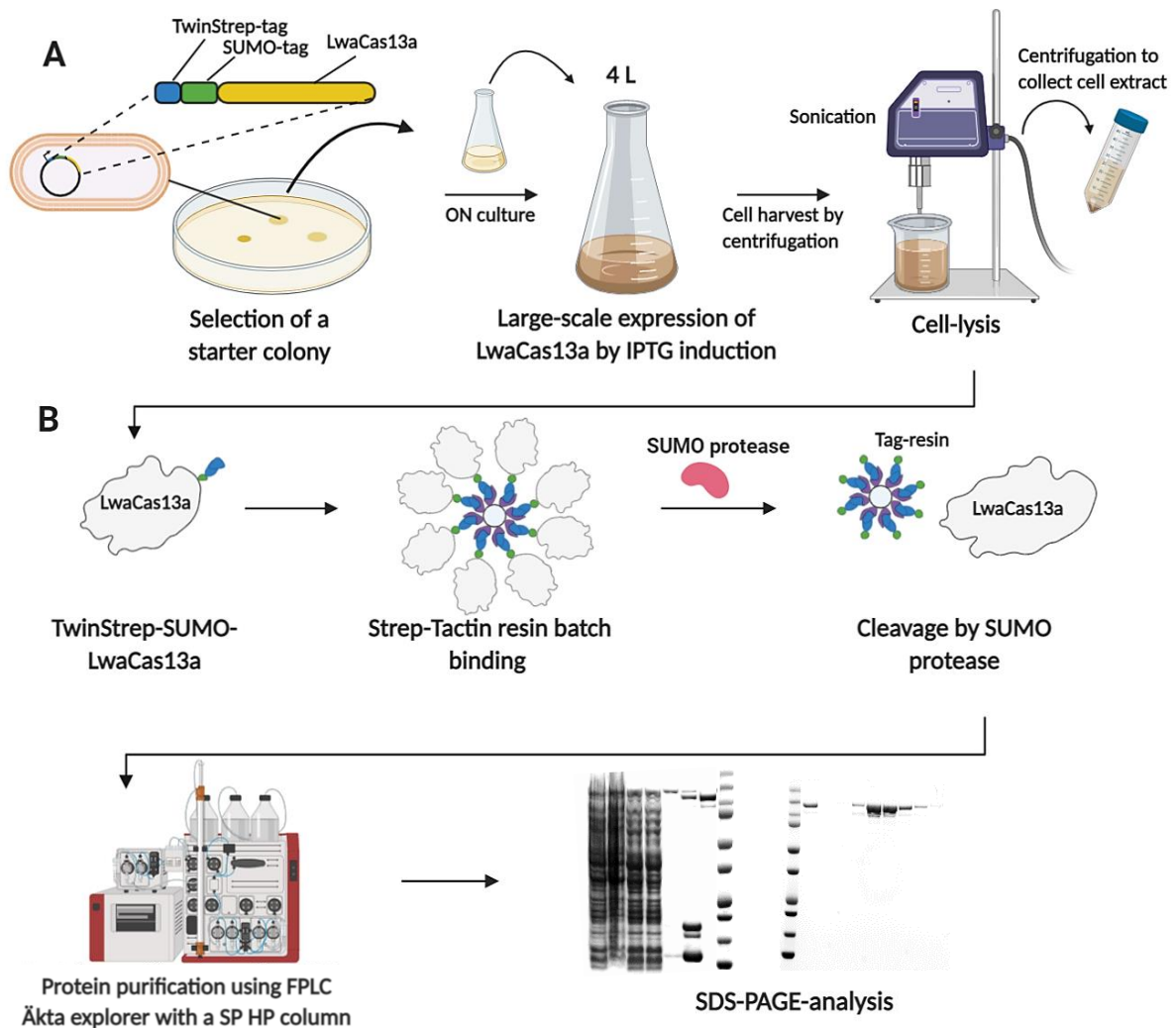
Figure 2.1: Flow chart of LwaCas13a expression and purification. A) Expression of LwaCas13a**. Pre-transformed competent Rosetta E-coli cells, including a TwinStrep-SUMO-LwaCas13a protein expression plasmid were grown on LB agar plate containing ampicillin for selection of a starter colony. After selection of a single colony and ON growth, the culture was added to Terrific Broth (TB) media containing ampicillin for large-scale expression of LwaCas13a by induction of IPTG. After induction of LwaCas13a, the cells were harvest and lysed using sonication and cell extract was collected using centrifugation. **B)** LwaCas13a purification and quantification. The protein was separated from other cell-components using strep-tag batch binding to a Strep-Tactin-resin. After batch binding, the protein was separated from the resin by SUMO protease cleavage of the SUMO-tag. The resulting native LwaCas13a protein-elute was further purified with cation exchange chromatography using a SP HP column in a Äkta explorer FPLC system. The purification process of LwaCas13a was visualized using SDS-PAGE® analysis. The figure is created with https://biorender.com/ and adapted from Kellner *et al.,* (36).

2.3.1 Expression

The LwaCas13a protein expression was done according step 4-8 (36), starting with an overnight culture (ONC) by selecting a single recombinant colony from a Luria-Bertani (LB)- agar plate containing ampicillin (100 µg/mL). 4 L of Terrific Broth (TB) media was used to express LwaCas13a. Resulting cell pellets were stored at -80°C for further protein extraction and purification. (Figure 2.1 A)

2.3.2 Purification with SUMO-tag

All steps for protein extraction and purification were performed at or close to 4°C. Sample buffer, SUMO protease cleavage solution and lysis buffer was freshly prepared. The LwaCas13a purification was executed from a total of 30 gram cell pellet resulting from a ≈ 1500 mL cell culture volume (Figure 2.1 B)

The pellet was resuspended in 200 mL lysis buffer and placed on ice for 30 minutes with repeated vortexing until homogeneous solution. Cells were then lysed by sonication for 3 x 30 seconds at 60 % amplitude. An aliquot of the resulting lysate was stored at 4°C for sodium dodecyl sulfate polyacrylamide gel electrophoresis (SDS-PAGE) and the rest was cleared by centrifugation for 20 minutes at 40,000 g in a pre-chilled 4°C centrifuge. Meanwhile, 1 mL of Strep-tactin Superflow Plus was washed three times with cold lysis buffer. An aliquot of the resulting supernatant was stored at 4°C for SDS-PAGE, the rest was divided into 5 x 50mL falcon flasks. The resin was mixed with lysis buffer to a total of 5 mL. 1 mL of the pre-washed Strep-tactin Superflow Plus resin was distributed to each falcon flask for LwaCas13a binding to Strep-tactin resin, by incubation at 4°C overnight with rotation. The protein-bound resin was centrifuged at 4°C with 3000 g for 3 min until clear distinction between protein bound resin and the buffer. The protein-resin from each tube was pooled in one 15mL tube. The protein bound resin was washed three times with ~10 mL cold lysis buffer and centrifuged at 3000 g for 3 min between each wash. Protein-resin was resuspended in 3 mL of freshly prepared SUMO protease cleavage solution and incubated overnight at 4°C with rotation for SUMO tag cleavage. The protein suspension was then centrifuged at 4°C, 3000 g for 3 min until clear distinction between Strep-tactin resin and SUMO cleaved mature protein, and the resulting protein suspension was transferred to a separate tube. The resin was washed 3 times with cold lysis buffer, and an aliquot was stored at 4°C for SDS-PAGE. The final mature LwaCas13a

elute was further purified with fast protein liquid chromatography (FPLC) using a HiTrap™ sulphopropyl (SP) High performance (HP) column cation exchanger except an aliquot that was stored at 4°C for SDS-PAGE.

2.3.3 Purification with Cation exchange chromatography

To separate the protein from potential contaminants like SUMO-protease and nucleases, the resulting protein elute was further purified using cation exchange chromatography. This technique allows the protein to be separated from other components based on a positive charged protein surface. LwaCas13a in a Tris pH 7.5 elutes at a salt concentration of ~550 milli molar (mM). The cation exchange chromatography program was executed according to step 21 in Kellner et al., (36), with some modifications. These are: the resulting protein extract post Strep-Tactin Sepharose-SUMO protease treatment was diluted to a lower salt concentration at 240mM by adding Buffer A to the protein elute. The solution was applied to a 1 mL HiTrap™ SP HP column in a FPLC (Äkta explorer) system and eluted over a salt gradient from 200 mM to 1M NaCl using elution buffers A (200mM NaCl) and B (1M NaCl). A 1 mL column was used instead of a 5 mL column, a flow rate of 1 mL/min was used instead of 5 mL/min, and the gradient elution was done in 25 x column volumes instead of 10.

Protein concentration was determined with Nanodrop spectrophotometer at 280nm using the extinction coefficient and the molecular weight of the protein (Table A6, appendix A). Protein containing fractions were analyzed further with SDS-PAGE for protein visualization (Appendix D). The three most concentrated fractions of LwaCas13a (7, 8, and 9), were pooled as a final LwaCas13a product, quantified with Nanodrop spectrophotometer, normalized to ensure protein storage conditions in the protein buffer (36), and stored for subsequent SHERLOCK experiments.

2.3.4 Nuclease test on protein extract

The LwaCas13a protein extract must be of high quality and free for contaminants to give sufficient and accurate LwaCas13a collateral cleavage reactions and avoid false positive results. Therefore, a nuclease test of the protein extract was conducted by incubating a 550 nt RNA

sequence (3,7µg/µL) with and without the LwaCas13a enzyme extract (diluted with sample buffer to 63,3 µg/mL) at 37 degrees with LwaCas13a reaction buffer (9 mM $MgCl_2$, 20 mM HEPES pH 7.0). After 20 minutes, 40 minutes and 1 hour, 5 µL of master mix was transferred to a PCR tube and mixed with 5 µL gel loading buffer II (Ambion). Next, samples were heated at 70 degrees for 3 minutes and loaded on a 6% polyacrylamide gel with urea. 1 x Tris-Borate-ethylenediamine-tetraacetic acid (TBE) was used as running buffer, and the samples migrated for 50 minutes at 130 V. The gel was stained for 30 minutes with 50 mL 1x TBE and 1,5 µL CYBRsafe and imaged using Bio-Rad Image Lab™ Software.

2.4   SHERLOCK crRNA design

For SHERLOCK reactions using LwaCas13a, specific crRNAs were designed to target synthetic DNA1 (DNA1-crRNA), SARS-CoV-2 *orf1b* (orf1b-crRNA), *orf1ab* (orf1ab-crRNA and orf1ab2-crRNA), MSA_T1 (MSA_T1-crRNA) and MSA_T2 (MSA_T2-crRNA). All crRNAs were designed in accordance with guidelines from Zhang lab and Kellner et al., with a 36-nt secondary structure loop for LwaCas13a recognition and binding, and a 28-nt protospacer complementary to the target sequence (36,82). The crRNAs for DNA1, *orf1b* and *orf1ab* were initially ordered as ssDNA oligomers from Eurofins Genomics with a T7 promoter added at the 5'end for *in vitro* transcription to mature crRNAs. Later, crRNAs for MSA_T1, MSA_T2 and orf1ab (orf1ab2-crRNA) were ordered as pre-synthesized RNA sequences by Eurofins genomics. To see if LwaCas13a reaction sensitivity improved, the orf1ab2-crRNA is equal in RNA sequence to the in vitro transcribed product of orf1ab-crRNA. All crRNAs sequences are available in Table S2.

2.5   In vitro transcription of crRNAs

Orf1b-crRNA, orf1ab-crRNA and DNA1-crRNA were *in vitro* transcribed from the respective ssDNA oligomers. MEGA Script Kit (Ambion) was used, in accordance to step 29-32 in Kellner *et al.*, with small modifications (36). These are: an initial crRNA template and T7-primer (T7-3G) input used for each crRNA template was 2 µmol/reaction except for the DNA-crRNA reaction with 100µmol of each primer. For all crRNAs, a ramp rate of 0,1 °C/s was used for the cooling process in the annealing reaction. The *in vitro* transcription was then executed at 37°C overnight (~16h).

2.5.1 Recovery of crRNAs

All crRNAs were purified with each method described **below** and analyzed with Tape Station Systems (Agilent) for quantification and to ensure correct products. crRNAs were then normalized to 300 ng/µL using a 0,5x TE buffer pH 7.5 and aliquots of 6 µL were made in PCR tubes and stored at -80°C for SHERLOCK.

Phenol: chloroform purification

To prepare crRNAs for SHERLCOK, the *in vitro* transcribed crRNA products were purified using phenol; chloroform extraction according to MEGAscript® Kit user guide (95). The method will remove all enzymes and almost all free nts used in the *in vitro* transcription, based on solubility of the molecules. Briefly, when using acidic phenol in combination with chloroform proteins and nts will precipitate while the crRNAs will remain in the aqueous phase. The chloroform increase efficiency of protein denaturation in the phenol while keeping the crRNAs separated in the aqueous phase (96,97) The remaining ssDNA templates will not be removed, but because they are present in such small amounts compared to the RNA products, their presence should be negligible in SHERLOCK. The addition of chloroform was done twice to remove excess phenol. The precipitation process with isopropanol was done overnight at -20°C. Resulting crRNA pellets were resuspended in 10mM Tris pH 7.5 solutions containing 0,5 mM ethylenediamine-tetraacetic acid (EDTA).

Purification with nanoparticles

A new extraction method developed by the Magnar Bjørås group at The Norwegian University of Science and Technology (NTNU) for extraction and isolation of SARS-CoV-2 RNA from clinical samples was used to purify the *in vitro* transcribed crRNA products (Appendix E). The method involves a lysis buffer to make RNA available and specially designed magnetic nanoparticle solutions for nucleic acid extraction and isolation (98). A buffer solution containing nuclease free water and 1% Tween 20 was used for crRNA elution.

2.6 Preparation of synthetic targets for SHERLOCK

To optimize SHERLOCK reaction conditions, trial SHERLOCK experiments were conducted using synthetic sequences, including SARS-CoV-2 like genes. Synthetic DNA 1 and sequences corresponding to areas within the SARS-CoV-2 *orf1b-* (T2) and *orf1ab-* (T3) genes was used as positive controls in the trial experiments (Table S1). To enable LwaCas13a nucleic acid detection without RPA as pre-amplification, the synthetic targets were converted to dsDNA products that included the T7 promoter using PCR. The targets were designed to fit SHERLOCK conditions, including a 28 nt stretch complementary sequence to associated crRNA in the LwaCas13a collateral cleavage reaction (Figure 1.5).

2.6.1 PCR

BIOTAQ™ PCR Kit (Bioline) and original associated primers designed for (RT-)RPA (Table S1) was used in the PCR reaction to amplify SARS-CoV-2-T2 and T3, respectively. In addition, three forward primers with different T7 promoter overhang sequences were combined with the DNA1 reverse primer to generate PCR products for a T7 promoter optimization assay (section 2.12). 50 µL reactions were prepared in PCR tubes on ice containing; 5 µL 10x NH4 buffer, 2 µL 50mM MgCl2, 0,4 µL deoxynucleotide tri-phosphate (dNTP) (25mM each, tot 100mM), 2 µL of forward and reverse primer (10uM) each, 0,4 µL BioTaq polymerase, 1 µL of template (0,01 pmol) and nuclease free water up to 50 µL. Cycling conditions included: 1-minute initial denaturation at 95°C for one round, 25 cycles including denaturation 95°C for 10 seconds, annealing at 72°C for 15 seconds, and extension at 72°C for 15 seconds, and an infinite final hold on 8°C.

2.6.2 SDS-PAGE and recovery of PCR products

30 µL of final PCR products were mixed with 4 µL orange 6x gel loading dye and run on a 2 % agarose gel. Quick load purple low molecular weight DNA ladder or Quick load purple 100 bp DNA ladder were used for the synthetic PCR products. 1x TAE was used as running buffer with SYBRsafe® DNA gel stain for visualization of the DNA fragments. The gel migrated at 90 V for 50 minutes. To avoid ultraviolet (UV)-light damage on the DNA fragments, a Safe Image™Transilluminator with blue light was used to visualize the PCR products. The DNA fragments were cut out of the gel and purified according to QIAquick Gel Extraction

purification protocol using a microcentrifuge (99). DNA extracts were quantified with Qubit 2.0 spectrophotometer using Qubit™ dsDNA HS Assay Kit. 1 µl of Qubit HS dsDNA reagent was mixed with 199 µL Qubit HS dsDNA buffer for each sample, an appropriate amount was mixed with each protein fraction and solutions stood for 2 minutes incubation in room temperature before measuring concentrations. The PCR products were then normalized in 0,5x TE buffer pH 8.0, and stored as aliquots of 6 µL in -20°C. Primers and templates used in this assay are available in Table S1.

2.7 Primers for (RT-)RPA in SHERLOCK

Specific primers are needed to proceed the isothermal (RT-)RPA pre-amplification step in SHERLOCK on the synthetic- or clinical targets (84). The RPA primers were designed using the primer design guidelines suggested by the TwistDx Assay Design Manual, and guidelines in Kellner et al., (36,85). To each forward primer, a 5' 25 nt T7 promoter overhang were introduced for T7 transcription of dsDNA (resulting from RPA) to RNA molecules, as LwaCas13a uses RNA as a substrate. All primers used in RPA are listed in Table S1.

2.7.1 RPA primer design for SARS-CoV-2

Several RPA primers were designed and tested for detection of SARS-CoV-2, to find optimal primer pairs for maximal amplification. Initially, original primer sets was designed for targeting two regions the *orf1b* and *orf1ab* genes (100) (Table S1). In addition, a new primer set for *orf1ab* and primers for two additional conserved regions in the SARS-CoV-2 genomes were designed (Table S1). The novel targets were identified through sequence analysis of the SARS-CoV-2 genome by Jon K. Lærdahl, research scientist and bioinformatician at MIK, OUH, and is referred to as MSA_T1 and MSA_T2 (conserved segment 2 and 1, respectively, Appendix P). Further, to identify the best (RT-)RPA primers, a primer screen experiment was conducted (section 2.16.3). Up to 5 different forward and reverse primers (Table S3, S4, S5 and S6) were designed for all SARS-CoV-2 regions except *orf1b*.

All primers for SARS-CoV-2 were designed using MN908947.3 obtained from GenBank as the SARS-CoV-2 reference genome.

2.7.2 RPA primer design for synthetic DNA 1

RPA primers for synthetic DNA 1 amplification were taken from table 2 in Kellner et al., (36). For possible improvements in the T7 transcription (section 2.12), two additional forward primers (24127F and 24128F) with a different T7 promoter sequence were designed (101).

PART II ASSAY OPTIMIZATION

2.8 Trial experiments excluding RPA from SHERLOCK

Early in the experiment period, there was no access to Twist Dx's RPA kit, and therefore several experiments were performed only with LwaCas13a nucleic acid detection using PCR generated dsDNA templates as direct input or RNase A. Both 96 and 384 well plates were tested with various optical settings to find optimal reading conditions of the fluorescent collateral cleavage reaction by LwaCas13a. The three experiments described below were executed according to section 2.9.2 using various concentrations of synthetic DNA 1 or RNase A as positive control. Synthetic DNA1-crRNA was used as guide to LwaCas13a. LwaCas13a reactions could proceed for 3 hours. More details about the experiments in question are described below.

2.8.1 Trial LwaCas13a detection of synthetic DNA 1

To investigate if the synthetic DNA 1 was detectable on a 96 well plate, a SHERLOCK experiment done on a 100x dilution series ($9,1*10^{+07}$ to $9,1*10^{-03}$ copies/reaction) of synthetic DNA PCR product. To see if the fluorescent signal was specific to the presence of target, the experiment included seven negative controls excluding one or more LwaCas13a reaction components.

2.8.2 Trial LwaCas13a reactions with RNaseA

To investigate if the use of RNase A as positive control gave higher detectable signal compared to synthetic DNA 1 a SHERLOCK experiment done on a 10x dilution ($9,1*10^{+06}$ copies/reaction) of synthetic DNA PCR product and three dilutions of RNase A (0,6 ng/µL, 0,06 ng/µL and 6 pg/µL). To see if the fluorescent signal was specific to the presence of target or RNase A, the experiment included several negative controls. The negative controls represented LwaCas13a reactions excluding one or more reaction components or an addition of

the storage buffer for LwaCas13a or elution buffer used to elute the PCR product from QIAquick Gel Extraction kit. The 96 well plate was used.

2.8.3 Trial LwaCas13a detection of synthetic DNA 1 using a 384 well plate

To investigate if the synthetic DNA 1 was detectable on a 384 well plate, a SHERLOCK experiment done on one sample of synthetic DNA PCR product ($3,6*10^{+07}$ copies/reaction). To see if the fluorescent signal was specific to the presence of target, the experiment included a water only negative control excluding target from the LwaCas13a reaction. A 384 well plate was used for fluorescent readouts.

2.9 Two pot SHERLOCK nucleic acid detection with LwaCas13a

The two-pot SHERLOCK nucleic acid detection method were chosen to target SARS-CoV-2. The newly published protocol by Kellner et al., (36) was used as a starting point for the SHERLOCK experiments, but was optimized and modified as described in detail below. For the fluorescent readout monitoring of the LwaCas13a reaction, the VICTOR Nivo multimode plate reader (PerkinElmer) was used. The LwaCas13a enzyme was used for nucleic acid detection with the 5'TEX615 reporter specific to LwaCas13a for collateral cleavage. To avoid contamination of reagents and work area which can generate false positive signals, pre- and post-amplification work areas was used when setting up the RPA and LwaCas13a reaction. Aliquots were made of RPA- and LwaCas13a reagents (that is (i.e) crRNA, LwaCas13a, and protein storage buffer, rehydration buffer from RPA kit), primers and ultrapure water solution. In the first optimization experiments only the LwaCas13a reaction part of SHERLOCK were done, excluding the RPA step (specified in the experiments in question).

2.9.1 (RT-)RPA

RPA reactions were executed in advance of the LwaCas13a detection assay as step 43-48 including some modifications (36). These modifications are: Samples used as input to RPA were thawed on ice. The RPA reaction mixture was altered; 1,25 µL RNase inhibitor Murine (NEB, 40,000 units/ml) was included per 1 pellet reaction, and 1-2 µL Super Script IV reverse transcriptase (200 U/µL) was also included if RT-RPA was executed. In each experiment, a positive (SARS-CoV-2 isolate or synthetic oligo), and a negative (ultrapure water input/no

target) control was included unless otherwise described. 1-2 µL input of extracted sample or synthetic sequence was added to each reaction. RPA was executed at 37°C in 30 minutes with agitation start after 5 minutes. RT-RPA reactions were incubated at 42°C for 30 minutes with agitation starting 7 minutes into incubation, unless otherwise described. After 15 and 25 minutes of incubation, the samples were flipped 3-4 times, spun down for 2-3 seconds using a minifuge and placed back in the incubator.
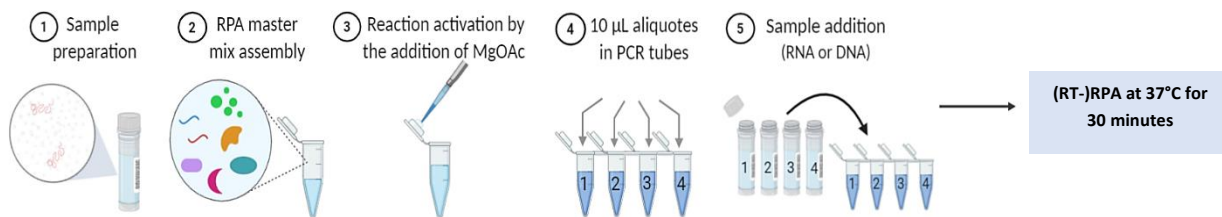
Figure 2.2: Workflow for the RPA reaction setup of clinical samples including: 1, sample preparation; 2, master mix assembly; 3, reaction activation by MgOAc; 4, master mix aliquoting of 10 µL into PCR tubes; 5, sample addition. Made in Biorender (https://biorender.com)/.

2.9.2 Fluorescent based LwaCas13a nucleic acid detection

The single-plex nucleic acid detection assay using LwaCas13a was performed as step 42-52(A) in Kellner et al., (36) with some modifications. These modifications are: the RNase inhibitor Murine (NEB, 40,000 units/ml), and the RNaseAlert Reporter (2 µM, from RNaseAlert Lab Test Kit v2) were excluded from the LwaCas13a master mix. For the various plate formats, the master mix assembly were altered. A water only input was included as negative control to each assay. When a standard, non-treated, black 384 transparent -round bottom well plate (Corning Life Sciences) was used for fluorescent readouts, a 70 µL of master mix were distributed in separate PCR tubes, where a 4 µL (RT-)RPA/water sample input was added. 20 µL of each sample-mix were pipetted as 3 technical replicates. For the use of 1536 well plates, a 31 µL master mix were distributed in separate PCR tubes, where a 2 µL (RT-)RPA/water sample input was added. 8 µL of each sample-mix were pipetted as 4 technical replicates for fluorescent readouts. A black 96 transparent plate with round wells was used on early trial experiments, to see how fluorescent signal was detected by the plate reader machine. A 50 µL master mix was mixed with 3 µL sample input (RNase A or synthetic DNA1) and plated as 50 µL reaction in a single well, unless otherwise described. Fluorescent monitoring was done over 1 hour if not specified in questioned sections.

2.9.3 Sterilization of surfaces, equipment, and surfaces

To prevent amplicon contamination from RPA products, which can result in false positive signals, an additional step was added to the two pot SHERLOCK nucleic acid detection assay, consisting of a careful sterilization on equipment, instruments, and surfaces. First, all surfaces and instruments were soaked for 20 minutes with 3 % chlorine containing sodium hypochlorite, washed with distillated water followed by 70 % ethanol. All pipettes were washed with 70% ethanol and soaked in 3% chlorine solution for 25 minutes. Next, the pipettes were rinsed with distillated water, sprayed with 70% freshly prepared ethanol before drying completely in an incubation cabinet at 60°C. The pipettes were then treated with UV radiation for 30 minutes using a laminar flow hood. All surface areas, instruments and pipettes used for RPA reaction assembly or LwaCas13a reaction was regularly swiped down with 1% bleach, and RNase Away. New buffer stocks were made of the original RPA primer sets.

2.10 Plate reader optimization

To optimize the fluorescent readings of the LwaCas13a reaction, the instrumental settings on the Victor Nivo multimode plate reader needed to be altered. Settings were altered for the use of a black 96-, 384- and 1536 round clear bottom, untreated well plates and 1536 round non-transparent bottom, untreated well plate. Tested parameters include excitation and emission filters and spot sizes, measurement time, z-focus and x,y area scan.

Signal to noise rates were calculated by the following equation:

Equation 1:

$$\frac{Signal}{Noise}\text{ratio} = \frac{\text{Average signal positive control}}{\text{Average background signal}}$$

2.10.1 Excitation and emission alterations

To optimize the fluorescence readings in the collateral cleavage reaction, it is important to adjust the instrument filters so that maximum excitation and emission wavelengths of the RNA reporter. The TEX615 RNA reporter used as cleavable agent in the LwaCas13a reaction have a maximal absorption and emission max at 596 and 615 nm respectively. The initial settings on the instrument was therefore adjusted to 570/10 and 600/10 nm to fit the reporter properties.

The excitation wavelength was further adjusted to 530/30 in this thesis. Different excitation spot sizes were also tried, representing the beam size when using the instrument.

2.10.2 Area scan

To identify highest fluorescent signal in the x,y plane, an end point area(x,y) was done using a 1000x dilution of RNase A (10 mg/µL) as positive control. Reactions were constructed and experiment executed according to section 2.9.2 with minor modifications: crRNA, LwaCas13a and T7-RNA polymerase were excluded from the reaction. The area scan was done after a 15-minute incubation of the reactions at room temperature.

2.10.3 Z-focus scan

To identify optimal fluorescence monitoring, an endpoint z-focus scan for fluorescent intensity was done on black 96, 384, 1536- well plates with transparent or nontransparent bottom. The z-focus scan represents a vertical end point well-scan in millimeter from the plate holder surface. The LwaCas13a reaction was assembled according 2.9.2 using RNase A (10 mg/mL) as positive cleavage agent. For the 1536 plate with non-transparent bottom a positive SARS-CoV-2 sample was used as positive control (U10, Table S8). RT-RPA was conducted as described in section 2.9.1 using RPA primer set orf1ab-original (table S1) with a 1µL sample input amount. orf1ab-crRNA purified with phenol: chloroform was used as guide for LwaCas13a. Since the end point experiment was done with RNaseA, fluorescent intensity measurement was done after 15 minutes incubation at room temperature.

2.10.4 Dichroic mirror changes

To improve separation of excitation and emission wave lengths a dichroic mirror (D590) was introduced to the plate reader and a new z-focus scan was done on black 1536- well plate nontransparent bottom. The D590 dichroic mirror separate wavelengths by reflecting unwanted wavelengths reflected from the specimen (<590 nm), allowing wanted wavelengths to pass through (> 590nm) to the detector. A 2 µL input of positive SARS-CoV-2 sample was used as positive control (U10, Table S8), and SHERLOCK reaction was done according to section 2.9. The orf1ab-new primer set for RT-RPA, and orf1ab-crRNA (nanoparticle purified) was used as

guide for LwaCas13a. The end point z-focus scan was done after 75 minutes of incubation at 37°C in the plate reader.

2.11 LwaCas13a reaction buffer optimization

To optimize the LwaCas13a collateral cleavage assay, several experiments were conducted where we tested different buffers, buffer concentration, pH, and metal ions at various concentrations.

2.11.1 Various buffers and Mg^{2+} concentrations and pH as variables

Buffer conditions in the LwaCas13a nucleic acid detection was optimized to improve sensitivity in the LwaCas13a collateral cleavage assay. The assay was executed according to section 2.9.2, using synthetic DNA 1 PCR product as positive control (final copy number of 1,53E+7 copies /reaction), DNA1crRNA was used as guide for LwaCas13a and a 384 well plate for fluorescence readings. Three different buffers titrated to 9 various pHs (5.5, 6.0, 6.5, 6.8, 7.0, 7.5, 8.0, 8.5, and 9.0) were tested. The three starting points for titrations were 2 M HEPES buffer at pH 7,5, a 2 M MES buffer at pH 6,5, and a 2M TAPS pH 7,7. Titration was done with 5 M NaOH, or 1 M HCl with the use of a pH meter. Finally, buffer solutions were diluted to 1 M and filtered through a 0,22 µm filter. The divalent ion concentration of Mg^{2+} was tested at 2, 6, 9, 12, 18 and 40 mM in the LwaCas13a reaction, added as a 1M, 0,5M or 0,25M stock to fit reaction volumes. The MgCl$_2$ stocks were made by dilution 1M MgCl$_2$ with distillated water and filtered through a 0,22 µm filter. 20 mM and 40 mM MES buffer of pH 6.5 and 20 mM HEPES buffer of pH 7.0 was used as reaction condition for LwaCas13a collateral cleavage assay combined with various Mg^{2+} concentrations. Reactions proceeded for 2 hours.

2.11.2 Changing Ions

Mg^{2+}, K$^+$ and Ca^{2+} metal ions were tested in the LwaCas13a reaction as described in section 2.9.2 to see the effect on enzyme activity. The divalent ion concentration of Mg^{2+}, Ca^{2+} and the monovalent K$^+$ were tested at 9 mM concentrations in combination with 20 mM HEPES pH 7, or 40 mM MES pH 6.5. 0,5 M ion stocks that were made by dilution of a 1-3 M start solutions with distillated water and filtered through a 0,22 µm filter. Synthetic DNA 1 PCR product was positive control (final copy number of 1,53E+7 copies /reaction), DNA1crRNA was used as

guide for LwaCas13a. A black 1536 well plate with transparent bottom was used for fluorescence monitoring.

2.12 Improving T7 RNA transcription

To investigate if T7 transcription of synthetic DNA 1 would increase in the LwaCas13a reaction. different T7 promoters were incorporated into RPA forward primers for synthetic DNA 1. Two new promoter sequences incorporated in the forward primers (24127F, 24128F) were collected from Paul et al., (table 2, named A6, B1 and C15, C62) (101). PCR products of synthetic DNA 1 containing each T7 promoter (table S1) were used as targets for LwaCas13a, with associated DNA1crRNA as guide. The PCR products were diluted 10x times in ultrapure water and added to the reaction with a final of 2,0E+07 copies / reaction. A LwaCas13a reaction was executed according to section 2.9.2, with the use of a 1536-well plate with round transparent bottom. Buffer condition included 20 mM HEPES, pH 7 and 9 mM $MgCl_2$. Fluorescent monitoring was done over 3 hours.

2.13 Two pot SHERLOCK on synthetic targets

SHERLOCK experiments were done on pre amplified PCR products of synthetic DNA 1 and synthetic sequences of SARS-CoV-2_T2 and SARS-CoV-2_T3. The SHERLOCK experiment was done according to section 2.9 with some modifications. A 100 x dilution series of each synthetic template was used as 1 µL inputs to separate RPA reactions with initial copy numbers of E+4, E+2 and E+0(1) per reaction, diluted with nuclease free water. Original RPA primers for *orf1b, orf1ab* and DNA1 was used in separate RPA reaction for respective targets, and associated crRNAs (orf1ab-crRNA, orf1b-crRNA and DNA1crRNA) were used as guides for LwaCas13a, respectively. Two buffers, pH 6.5 (MES) and pH 7.0 (HEPES), was used in the LwaCas13a fluorescent detection reaction for sensitivity optimization on the assay.

The same experiment was then repeated, but the RPA reaction was this time conducted in 5, 10, 15 and 30 minutes on each dilution series to see the amplification effect of the RPA reaction. The LwaCas13a reaction was only done using HEPES pH 7,0 as buffer. No negative RPA control was included in either experiments

2.13.1 Making an empirical background for RPA on synthetic sequences

Because the experiments on synthetic sequences SARS-CoV-2_T1, SARS-CoV-2_T2 and synthetic DNA1 did not include a negative control for the RPA reaction, 16 series with 4 replicates of water inputs to RPA reactions containing orf1ab-original primer set were used to make an average background value to compare with positive samples. The experimental setup for negative controls were conducted the same way as in section 2.9.

2.14 Examination of background signals in the SHERLOCK assay

An optimization of the SHERLOCK assay had to be done, because of high background signal from negative controls. The background signal makes the detection of nucleic acids difficult, as signal from negative and positive samples is harder to separate. For this purpose, SHERLOCK experiments were conducted according to section 2.9, except excluding reaction components from either RPA or LwaCas13a nucleic acid detection reaction. Original primers for *orf1b*, *orf1ab* and DNA1-primers were variously used in the experiments. A SARS-CoV-2 RNA extract was used as positive control (various start concentrations 8,5E+03 to E+06 copies/reaction) using 1µL as input. Synthetic DNA 1 PCR product was used as negative control input to RPA reaction with primers for *orf1ab*, added at 1,53E+05 or 1,53E+06 copies /reaction. A black 1536 well plate with round, transparent bottom was used for fluorescent monitoring over 1-3 hours. crRNAs used in these assays were purified with phenol: chloroform.

2.14.1 LwaCas13a nucleic acid detection reaction without crRNA

Because of unspecific fluorescent signal in the LwaCas13a reaction, orf1ab- and orf1b-crRNA and synthetic DNA 1 was removed, as these components are required for collateral cleavage of the RNA reporter. A RNase inhibitor was also added to a LwaCas13a reaction to exclude RNase activity. Associated crRNA orf1ab-crRNA, orf1b-crRNA and DNA 1-crRNA and/or RNase inhibitor was excluded from the reaction to respective targets.

2.14.2 SHERLOCK on negative RPA controls

To investigate the unspecific fluorescent signal, a SHERLOCK experiment was conducted using RPA reaction excluding one or more RPA reaction components. Reverse transcriptase, reverse and/or forward original RPA primers for *orf1ab* and RPA mix was excluded. Orf1ab-crRNA (Table S2) was used as guide for LwaCas13a to target *orf1ab*.

2.14.3 SHERLOCK with negative Cas13 reactions

To investigate the LwaCas13a reaction kinetics generating unspecific fluorescent signal, a SHERLOCK experiment was conducted with LwaCas13a reactions excluding one or more reaction component (crRNA, LwaCas13a, T7-RNA polymerase, RNA reporter, Target). Orf1ab-crRNA was used as guide for LwaCas13a (Table S2) to target *orf1ab*.

2.14.4 Water only input to RPA reaction

It was investigated whether the background noise would vary in negative water only controls in the LwaCas13a reaction before and after the strict surface sterilization. Two SHERLOCK experiments were done on 4 series (m=4) of water as 2µL inputs to RT-RPA using the original water source and then a new water source. RPA primer set orf1ab-original was used in the RPA reaction (table S1). The SHERLOCK experiment was done according to section 2.9, using a black 1536 well plate with round transparent bottom. Orf1ab-crRNA was used as guide for LwaCas13a (Table S2).

2.15   (RT-)RPA optimization

In search of higher assay sensitivity, the RPA reaction was optimized. This was done by testing RPA primer combinations for *orf1ab,* RPA reaction time and reverse transcriptase concentration in separate experiments. Up to 8 clinical SARS-CoV-2 samples were tested in each assay (Table S10) including a positive SARS-CoV-2 sample as positive control (Table S8, U1). One additional negative control sample (N2, Table S10) with no SARS-CoV-2 viral load and synthetic DNA1 were included as negative RT-RPA controls. orf1ab-crRNA purified with nanoparticles was used as guide for LwaCas13a, and a black 1536 well plate with non-transparent bottom was used for fluorescent readings. In the first experiment, combinations of the original and new primers for *orf1ab* in SARS-CoV-2 were used to target *orf1ab* in clinical

SARS-CoV-2 samples. In the second experiment, RT-RPA was executed in 30 and 60 minutes. In the third experiment, variable concentrations of Superscript IV reverse transcriptase were used: 2,0 µL, 1,3 µL, 1,0 µL or 0,67 µL /RPA pellet in the RT-RPA reaction. The three experiments were conducted according to section 2.9, using a 2 µL sample input to RT-RPA. In the two last experiments orf1ab primers (24138F, 24276R, Table S1), now referred to as orf1ab-combo was used in RT-RPA.

2.16 Optimization of primers and targets for SHERLOCK detection of SARS-CoV-2

It was investigated if an optimal primer combination and target sequence could increase SHERLOCK assay sensitivity. Therefore, several SHERLOCK experiments were conducted, in accordance with section 2.9 targeting SARS-CoV-2 *orf1ab* and two new target areas MSA_T1 and MSA_T2 (section 2.15.2) in the SARS-CoV-2 genome. A 2 µL sample input was used for RT-RPA. All assays described below were executed with 1 µL /pellet reverse transcriptase in RT-RPA reactions. In each SHERLOCK experiment, one additional negative control sample, with no SARS-CoV-2 viral load were included as negative RT-RPA control (Table S10, N2). Further, 3-5 positive SARS-CoV-2 samples were used (Table S10) in each experiment. A black 1536 plate with round black wells was used for fluorescence monitoring. Various primers, crRNAs and targets tested in each assay are specified in sections below and crRNAs were purified with magnetic particles.

2.16.1 SHERLOCK on new SARS-CoV-2 targets

In search of higher assay sensitivity, the detection of two new target areas in SARS-CoV-2, MSA_T1 and MSA_T2, along with *orf1ab* were tried on clinical SARS-CoV-2 samples. RPA orf1ab-combo primer set, MSA_T1 and MSA_T2 primer set to amplify RNA. It was then investigated if pre-synthesized crRNAs provided higher assay sensitivity than manually *in vitro* transcribed crRNAs. orf1ab-crRNA (nanoparticle purified), and pre synthesized crRNAs: orf1ab-2crRNA, MSA_T1crRNA and MSA_T2crRNA (Table S2) were used as guides for LwaCas13a respectively to each target.

2.16.2 Primer screen on *orf1ab*, MSA_T1 and MSA_T2

To improving RT-RPA reaction rate and reduce primer noise, primer screens were done to increase SHERLOCK assay sensitivity. Each primer screen involves two SHERLOCK experiments where combinations of primers are tested in RT-RPA. Several primers were tested in each screen to target SARS-CoV-2 *orf1ab*, MSA_T1 and MSA_T2 in clinical SARS-CoV-2 samples specified further in each section below. orf1ab2-, MSA_T1- and MSA_T2-crRNAs were used as guides for LwaCas13a to sense each target, respectively.

Experiment 1: Primary primer screen SARS-CoV-2 *orf1ab*
Six forward and reverse RPA primers were used in the primary screen, partly overlapping each other in sequence (Figure ST4, Table S3). First, the forward primer giving the shortest amplicon was screened against all reverse primers. The resulting most sensitive reverse primer was further screened against all forward primers to give the most sensitive primer pair. To see if increased sensitivity was reached, the samples used as targets had increasing Ct values (20,68, 30,34 and 34,79, 35,59 and 37,58).

Experiment 2: Secondary primer screen SARS-CoV-2 *orf1ab*
To find even more sensitive primers for targeting *orf1ab*, four forward and reverse RPA primers were used in the secondary screen, differing only by 1-2 bases in sequence (Table S4, Figure TS4). The F3 and F4 forward primers and R3 reverse primers were used as basis for the secondary primer design. First, the forward primer resulting in the shortest amplicon was screened against all reverse primers. Then, the reverse primer with highest sensitivity was screened against all forward primers. To see if increased sensitivity was reached, the samples used as targets had increasing Ct values (20,68, 28,28, and 32,83). Only the last screen included a negative SARS-CoV-2 sample (N2, Table S10).

Experiment 3: Primary primer screen SARS-CoV-2 MSA_T1 and MSA_T2
Five forward and reverse RPA primers were used in each primary primer screen to target MSA_T1 (Table S5, Figure TS5) and MSA_T2 (Table S6, Figure TS6). The screen was done as experiment 1 described in the section above for "Primary primer screen of SARS-CoV-2 *orf1ab*". Only exception was that four new SARS-CoV-2 samples with increasing Ct values were tested (Table S11).

PART III SHERLOCK on clinical SARS-CoV-2 samples

2.17 Trial SHERLOCK on one SARS-CoV-2 RNA extract

To investigate if SHERLOCK was able to detect viral SARS-CoV-2, RNA extracted from a clinical SARS-CoV-2 sample was used in a SHERLOCK experiment targeting *orf1b* and *orf1ab*. DNA 1 PCR product was included as positive control. The SHERLOCK experiment was done according to section 2.9. A 1 µL sample inputs with initial copy numbers of E+4, E+2 and E+0, diluted with nuclease free water of each target was included. Original primers for *orf1b, orf1ab* and DNA1-primers were used in RT-RPA. Reaction buffer with pH 7.0 (HEPES) was used with associated crRNAs (orf1ab-crRNA, orf1b-crRNA and DNA1crRNA) purified with phenol: chloroform as guide for LwaCas13a. A black 1536 well plate with round, transparent bottom was used for fluorescent monitoring. LwaCas13a reaction was done over 3 hours.

2.18 SHERLOCK on several SARS-CoV-2 samples

The SHERLOCK platform's sensitivity and specificity was investigated, where several clinical SARS-CoV-2 samples was tested in various SHERLOCK experiments. All SHERLOCK experiments were done according to section 2.9, using 2 µL sample inputs targeting *orf1ab* in SARS-CoV-2. A black 1536 well plate with round, transparent bottom was used for fluorescent readouts. orf1ab-crRNA purified with nanoparticles was used as guide for LwaCas13a (Table S2).

2.18.1 SHERLOCK blind test on clinical SARS-CoV-2 samples

Four clinical SARS-CoV-2 samples and one positive SARS-CoV-2 control (Table S7) to see if the SHERLOCK platform could identify positive SARS-CoV-2 samples. The RPA original and new primer sets for *orf1ab* were used in RT-RPA separately (Table S1).

2.18.2 SHERLOCK on ten positive SARS-CoV-2 samples

To investigate signal intensity from positive SARS-CoV-2 samples, ten positive clinical SARS-CoV-2 samples (Table S8) were tested in a SHERLOCK experiment. The original RPA primer set for *orf1ab* was used in RT-RPA.

PART IV Final validation of the SHERLOCK platform

2.19 Validation of the SHERLOCK platform

The SHERLOCK sensitivity and specificity was validated by testing negative and positive SARS-CoV-2 samples in two separate SHERLOCK experiments, executed according to section 2.9. 2 µL sample inputs were used in RT-RPA reactions including the new primers for targeting *orf1ab.* Negative controls with no viral load (Table S10, N1-N3) was included as negative inputs to RT-RPA besides ultrapure water. In each LwaCas13a reaction, orf1ab-crRNA purified with nanoparticles was used as guide for LwaCas13a. The D590 dichroic mirror was used for all fluorescence readouts. Final optical parameters included excitation and emission spot sizes, 1.0/2.0 mm; Z-focus, 7,1 mm; measurement time/direction, 250 ms/top; dichroic mirror, D590; excitation/emission filter, 530/30 and 600/10 nm

To test specificity in the SHERLOCK platform, 19 samples containing viral load besides SARS-CoV-2 were tested (Table S9). A Positive SARS-CoV-2 sample (U1, Table S10) was used as positive control for indication of a successful detection of the SARS-CoV-2 *orf1ab* gene. To test platform sensitivity, a SHERLOCK experiment was done on 72 positive clinical SARS-CoV-2 samples targeting *orf1ab* in SARS-CoV-2.

3 Results

PART I Preparing SHERLOCK components

3.1 LwaCas13a expression and purification

LwaCas13a purity is particularly important for achieving specificity and preventing non-specific cleavage of the quenched-RNA reporter. The LwaCas13a protein was expressed and purified as described in section 2.3. The SDS-PAGE® analysis of the eluted protein fractions revealed a band between 100-150 kilo Dalton (kDa) corresponding to the expected size of LwaCas13a at 138,5 kDa (Figure S2A). The protein was further purified by cation exchange chromatography, using an Äkta explorer protein purification system (Figure S2B) to separate LwaCas13a from potential nucleases and SUMO proteases. An SDS-PAGE® analysis of the seven most concentrated protein fractions revealed exclusively an expected band size between 100 and 150 kDa (Figure S2C), indicating successful protein purification.

3.1.1 Nuclease activity test

To ensure optimal sensitivity and specificity in the SHERLOCK assay the purity of LwaCas13a must be high, as contaminants such as nucleases could result in false positive signals. To verify the absence of nuclease activity in the purified LwaCas13a fractions from FPLC, a nuclease test was conducted using an RNA construct as cleavable target (section 2.3.4). The resulting products were analyzed by SDS-PAGE ® revealing no significant nuclease activity in reactions with the purified LwaCas13a protein (Figure S3).

3.2 SHERLOCK crRNA design and preparation

crRNAs are used in SHERLOCK to guide the LwaCas13a protein to a target RNA sequence complementary to the crRNA spacer sequence and thereby induce a "detection" signal. In this thesis, the crRNAs were in vitro transcribed and purified with both nanoparticles and chloroform extraction to compare yield between the methods. A Tape Station analysis of the purified *in vitro* transcribed RNA products revealed bands corresponding to the 64 nt expected size of the crRNAs (Figure S4). Bands representing same products showed almost identical yield (band intensity) independent of purification method (Figure S4A). However, a sample intensity graph showing the *in vitro* transcribed product of orf1ab-crRNA purified with phenol:

chloroform reveals a peak at 72 nt (Figure S4B). Magnetic nano-particle purification of crRNAs was thus chosen as the purification technique for final SHERLOCK assays.

3.3 Preparing synthetic targets for SHERLOCK

To verify SHERLOCK assay design and run trial LwaCas13a nucleic acid detection for fluorescent reaction optimization, synthetic targets of DNA 1 and SARS-CoV-2 (T2 and T3) were used. A PCR was prepared for each synthetic target using RPA primers to generate a double stranded template for T7 transcription in the LwaCas13a reaction. An SDS-PAGE® confirmed the sizes of PCR amplicons (100-150 bp) corresponded to the length of the expected PCR products (Figure S5A-C). The synthetic targets were therefore subsequently isolated, normalized and stored for use in the SHERLOCK assay.

PART II ASSAY OPTIMIZATION

3.4 Trial experiments excluding RPA from SHERLOCK

Several preliminary optimization experiments for fluorescent measurements were done using LwaCas13a combined with positive (synthetic DNA 1 dilutions or RNaseA) and negative controls in 96- and 384 well plates (section 2.8). The optimization tests showed that sufficient fluorescent signal was achieved with the 384 well plate type (Figure S6) and that the signal increased with incubation time up to two hours (Figure S6C). The 96 well plate only exhibited signal when using RNaseA and resulted in evaporization of the reactions after two hours (Figure S6A-B).

3.5 Optimization of optical parameter in the plate reader

For a final optimization of fluorescent signal sensitivity and to test for possible effects of plate types, a comprehensive parameter optimization was done using the plate reader for each plate format (96, 384, 1536 wells) (section 2.10).

The parameter optimizations included area scans (for 96 and 384 well plates) to find optimal x and y coordinates for maximal fluorescence signal and z-focus scans to identify highest signal-to-noise (S/N) ratio for all plate types. The Area scan showed that the optimal area coordinates

for maximal fluorescence is approximately (0,0) for both 96 and 384 well plates (Figure S7). This setting was therefore further used in all subsequent assays, also for 1536 well plates. Optimal z-focus (i.e. highest S/N ratio) was different for each pate type (Figure 3.1, Figure S8). Next, signal: noise ratios differed substantially between the plate types with the ranking 96 < 384 < 1536 (Figure 3.1). Furthermore, lowering of the excitation filter to 530/30, changing to larger spot sizes, switching to black colored well bottoms, and using a 590 dichroic mirror increased sensitivity of fluorescent readings (Figure S8A-H). The results show that optimal fluorescent reading sensitivity is highly dependent on the optical settings on the plate reader and the plate format (Figure 3.1). Highest S/N ratio and fluorescence signal were obtained when using the black 1536-well plate with colored bottom, combined with a 590 dichroic mirror (Figure 3.1). These settings were therefore used in the final experiments.

Number of wells	96	96	384	384	1536	1536	1536	1536
Transparent well bottom	Yes	Yes	Yes	Yes	Yes	Yes	No	No
Ex/Em Spot Size (mm)	0.5/1.0	0.5/1.0	0.5/1.0	1.0/2.0	0.5/1.0	1.0/2.0	1.0/2.0	1.0/2.0
Z-Focus (mm)	8,9	7,1	5,3	7,1	8,6	7,2	6,9	7,1
Measuement time (ms)	500	500	250	250	250	250	250	250
Dichroic mirror	General (50/50)	General (50/50)	General (50/50)	General (50/50)	General (50/50)	General (50/50)	General (50/50)	D590
Excitation filter (nm)	570/10	530/30	530/30	530/30	530/30	530/30	530/30	530/30

Figure 3.1: A comparison of maximum signal to noise ratios using different types of black plates; 96, 384, 1536 (transparent and nontransparent) wells, and optical parameters on the VICTOR Nivo Multimode plate reader, for fluorescent intensity readings. Maximal average signal to background noise ratio (columns) for each condition are plotted against average background subtracted fluorescence (line) resulting from the same settings. Optical parameters include excitation and emission spot sizes (mm) termed "Ex/Em Spot Size", Z-focus (mm), measurement time (ms), dichroic mirror and excitation filter (nm). Other constant parameters were: emission filter, 600/10 nm, area (x,y) focus, (0,0), and a top measurement. RNase A (0,6 ng/µL) was used as positive control for the Z-focus scan on the transparent 96, 384 and 1536 well plates. RT-RPA product of SARS-CoV-2 *orf1ab* using orf1ab-new primer set on a positive SARS-CoV-2 sample (U 10, Table S8) was used as positive control with orf1ab-crRNA for the 1536-well plate with non-transparent, round bottom, and RNase A (0,6 ng/µL) was used as positive control for the 96- and 384- and 1536 well plates with transparent, round bottom. n=3 (n=1 of the 96 well plates)

3.6 LwaCas13a reaction buffer optimization

To optimize enzyme activity and thereby increase assay sensitivity, LwaCas13a buffer optimization experiments were conducted (section 2.11). Various $MgCl_2$ concentrations in combination with buffers, buffer concentration and pH were tested. Keeping in mind that normal cytoplasmic pH conditions in bacterial cells varies around 7.0 (102), we assessed different pH ranging from 5,5-9. The resulting LwaCas13a enzyme kinetics revealed an inhibition of enzyme activity when using a pH below 6.0 and above 7.5 (Figure S9, Figure 3.2A). LwaCas13a was most active around pH 6,5-7,5 in 20 mM HEPES or 40 mM MES using 6-12 mM salt (Figure 3.2A). Highest fluorescent signal after 30 and 60 minutes of LwaCas13a reaction was obtained using 40 mM MES pH 6,5 with 9 mM Mg^{2+} (Figure 3.2A).

We hypothesized that LwaCas13a function could be impacted by varying metal ion concentration in the reactions, based on previous studies of Cas13b orthologues by Gootenberg et al., (42). We thus replaced Mg^{2+} with the divalent Ca^{2+} ion or the monovalent K^+ ion at 9 mM concentration and assessed enzyme activity in the collateral reactions. Results reveals that LwaCas13a prefers Mg^{2+} as reaction stabilizer for collateral cleavage and that the strongest signal is obtained using 40 mM MES pH 6.5 as combined (Figure 3.2B). No signal was detected with either K^+ or Ca^{2+} in the reaction buffer (Figure 3.2B). Based on these findings, a 40 mM MES buffer with pH 6.5 and a 20 mM HEPES buffer at pH 7.0 was further used in subsequent assays including 9 mM $MgCl_2$.
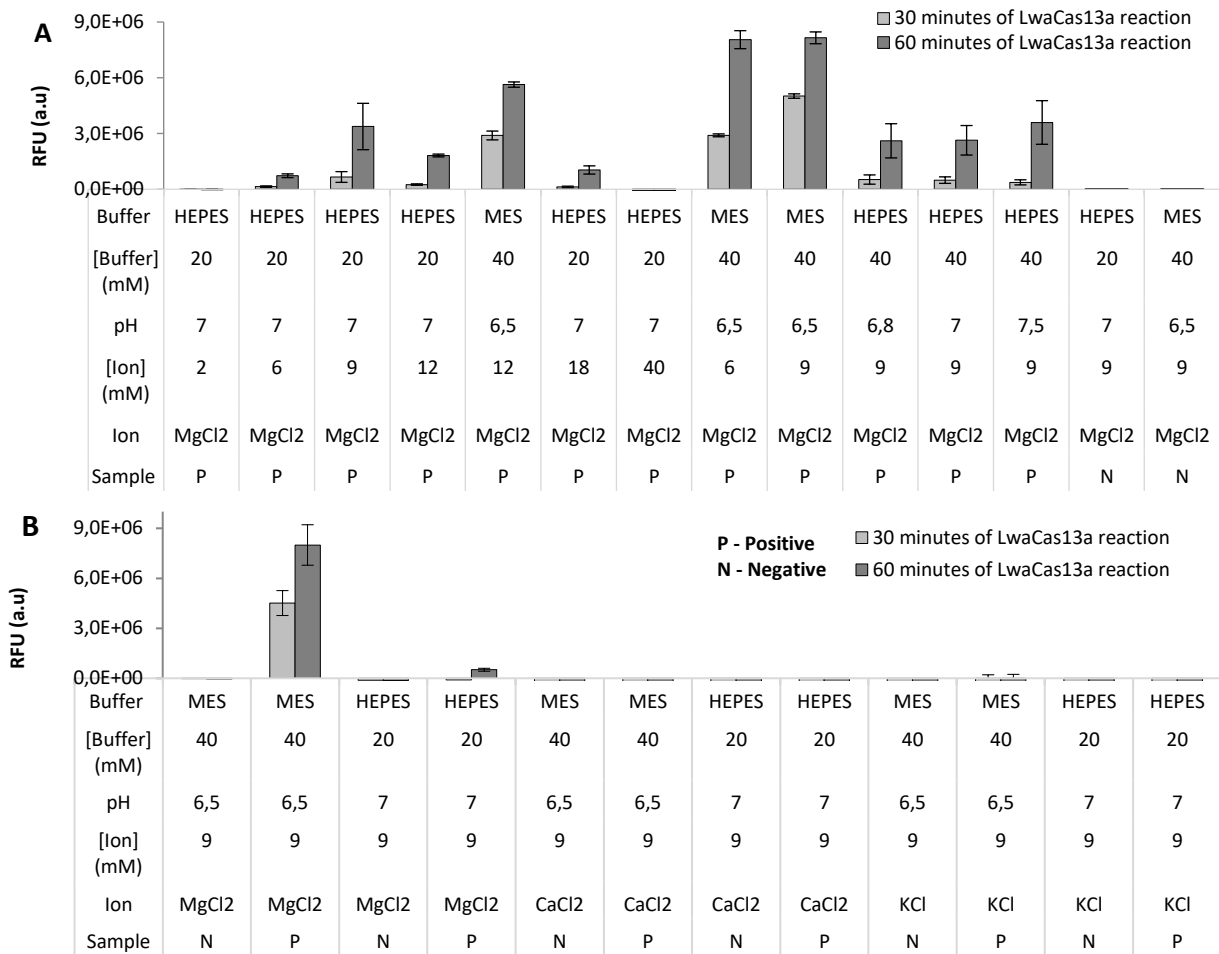
Figure 3.2: LwaCas13a reaction buffer optimization. Average fluorescent signal in RFU ± SD after 30 (light) and 60 minutes (dark) of LwaCas13a collateral cleavage reaction. Synthetic DNA 1 PCR product using DNA1-primers was used as positive control (**P**), added to the reaction at a final concentration of 2,0E+07 copies/reaction and DNA1-crRNA was used as guide for LwaCas13a. (**A**) Using HEPES or MES buffer at various concentrations and pH combined with several ion concentrations of Mg^{2+}. A black 384-well plate with round transparent bottom was used for fluorescent readouts. Two negative controls (**N**) include a water only input to LwaCas13a reaction using 20 mM HEPES pH 7,0 and 20 mM MES pH 6,5 with 9 mM MgCl2. (**B**) 20mM HEPES pH 7,0 or MES pH 6,5 combined with Mg2+, K+ or Ca2+ metal ions as LwaCas13a reaction buffer. A black 1536-well plate with round transparent bottom was used for fluorescent readouts. A water only input to Cas13a reaction was included for each buffer condition (**N**). n=3.

3.7   Improving T7 RNA transcription

A main factor that can influence SHERLOCK assay sensitivity is the T7 RNA transcription which takes place in the LwaCas13a reaction to convert amplicons from RPA to RNA available for LwaCas13a. We hypothesized that an optimized T7-promoter could enhance T7-transcription and thereby increase LwaCas13a sensitivity. Two T7 promoter sequences were tested as alternative T7 promoter overhang in the forward primer to DNA1 (Figure 3.3A) in SHERLOCK (section 2.12) (101). Our results revealed no sign of fluorescent signal from

41

reactions with mutant T7 promoters (Figure 3.3B) and proceed with using the original T7 promoter in following experiments.
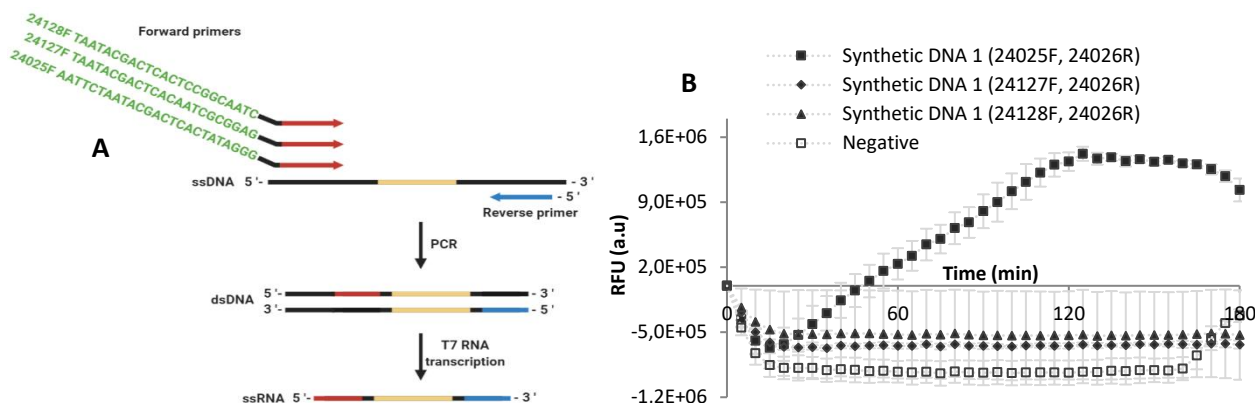
Figure 3.3 Optimization of T7 transcription. **(A)** Flow illustration of the three T7 promoters (green) used to create PCR products of synthetic DNA 1 for subsequent T7 RNA transcription to make RNA template for the LwaCas13a. 24127 and 24128 T7 promoters taken from Table 2, Paul *et al*., patent under W02014013067A1 (101). **(B)** Reaction kinetics of LwaCas13a collateral cleavage in relative fluorescence units (RFU) as means ± SD over three hours targeting three different PCR products of synthetic DNA 1 differing in T7 promoter sequence. A black 1536-well plate with round transparent bottom was used for fluorescent readouts. Synthetic DNA 1 PCR product was used as positive control, added to the reaction at a final concentration of 2,0E+07 copies/reaction and DNA1-crRNA was used as guide for LwaCas13a. A water only input to LwaCas13a reaction was used as negative control. n=3

3.8 Two pot SHERLOCK on synthetic targets

Before testing SHERLOCK on clinical samples, we performed an assay validation on synthetic sequences of SARS-CoV-2 (_T2 and _T3) and synthetic DNA 1 PCR products (section 2.13). The SHERLOCK assay was performed using a dilution series of target sequences with two promising buffer condition, HEPES at pH 7.0 and MES at pH 6.5 (section 3.6, Figure 3.2A and Figure S9). Except for one target sequence dilution (T2_4), all reactions produced much stronger signal compared to the background signal (black graphs) from the RPA reaction (black line), as shown in figure 3.4. There was also no signal from negative LwaCas13a water input as expected (Figure 3.4). Results also reveals a slightly more rapid activation enzyme activity using pH 7.0, but that a MES buffer with pH 6.5 enhances the LwaCas13a enzyme activity gradually with a higher resulting fluorescent signal after 60 minutes (Figure 3.4). Based on these findings, the HEPES buffer at pH 7.0 was used in further SHERLOCK assays, since this condition showed faster collateral cleavage activity.
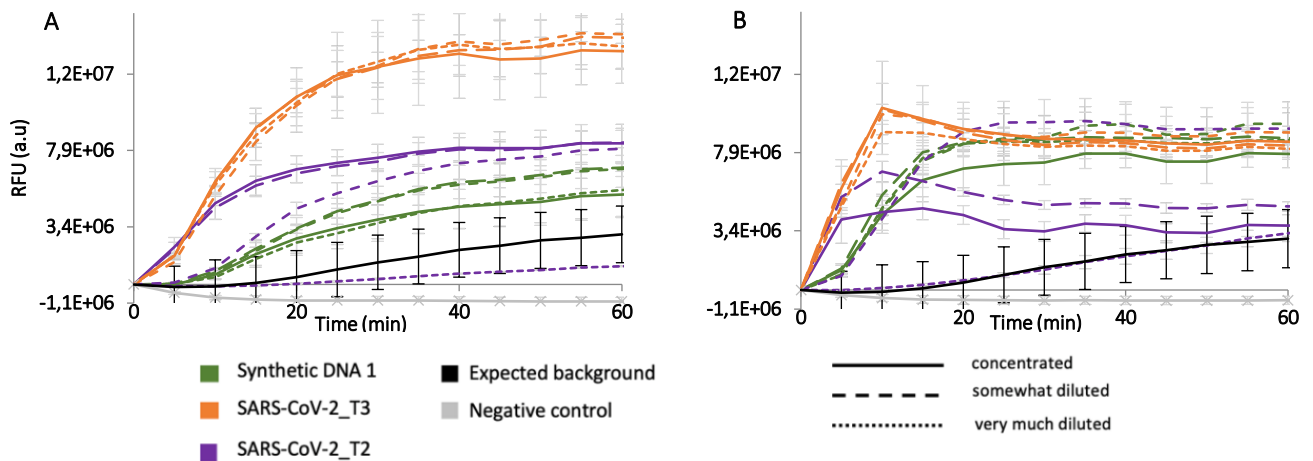
Figure 3.4: SHERLOCK detection of synthetic sequences. SHERLOCK reaction kinetics with relative fluorescent signal in means ± SD of LwaCas13a collateral cleavage over one hour targeting three RPA products; synthetic DNA 1 PCR product using DNA1-primer set, SARS-CoV-2_T2 PCR product using orf1b-original primer set and SARS-CoV-2_T3 PCR product using orf1ab-original primer set for RPA executed in 30 minutes. For each target, a 100x dilution series were made using nuclease free water to give 1,0E+04 (concentrated), 1,0E+02 (somewhat diluted) and 1 (very much diluted) copies / reaction. Either **(A)** 40 mM MES pH 6,5 or **(B)** 20 mM HEPES pH 7,0 was used in the LwaCas13a reaction buffer. A black 1536-well plate with round transparent bottom was used for fluorescent readouts. Associated DNA1-crRNA, orf1ab-crRNA and orf1b-crRNA was used as guide for LwaCas13a targeting each RPA product, respectively. A negative water only input to LwaCas13a reaction was used as negative control. n=3

To investigate the impact of RPA reaction time on SHERLOCK assay sensitivity, the same dilution series (Figure 3.4) were tested in a new SHERLOCK experiment with various RPA incubation times using pH 7.0 in the LwaCas13a reaction. Results revealed no clear effect of increasing RPA time on assay sensitivity. After only 5 to 10 minutes of RPA reaction, a maximal amplification is achieved (Figure S10). Because the SHERLOCK method is still staged under optimization, we chose to perform the RPA reaction for 30 minutes to ensure maximum amplification.

3.9 Examination of background signals in the SHERLOCK assay

The SHERLOCK assay is based on an enzymatic cleavage reaction driven by LwaCas13a when in complex with its associated crRNA in the presence of a target sequence. However, other types of enzymes, such as RNases, can putatively induce similar cleavage reactions and thus elevate the assay background signal which reduces assay sensitivity. To test for RNase activity interactions with our SHERLOCK assay, three separate SHERLOCK experiments were conducted (section 2.14) by investigating if the fluorescence signal was independent of: (i) the

presence of crRNA, target and RNase inhibitor, (ii) RPA reaction components (i.e. primers, reverse transcriptase) and (iii) LwaCas13a reaction components.

Figure 3.5A reveals that fluorescence signal in positive controls (Target is present) are dependent on the presence of crRNA. The addition of RNase inhibitor significantly lowers the fluorescence signal in the orf1b-target, but not completely (Figure 3.5A). However, a fluorescence signal is detected in the negative control containing orf1ab-crRNA but no target or RNase inhibitor (Figure 3.5A). The LwaCas13a kinetics show that the highest sensitivity is displayed after 5-20 minutes but that the sensitivity becomes engulfed by background noise over time (Figure S11). This led to a signal decrease in the positive orf1ab target and DNA 1, while orf1b shows a slight increased signal over time (Figure S11). Figure 3.5B shows that all RPA reaction components including target must be present to generate strong fluorescence signal. Further, a lower fluorescence signal was detected in three negative controls, including the reaction with no RPA (Figure 3.5B), thus independent of some RPA reaction components. Figure 3.5C show the same trend as in figure 3.5A, where a fluorescence signal is generated in the presence of all LwaCas13a reaction components, without the target present. Because of the observed signals in negative controls, we chose to further investigate what caused the background signals.
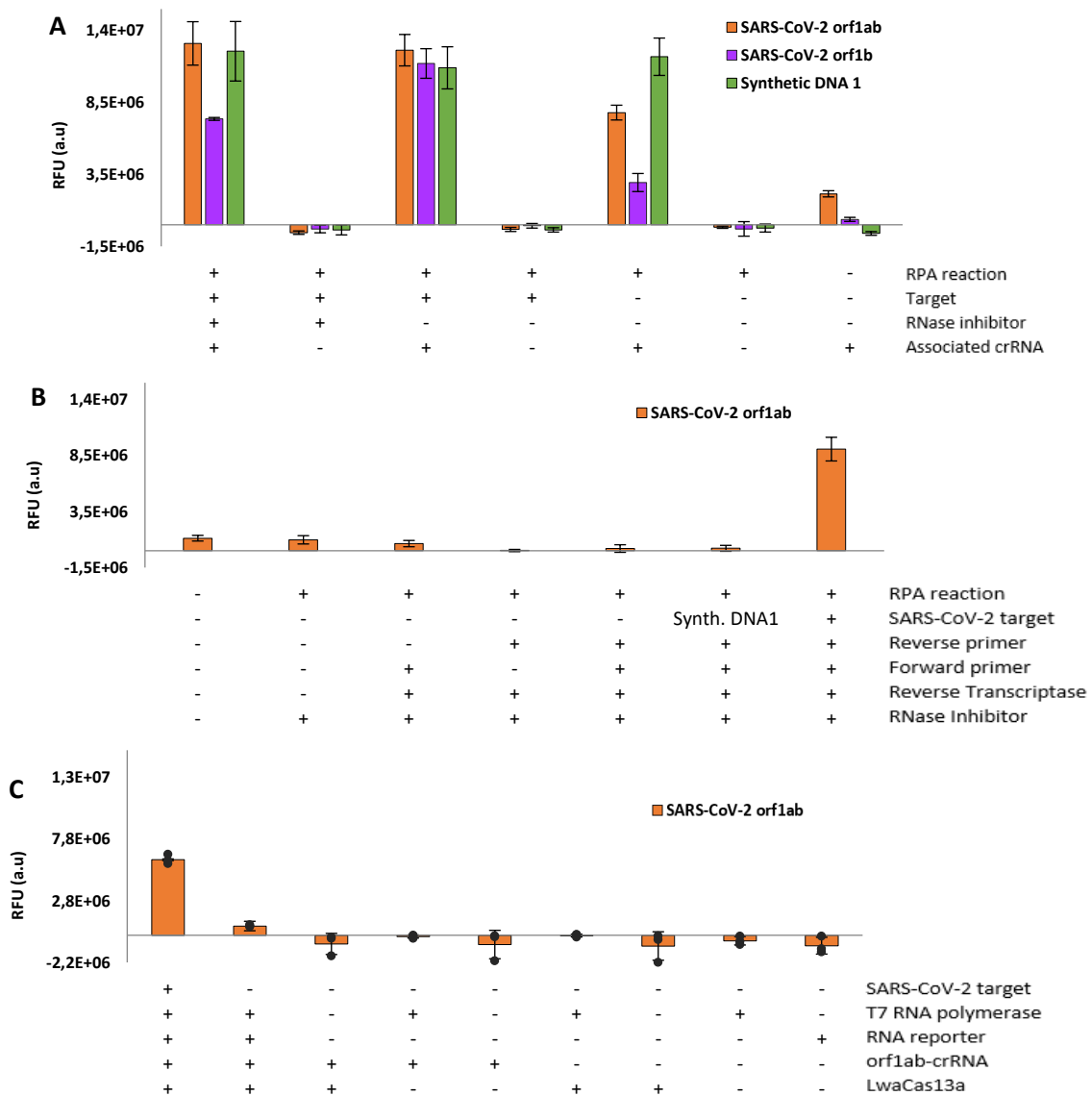
Figure 3.5: Investigation of SHERLOCK background. Three separate SHERLCOK experiments to examine the origins of background signals, where RT-RPA and LwaCas13a collateral cleavage reaction were executed for 30 and 60 minutes, respectively. Relative fluorescence units (RFU) are represented as means ± SD. **(A)** A SHERLOCK on a SARS-CoV-2 extract (8,5E+06 copies/RT-RPA reaction, targeting *orf1b* and *orf1ab,* and synthetic DNA 1 (1,53E+06 copies/reaction, Synth.DNA1). Targets, associated crRNA, or RNase inhibitor were excluded **(-)** or included **(+)** in the LwaCas13a reaction. **(B)** A SHERLOCK on a SARS-CoV-2 extract (8,5E+05 copies/RT-RPA reaction, targeting *orf1ab*. RT-RPA reactions were executed in the presence **(+)** or absence **(-)** of various RPA reaction components. A water only input and synthetic DNA 1 (1,53E+05 copies/reaction) were included as negative RT-RPA controls. **(C)** A SHERLOCK on a SARS-CoV-2 extract (8,5E+03 copies/RT-RPA reaction, targeting *orf1ab*. LwaCas13a reactions were executed in the presence **(+)** or absence **(-)** of various LwaCas13a reaction components. Orf1ab-original, orf1b-original, and DNA1-primers primer sets were used respectively for each target in the RT-RPA reaction. A black 1536-well plate with round transparent bottom was used for fluorescent readouts. Associated DNA1-crRNA, orf1b-crRNA and orf1ab-crRNA was used as guide for LwaCas13a with each RPA product, respectively. Each replicate is noted in the graph (black dot).

3.9.1 Examination of water source

A common problem causing false positive signal is contamination from reagents, surfaces, equipment, or when working with an initially high copy number of a target. Since we observed fluorescence signals from negative controls, we hypothesized that contamination could have caused this. A careful decontamination process was executed as described in section 2.9.3. To investigate if the water source was contaminated, two SHERLOCK experiments were executed using negative controls with water as input to RPA, one (i) before decontamination of equipment and surfaces using the original water source, and one (ii) after decontamination using a new water source (section 2.14.4). Figure 3.6 reveals that a detectable fluorescent signal is generated using both water sources. To minimize the probability of contamination in further assays a careful decontamination procedure was done prior to SHERLOCK assays.
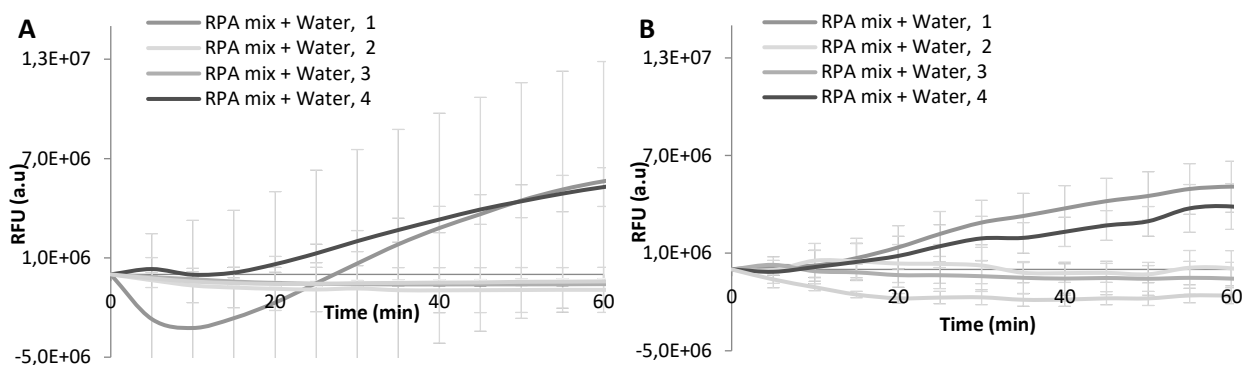
Figure 3.6 Testing Water source in SHERLOCK. Two separate SHERLOCK experiment on four series of water only input to RPA including orf1ab-original primer set. LwaCas13a reaction kinetics is shown in relative fluorescent represented as means ± SD, n=3. The original water source **(A)** and a new water source **(B)** was tested to investigate whether the original water source was the cause of false positive signal in SHERLOCK. A negative water only input to LwaCas13a reaction is included in each experiment.

3.10 Optimizing (RT-)RPA

A key component to the high sensitivity of the SHERLOCK platform is the isothermal RPA amplification step performed prior to LwaCas13a detection. One hypothesis was therefore that an improvement in the RT-RPA response may give an increasing sensitivity to the detection of SARS-CoV-2. Three individual two-pot SHERLOCK experiments were executed (section 2.15) where we investigated three factors that can improve RPA reaction and, thus detection

sensitivity of SARS-CoV-2; (i) primer combination (ii) RT-RPA reaction time and (iii) reverse transcriptase concentration.

The first experiment (i) revealed that a new primer combination (24138F-24276R) resulted in a higher assay sensitivity giving a significant signal from the SARS-CoV-2 sample with Ct-value=35,59 (Figure 3.7A). Samples with lower Ct-values however were not detectable using the same pair (Figure 3.7A). All primer pairs detected the positive control and the SARS-CoV-2 samples of Ct-values < 25, while the negative controls gave no significant signals from either pair (Figure 3.7A). We decided to use primer combination of 24138F and 24276R, termed orf1ab-combo primer pair, in further optimization of the RT-RPA.

Results from (ii) show that RT-RPA reaction is not more effective when samples are incubated in 60 minutes, and that the LwaCas13a collateral signal was lower when RT-RPA time increases (Figure 3.7B). Notably, figure 3.7B shows no detectable signal from the SARS-CoV-2 sample with Ct-value=35,59 as previously observed (Figure 3.7A).

Results from (iii) illustrated in figure 3.7C reveal that the SARS-CoV-2 detection in most sensitive when using 1,33 µL and 1 µL of reverse transcriptase / pellet. These concentrations provided a significantly detectable signal in the SARS-CoV-2 sample of a Ct= 35,59 and 37,58, respectively (Figure 3.7C). In further experiments, it was therefore decided that 1 µL reverse transcriptase should be used per RT-RPA reaction pellet.
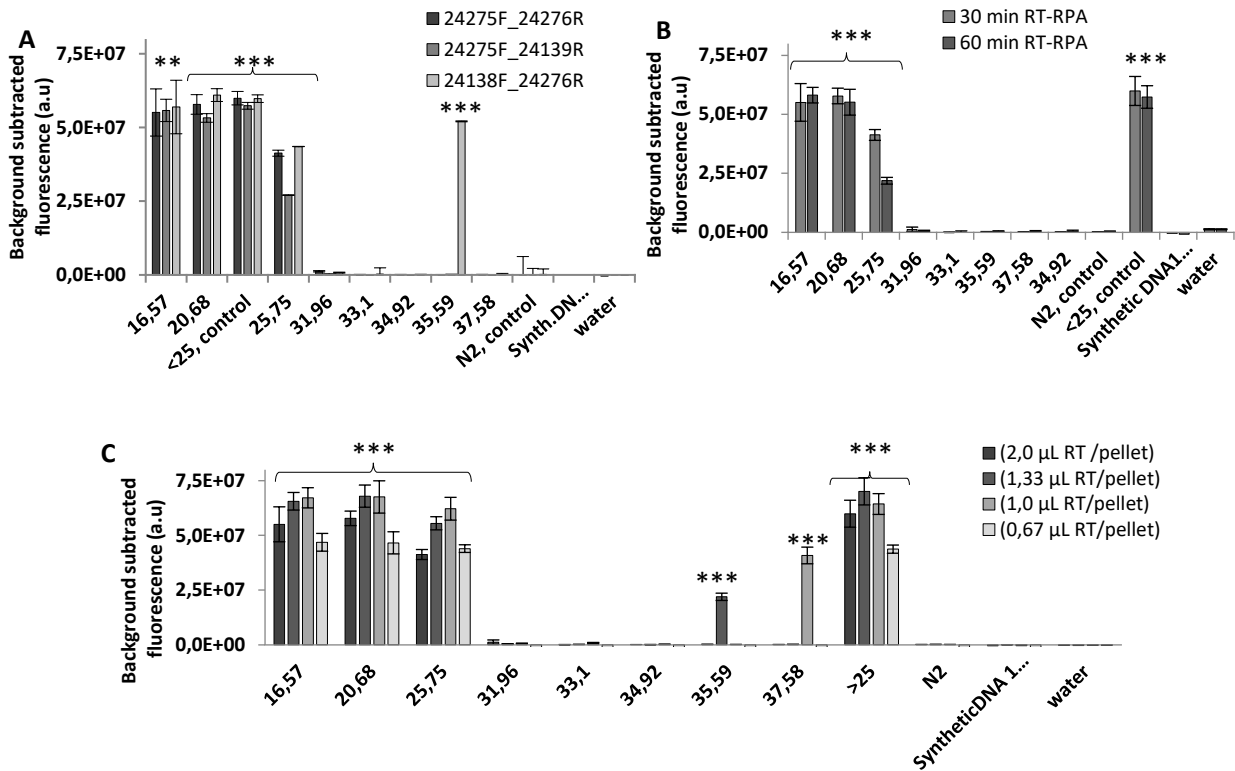
Figure 3.7: Optimizing RT-RPA reaction in SHERLOCK, using 8 positive SARS-CoV-2 samples. Three individual two-pot SHERLOCK experiments on 8 positive SARS-CoV-2 samples targeting SARS-CoV-2 *orf1ab*, were done, conducting RT-RPA in various ways for assay sensitivity optimization. Each bar represents the detected LwaCas13a collateral cleavage activity in mean ± SD of background subtracted fluorescence measured from four technical replicates of the SARS-CoV-2 samples given a Ct-value by RT-qPCR of the *E-gene*. One negative SARS-CoV-2 sample (N2) was used as negative input tor RT-RPA and a water only input was used as negative to LwaCas13a reaction. SARS-CoV-2 sample U1 (Ct<25, Table S8) was used as positive control. Associated orf1ab-crRNA was used as guide for Cas13a. A black 1536-well plate with non-transparent bottom was used for fluorescent readouts. **(A)** Test of RPA primer combinations. Samples were detected with a 30-minute RT-RPA incubation followed by 30 minutes of LwaCas13a nucleic acid detection. Combinations of orf1ab-original and -new primer sets were used to detect the SARS-CoV-2 samples. **(B)** RT-RPA reaction time was tested. Samples were detected with a 30- or 60-minute RT-RPA incubation followed by 30 minutes of LwaCas13a nucleic acid detection. orf1ab-combo primer set (24138F and 24276R) were used to amplify the SARS-CoV-2 samples. **(C)** Various concentrations of reverse transcriptase were tested for each reaction pellet which means 4 individual reactions. Samples were detected with a 30-minute RT-RPA incubation using various Reverse transcriptase concentrations, followed by 30 minutes of LwaCas13a nucleic acid detection. Orf1ab-combo primer set (24138F and 24276R) was used to amplify the SARS-CoV-2 samples. Significant levels are shown on samples with detectable signal; ns≥0,05. *p≤ 0.05. **p≤ 0.01. ***p≤ 0.001, compared to water only input for RT-RPA on respective targets.

3.11 Identification of novel targets and primers for SHERLOCK detection of SARS-CoV-2

To obtain higher sensitivity than observed in the SHERLOCK validation assay (section 3.14, Figure 3.14B) a search for other potentially superior targets for the SHERLOCK detection of SARS-CoV-2 was done by Jon K. Lærdahl, research scientist and bioinformatician at MIK, OUS (Appendix P). The analysis resulted in two new conserved potential target sequences

(MSA_T1 and MSA_T2, Table S1*) in N-gene region of SARS-CoV-2 (Figure 3.8C) that were selected for SHERLOCK. Positive SARS-CoV-2 samples were tested in a SHERLOCK experiment for the detection of *orf1ab*, MSA_T1 and MSA_T2 as described in section 2.16.1 (Figure 3.8C). To see if pre-synthesized crRNAs provides higher SHERLOCK activity compared to the *in vitro* transcription product the orf1ab-crRNA, the pre-synthesized crRNA (orf1ab2-crRNA), was also used for the detection of *orf1ab*. Figure 3.8A reveals that all targets were significantly detectable in the most concentrated SARS-CoV-2 sample. Moreover, the MSA_T1 target showed highest sensitivity, and could detect the SARS-CoV-2 sample with Ct-value of 30,34 (Figure 3.8A). orf1ab-crRNA and orf1ab2-crRNA have almost similar efficiency as guides for LwaCas13a (Figure 3.8B). MSA_T2 showed weaker detection than the *orf1ab* (Figure 3.8B).
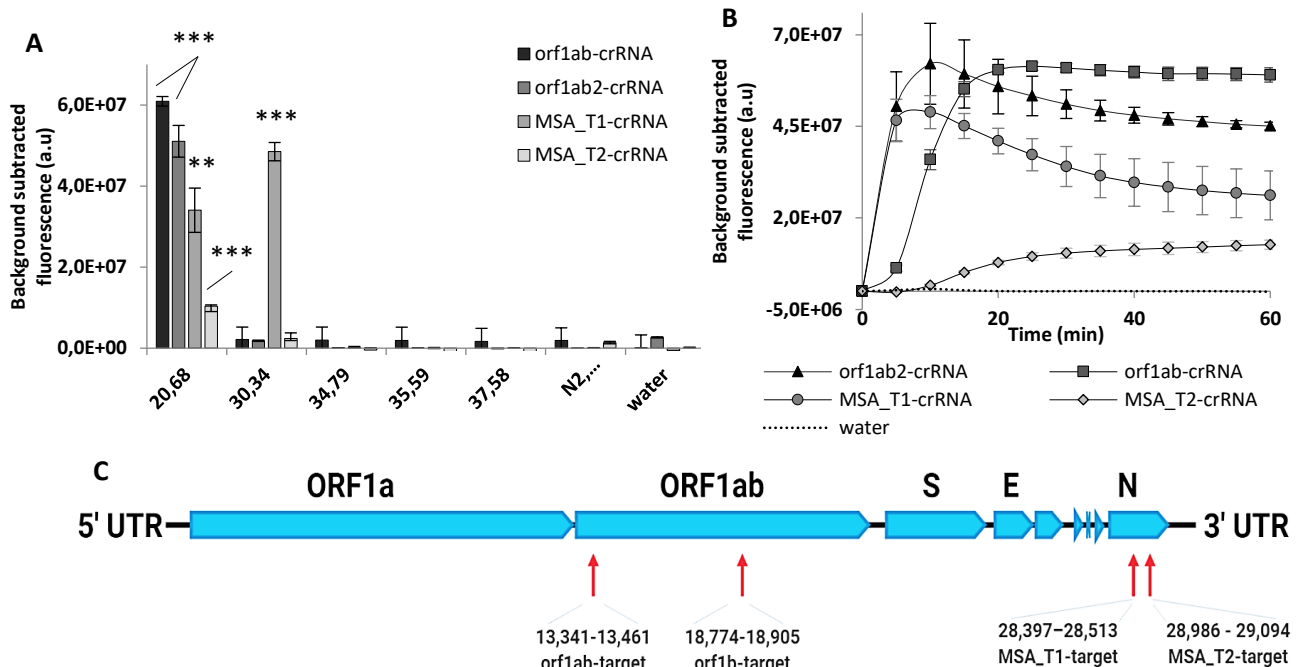
Figure 3.8: Finding new targets for SHERLOCK on SARS-CoV-2 A two pot SHERLOCK experiments on 5 positive SARS-CoV-2 samples targeting SARS-CoV-2 *orf1ab*, MSA_T1 and MSA_T2. Samples were detected with a 30-minute RT-RPA incubation followed by 60 minutes of LwaCas13a nucleic acid detection. The Ct-values were given by a RT-qPCR analysis of the SARS-CoV-2 *E-gene* in advance. orf1ab-combo, MSA_T1- and MSA-T2- primer sets were used to detect the SARS-CoV-2 samples targeting *orf1ab*, MSA_T1 and MSA_T2, respectively. One negative SARS-CoV-2 sample (N2), and water was used as negative inputs for each RT-RPA reaction and a water only input was used as negative to LwaCas13a reaction. Associated orf1ab-crRNA, orf1ab2-crRNA, MSA_T1-crRNA or MSA_T2-crRNA were used as guides for LwaCas13a for the detection of respective targets. A black 1536-well plate with non-transparent bottom was used for fluorescent readouts. Ct values were given to the samples by RT-qPCR analysis of the SARS-CoV-2 *E-gene*. **(A)** Each bar represents the detected LwaCas13a collateral cleavage activity after 30 minutes in mean ± SD of background subtracted fluorescence measured from four technical replicates of each SARS-CoV-2 sample, detecting *orf1ab*, MSA_T1 or MSA_T2. **(B)** LwaCas13a collateral cleavage activity over one hour in mean ± SD of background subtracted fluorescence measured from four technical replicates of the SARS-CoV-2 sample with Ct= 20,86, detecting *orf1ab*, MSA_T1 or MSA_T2 targets. **(C)** SARS-CoV-2 genome map visualizing target areas ORF1ab, ORF1b, MSA_T1 and MSA_T2 from the 5' untranslated region (UTR) to the 3'UTR used in this study to detect SARS-CoV-2. Significant levels are shown on samples with detectable signal; ns≥0,05. *p≤ 0.05. **p≤ 0.01. ***p≤ 0.001, compared to water only input for RT-RPA on respective targets.

3.11.1 Primer screens for SARS-CoV-2 *orf1ab* gene, MSA_T1 and MSA_T2

Since it was observed that a higher assay sensitivity was obtained by changing primer combinations (Figure 3.9A), the primers used in RT-RPA were further modified for detecting orf1ab, MSA_T1 and MSA_T2 (Figure TS4, TS5, TS6). Results from the primary primer screen *on orf1ab* revealed first that R3 serves as the most sensitive reverse primer in combination with F1 (Figure 3.9A, S12C) and was therefore screened against the other forward primers. The second screen showed that primer pair R3-F3 resulted in highest detectable signal from the SARS-CoV-2 sample with Ct-value of 30,34. (Figure 3.9B, S12J). Further, none of the primer combinations resulted in significant signals from SARS-CoV-2 samples having higher Ct value than 30,34 (Figure 3.9A-B). There was no detectable signal from the negative samples as expected (Figure 3.9A-B). A secondary primer-screen on SARS-CoV-2 *orf1ab* was therefore conducted for further improvement of assay sensitivity.

The orf1ab-Fa secondary screen against all reverse primers revealed that the Fa-Rd combination gave in highest detectable signal from the SARS-CoV-2 sample with a 28,28 Ct-value (Figure 3.9C, S13D). The Rd-primer was therefore screened against the forward primers, and results (Figure 3.9D) revealed that only primer pair Fb-Rd gave a detectable signal from the SARS-CoV-2 sample of Ct= 32,83, however not significant (Figure S13F).

For the primer screen on MSA_T1 and MSA_T2, the original primer sets (MSA_T1-24271F-24727R and MSA_T2-24273F-24274R) were used as basis for the design of primary primers (Figure TS5-TS6). The primer screen on MSA_T1 revealed two set of primers (MSA_T1-R1-F1 blue bars, -R1-F4 orange bars) that resulted in a significant signal (p<0,001) in all positive SARS-CoV-2 samples after 30 minutes of reaction, excluding the negative controls (Figure 3.10A-B). The MSA_T1 shows higher sensitivity, by the detection of higher Ct values, compared to the *orf1ab*-target (Figure 3.10). The MSA_T2 primer screen did not provide primer pairs with the same sensitivity of the detection of SARS-CoV-2, compared to the MSA_T1-target (Figure 3.10C-D). The most sensitive primer pair significantly detected four out of five SARS-CoV-2 samples with a detection limit equal a Ct-value of 30,45 (Figure 3.10D, purple bars). However, a significant signal was observed in the negative LwaCas13a water control (Figure 3.10C-D white bars)
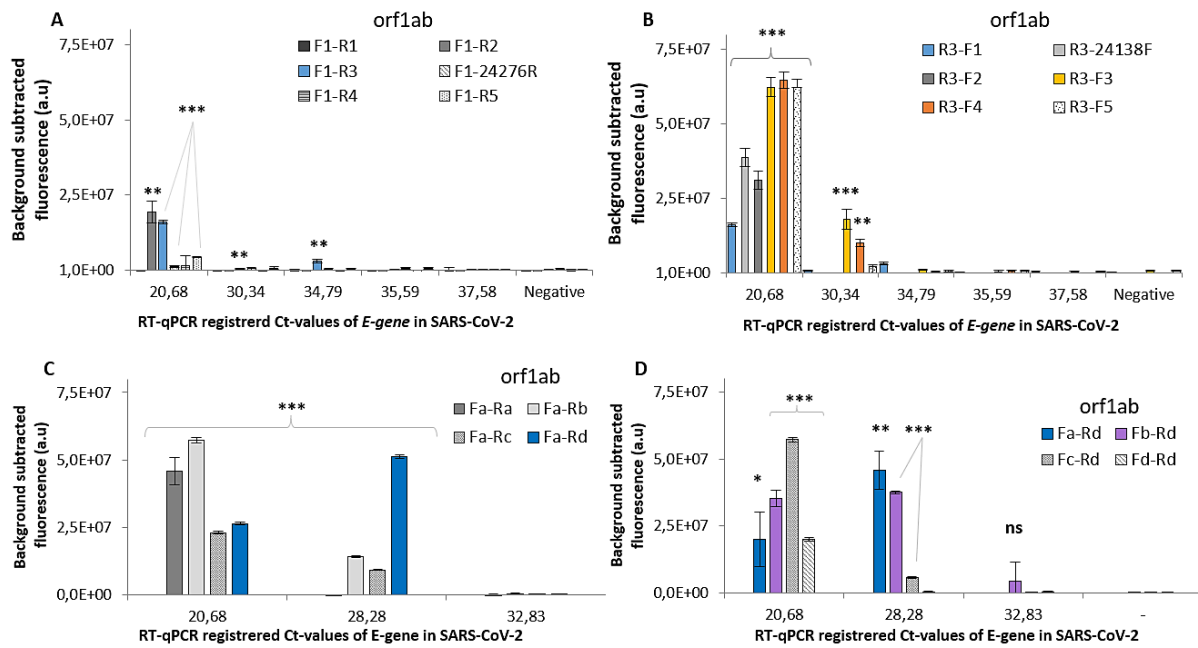
Figure 3.9 Primer screen for the detection of SARS-CoV-2 *orf1ab*. A primary and secondary primer screen on for *orf1ab* in SARS-CoV-2 using up to five clinical SARS-CoV-2 samples (from Table S10). Samples were detected with a 30-minute RT-RPA incubation followed by 60 minutes of LwaCas13a nucleic acid detection. Bars represent background subtracted fluorescence (a.u) in means ± SD after 60 minutes of SHERLOCK-Cas13a collateral reaction from four technical replicates of each sample. **(A)** Combinations of orf1ab-F1 primer with orf1ab- R1, R2, R3, R4 or R5 primers were tested in the RT-RPA reaction. **(B)** The most sensitive reverse primer from reverse screen, orf1ab-R3 (light blue), were combined with forward primers F1, F2, F3, F4 and F5 in RT-RPA. A negative SARS-CoV-2 sample (N2) was included for each primer pair for RT-RPA in the primary screen **(A-B)**. Resulting primer pairs with highest sensitivity in the primary scan are marked as orange and yellow bars. **(C)** A secondary primer screen on SARS-CoV-2 *orf1ab* using combinations of orf1ab-Fa primer with orf1ab- Ra, Rb, Rc or Rd primers in the RT-RPA reaction. **(D)** The resulting most sensitive reverse primer, orf1ab-Rd (blue), were combined with forward primers Fa, Fb, Fc or Fd in RT-RPA. A negative SARS-CoV-2 sample (N2) was included. Resulting primer pair with highest sensitivity in the secondary scan is marked as purple bars. Associated orf1ab2-crRNA was used as guide for LwaCas13a. A black 1536-well plate with round non-transparent bottom was used for fluorescent readouts. Significant levels are shown on samples with detectable signal; ns≥0,05. *p≤ 0.05. **p≤ 0.01. ***p≤ 0.001, compared to water only input for RT-RPA using respective primers.
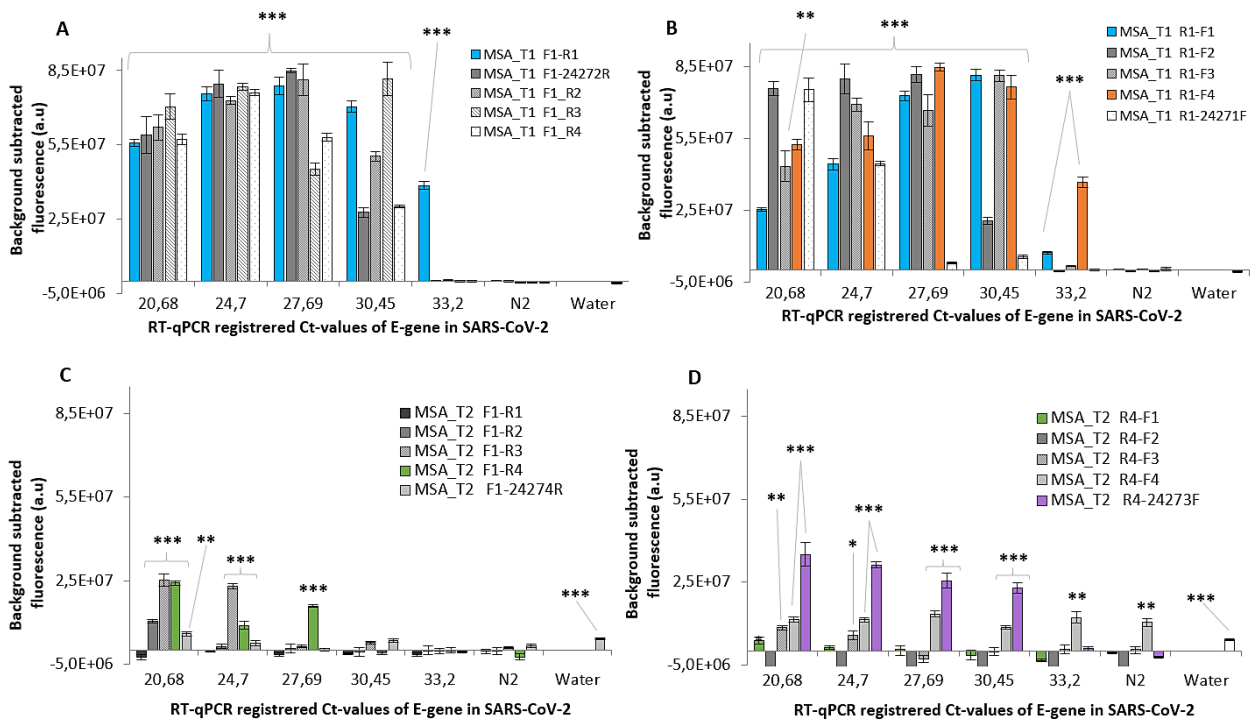
Figure 3.10 Primary primer screen for the detection of SARS-CoV-2 MSA_T1 and MSA_T2. A primary primer screen on for MSA_T1 and MSA_T2 in SARS-CoV-2 using five clinical SARS-CoV-2 samples (Table S11) and a negative control (N2, Table S10). Samples were detected with a 30-minute RT-RPA incubation followed by 30 minutes of LwaCas13a nucleic acid detection. Bars represent background subtracted fluorescence (a.u) in means ± SD after 30 minutes of SHERLOCK-Cas13a collateral reaction from four technical replicates of each sample. **(A)** MSA_T1-F1 primer screen, combinations of MSA_T1-F1 primer with MSA_T1- R1, R2, R3, R4 and 24272R primers were tested in the RT-RPA reaction. **(B)** MSA_T1-R1 primer screen. The most sensitive reverse primer from reverse screen, MSA_T1-R4 (light blue), were combined with forward primers F1, F2, F3, F4 and 24271F in RT-RPA. The resulting primer pair with highest sensitivity is marked in orange. **(C)** MSA_T2-F1 primer screen, combinations of MSA_T2-F1 primer with MSA_T2- R1, R2, R3, R4 and 24274R primers were tested in the RT-RPA reaction. **(D)** MSA_T2-R4 primer screen. The most sensitive reverse primer from reverse screen, MSA_T2-R4 (green), were combined with forward primers F1, F2, F3, F4 and 24273F in RT-RPA. The resulting primer pair with highest sensitivity is marked as purple bars. Associated MSA_T1-crRNA and MSA_T2-crRNA were used as guide for LwaCas13a to detect SARS-CoV-2 MSA_T1 and MSA_T2, respectively. A black 1536-well plate with round non-transparent bottom was used for fluorescent readouts. Significant levels are shown on samples with detectable signal; ns≥0,05. *p≤ 0.05. **p≤ 0.01. ***p≤ 0.001, compared to water only input for RT-RPA using respective primers and targets.

PART III SHERLOCK on clinical SARS-CoV-2 samples

3.12 A two-pot SHERLOCK on one SARS-CoV-2 RNA extract

We investigated if SARS-CoV-2 was detectable when using the associated RPA primers and crRNAs for the *orf1b* and *orf1ab* target genes. A single positive SARS-CoV-2 extract with known RNA concentration was used in a SHERLOCK experiment as described in section 2.17. A fluorescence signal was detected from all samples beside the negative control where no RPA reaction was added (Figure 3.11A). After 30 and 60 minutes of LwaCas13a collateral cleavage,

there is no significant signal from SARS-CoV-2 orf1b samples or synthetic DNA 1 when negative RPA background is subtracted. The limit of detection (LOD) is described as the smallest amount of analyte or sample concentration in a test-sample that can be identified and distinguished from a defined baseline (103). The detection limit of orf1ab in a SARS-CoV-2 extract is 8,5*104 copies/µL (142 aM) with low levels of significance (Figure 3.11B). Based on these results, the orf1ab was used as target is subsequent SARS-CoV-2 detection assays.
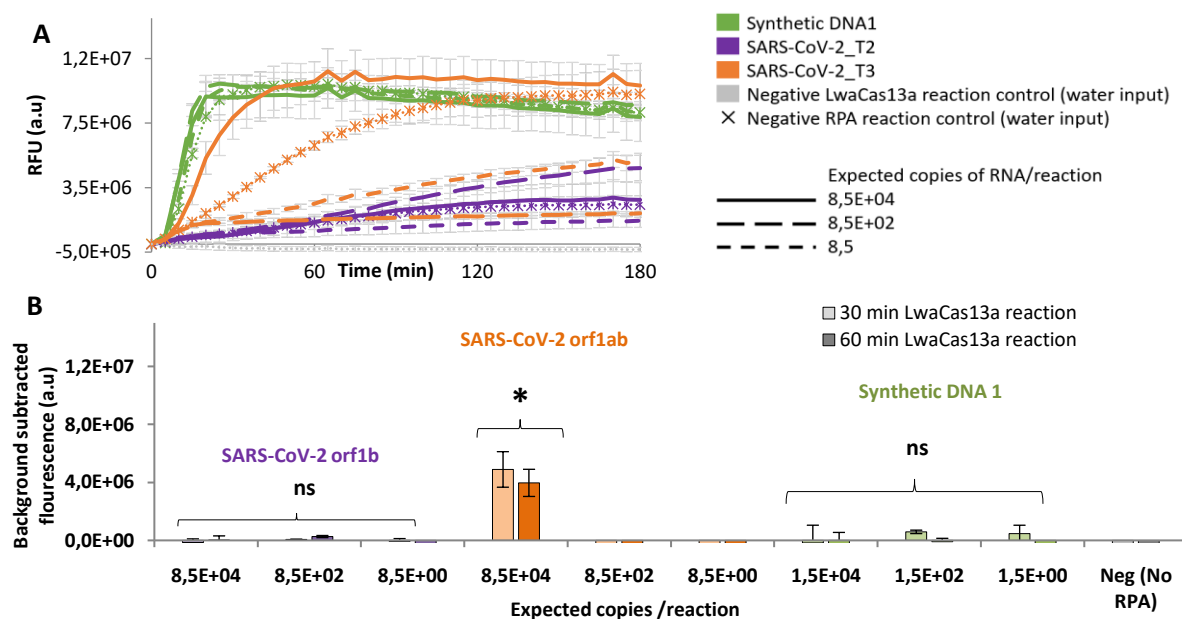
Figure 3.11: SHERLOCK on a positive SARS-CoV-2 RNA extract. A SHERLCOK experiment targeting *orf1ab* and *orf1b* in SARS-CoV-2 RNA extract and synthetic DNA 1 diluted with nuclease free water to give a final of 8,5E+04, 8,5E+02 and 8,5E+00, copies/RT-RPA reaction initially. (**A**) LwaCas13a reaction kinetics over three hours as relative fluorescence units (RFU). (**B**) Background subtracted fluorescence from the LwaCas13a collateral cleavage reaction after 30 and 60 minutes, expressed in means ± SD from three technical replicates for each series. RT-RPA was done over 30 minutes using orf1ab-original primer set, and DNA1-primers for synthetic DNA1 amplification. A water only negative control was included for each RT-RPA reaction mix. A black 1536-well plate with round transparent bottom was used for fluorescent readouts. Associated DNA1-crRNA and orf1b-crRNA and orf1ab-crRNA was used as guides for LwaCas13a targeting each RPA product, respectively. A negative water only input to LwaCas13a reaction was used as negative control. Significant levels are shown on samples with detectable signal; ns≥0,05. *$p \leq 0.05$. **$p \leq 0.01$. ***$p \leq 0.001$, compared to water only input for RT-RPA on respective targets.

3.13   SHERLOCK blind test on clinical SARS-CoV-2 samples

To see if the SHERLOCK assay could distinguish between positive and negative SARS-CoV-2 samples, a blind test SHERLOCK experiment was conducted as described in experiment 1 section 2.18.1 using two sets of primers on 5 clinical SARS-CoV-2 samples with unknown identity (Table S7). After 60 minutes of LwaCas13a reaction, only one positive sample was detectable with low significance (R2, $p \leq 0.05$) when using the original primer set for *orf1ab*

(Figure 3.12A). The new primer set (Figure 3.12B) resulted in higher significant signal from two positive samples (R1, R5), however also significant signal from negative controls. The SHERLOCK results did not correlate with results from RT-qPCR and detected in one false positive sample with significant signal with the new primer set for *orf1ab* (Figure 3.12).
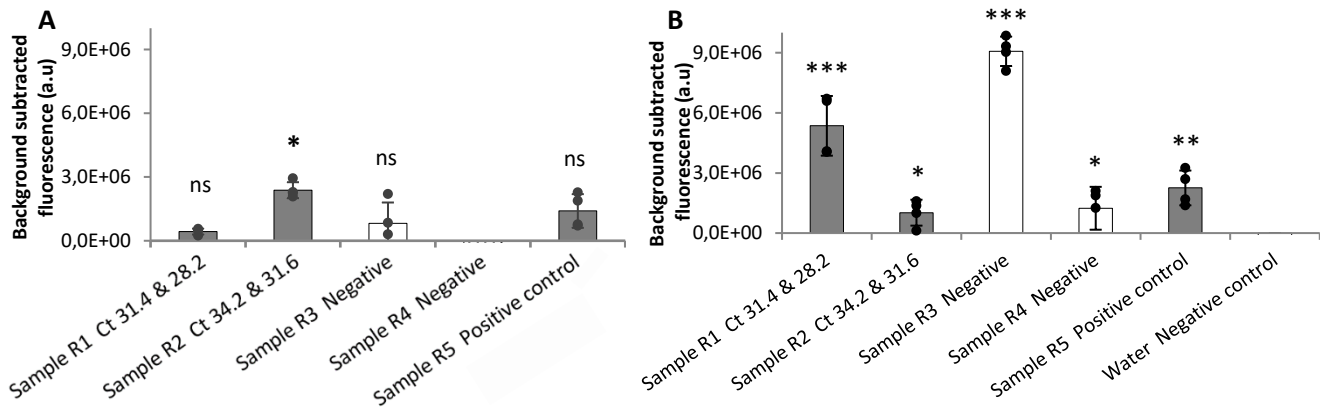
Figure 3.12. SHERLOCK on 5 SARS-CoV-2 samples. A SHERLOCK assay on four clinical SARS-CoV-2 samples, and one SARS-CoV-2 positive control, received from Oslo University hospital. Ct values for each sample represent a RT-qPCR detection analysis of the SARS-CoV-2 E-gene, done in advance by employees at Oslo University hospital to decide if samples were SARS-CoV-2 positive or negative. Values are represented as average background subtracted fluorescence in means ± SD after 60 minutes of LwaCas13a nucleic acid detection using **(A)** the original orf1ab primer set for RT-RPA, **(B)** the new orf1ab primer set for RT-RPA. orf1ab-original primer set was used to target SARS-CoV-2 *orf1ab,* and orf1ab-crRNA was used as guide to LwaCas13a. A black 1536-well plate with round transparent bottom was used for fluorescent readouts. Significant levels are shown on samples with detectable signal; ns$\geq$0,05. *p$\leq$ 0.05. **p$\leq$ 0.01. ***p$\leq$ 0.001, compared to water only input for RT-RPA. n=3

To investigate the SHERLOCK detection assay consistency, ten positive SARS-CoV-2 samples were tested in a SHERLOCK experiment described in experiment 2 section 2.18.2. After 20 minutes of LwaCas13a nucleic acid reaction there were significant fluorescent signal detected in all ten clinical SARS-CoV-2 samples, consistent with the RT-qPCR Ct values (Figure 3.13A). After 60 minutes the signal was considerably lower, but still significantly higher than the background signal (Figure 3.13B). Increasing background noise from the negative water only input to RPA (RPA + water) is observed over time (Figure 3.13D), consequently lowering the resulting background subtracted fluorescence (Figure 3.13C). No fluorescence signal was detected from the negative water only input in LwaCas13a nucleic acid detection reaction (Figure 3.13C-D)
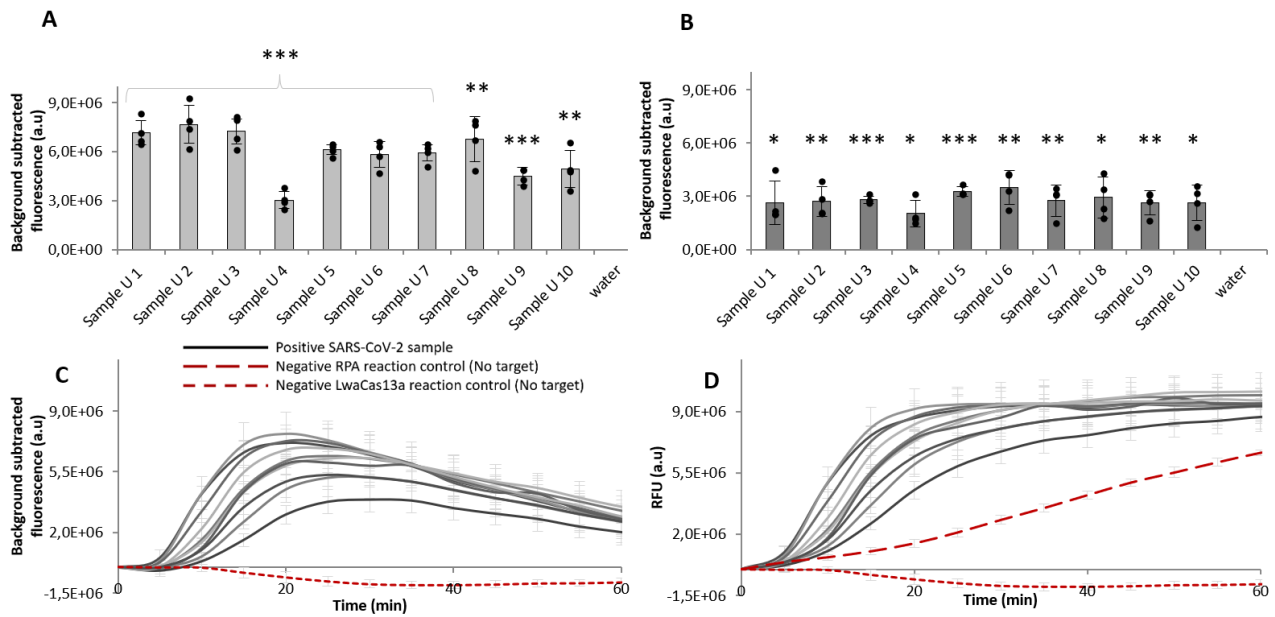
Figure 3.13. A SHERLOCK assay on ten positive clinical SARS-CoV-2 samples. Ct values <25 for each sample, found by RT-qPCR detection analysis of the SARS-CoV-2 *E-gene,* done in advance by employees at the department. A water only input to the RT-RPA reaction was included to create a subtractable background in the LwaCas13a nucleic acid detection reaction. A water only input to the LwaCas13a reaction was also included to ensure no signal from LwaCas13a reaction components. **(A)** background subtracted fluorescent after 20 minutes of collateral cleavage reaction, **(B)** background subtracted fluorescent after 60 minutes of collateral cleavage reaction, **(C)** LwaCas13a reaction kinetics over one hour with background subtracted fluorescence, **(D)** LwaCas13a reaction kinetics over one hour with relative fluorescence, is represented as means ± SD, of three technical replicates. Orf1ab-crRNA was used as guide to LwaCas13a. The original primers for amplification of *orf1ab* was used in RT-RPA. A black 1536-well plate with round transparent bottom was used for fluorescent readouts. Significant levels are shown on samples with detectable signal: ns $p \geq 0.05$. *$p \leq 0.05$. **$p \leq 0.01$. ***$p \leq 0.001$. compared to water only input for RT-RPA with respective primer sets.

PART IV Final validation of the SHERLOCK platform

3.14 SHERLOCK specificity and sensitivity validation

To test the specificity (equation 1, Appendix O) of the SHERLOCK assay, 19 negative SARS-CoV-2 samples tested for the presence of *orf1ab* gene in SARS-CoV-2 as described in section 2.19. Results revealed a significant signal from the positive SARS-CoV-2 control (U1), and only one negative SARS-CoV-2 sample (5% of negatives) confirming assay specificity (Figure 3.14A). Further, none of the negative RT-RPA and LwaCas13a reaction controls showed signal, as expected (Figure 3.14A). When defining a positive signal threshold to 2,0E+06, the resulting assay specificity was 95% (Appendix O).

To validate the SHERLOCK assay sensitivity (equation 2 Appendix O) and compare this method with RT-qPCR diagnostic for the detection of SARS-CoV-2, 72 clinical SARS-CoV-2 samples were tested in SHERLOCK experiments for the detection of *orf1ab*. When defining a positive signal threshold to 2,0E+06, the resulting assay sensitivity is 86%, where 60/72 positive samples were detected (Appendix O). The SHERLOCK method managed to detect SARS-CoV-2 *orf1ab* in samples with Ct values ≤ 31 for the *E-gene* (Figure 3.14B) after 60 minutes of LwaCas13a nucleic acid detection. The detection of the SARS-CoV-2 *orf1ab* gene varies greatly when Ct-values > 28 (Figure 3.14B). By increasing LwaCas13a detection to 60 minutes, a stronger signal is detected from samples with low copy number (Figure 3.14B, black dots).
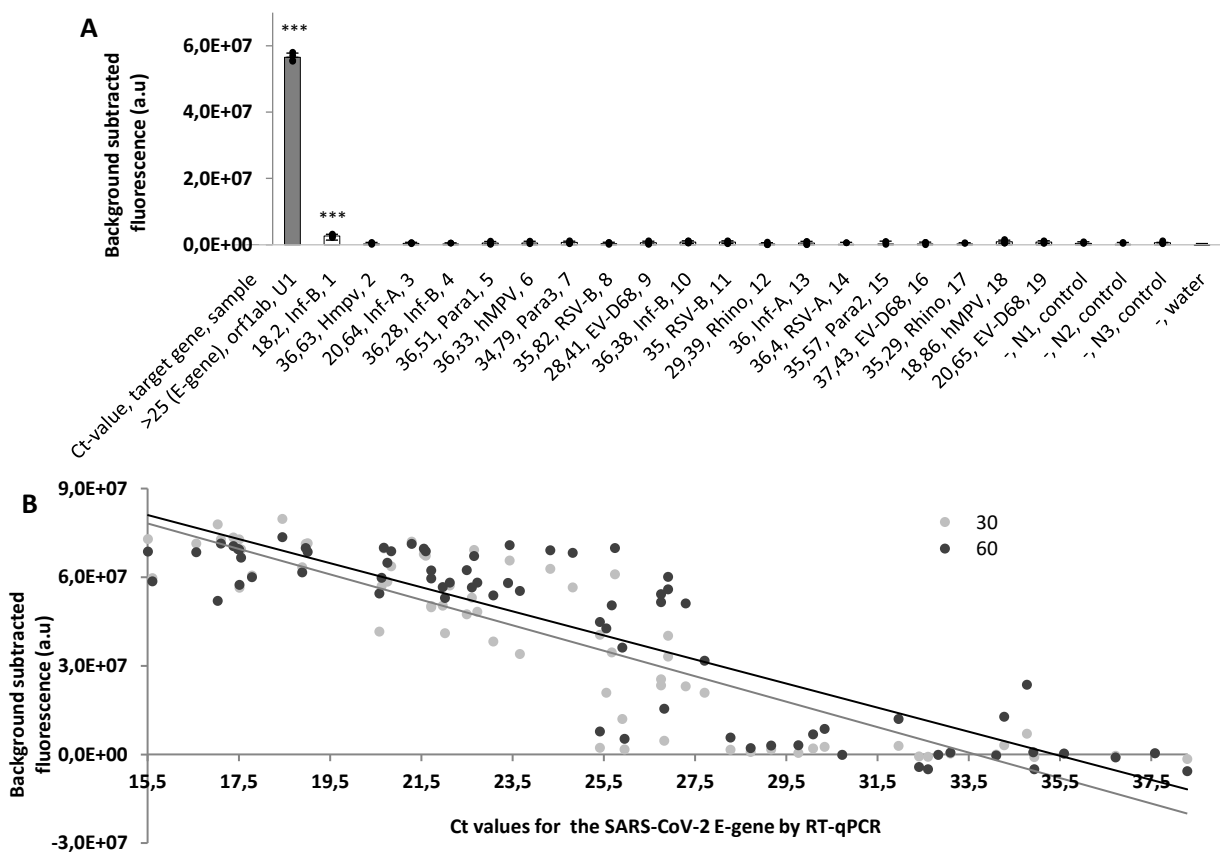
Figure 3.14: SHERLOCK specificity and sensitivity validation. Samples were detected with a 30-min RT-RPA incubation followed by 60 minutes of LwaCas13a nucleic acid detection. Orf1ab-new primer sets were used to detect the synthetic SARS-CoV-2 targets. Associated orf1ab-crRNA was used as guide for LwaCas13a. A black 1536-well plate with non-transparent bottom was used for fluorescent readouts. **(A)** Specificity test using 19 negative SARS-CoV-2 samples containing genes from various bacteria or virus was tested in the specificity test. Each bar represents the detected collateral cleavage activity in mean ± SD of background subtracted fluorescence measured from four technical replicates. Three negative SARS-CoV-2 samples (N1-N3) were used as negative for RT-RPA and a water was used as negative to LwaCas13a reaction. **(B)** Sensitivity test using 72 (m=72) positive SARS-CoV-2 samples confirmed by the presence of the *N-gene* was used in the sensitivity test. A comparison of the detected collateral cleavage activity (dots) in means of background subtracted fluorescence measured from four technical replicates (n=4) after 30-(light gray) and 60-(black) minutes of LwaCas13a nucleic acid detection and corresponding Ct values given the samples by RT-qPCR of the SARS-CoV-2 *E-gene*. Significant values were calculated by including a threshold for positive signal to 2,0E+06 (Appendix O).

4 Discussion

PART I Preparing SHERLOCK components

4.1 Nanobeads can simplify crRNA purification

A fast and efficient preparation of reaction components is desirable in any diagnostic assay with the least possible dependence on suppliers. CrRNAs were initially ordered as templates for *in vitro* transcription. As mentioned in Kellner *et al.,* both crRNA and LwaCas13a purification can be obtained commercially (36). However, this will increase the cost of the entire platform, and the dependence on manufacturers and suppliers which is a common problem for diagnostic tests using RT-qPCR (37). The *in vitro* transcription approach have also been successfully executed in similar studies that resulted in functional products (36,40,42). Using this approach, products must be purified and phenol: chloroform purification was initially used for crRNA extraction, as this was recommended in the MEGA script manual used for *in vitro* transcription (95). The method has been used for purification of single-guided RNAs *in vitro* transcription products in other studies (104). Subsequently, a novel RNA extraction method based on magnetic nanoparticles was developed by the Magnar Bjørås-group at NTNU and this method was used to purify the crRNAs (98). The nanoparticle-extraction method was optimized for efficient extraction of nucleic acids from clinical SARS-CoV-2 samples and is both significantly faster and simpler than the phenol: chloroform extraction method. Phenol: chloroform purification leads to yield reductions due to difficulties with phase separation (95). It was further suggested that the method could be used for crRNA extraction, possibly resulting in higher yield. Tape-station yield, and integrity analysis of the resulting crRNA products revealed an almost identical yield by comparing bands from the two extraction methods (Figure S4A), thereby contradicting the yield loss hypothesis. The results point to nanoparticle-purification as the best method to use for crRNA preparation, since the approach is faster than the use of phenol: chloroform and gives same yield. Automatization is the ultimate solution for preparation of reaction components. Since phase separation in phenol chloroform extraction can be difficult using a robot, an automized purification process is easier using nanoparticles.

Next, the purity of these components needs to be kept in mind during the establishment of a diagnostic platform in terms of expected assay sensitivity and specificity. Data from the crRNA *in vitro* transcription (Figure S4A-B) suggest the presence of the expected crRNA product but

also the presence of both truncated and overextended products. The results from this thesis however confirm functional crRNAs (Figure 3.2-3.5, Figure S10. Figure S11), although there might be bi products in the crRNA extract. Directly synthesized crRNAs were tested as guides in search of higher crRNA activity. No significant difference in sensitivity was observed between the directly synthesized and manually in vitro transcribed crRNA for the orf1ab target (Figure 3.8A-B). In conclusion, the in vitro transcribed crRNAs should be used in further SHERLOCK assays, using an automized version of the nanobead-crRNA purification if possible. Moreover, sequencing, may be necessary to confirm the presence of the desired crRNA.

PART II ASSAY OPTIMIZATION

The original research papers on Cas13a only focused on the biochemical aspects of the assay and did not address the importance of correct instrument optimization (36,40,42). Here we set out to understand the importance of optimization of the instruments and equipment used for fluorescence monitoring in SHERLOCK.

4.2   Plate types significantly impact flourescence reading

In the preliminary SHERLOCK experiments, 96 and 384 well plate formats were used for fluorescence monitoring of the LwaCas13a nucleic acid detection reaction. Since the LwaCas13a reaction results in a fluorescence signal black plates were chosen as they absorb scattered light and reduce background noise and crosstalk which is produced by fluorescence signals leaking into adjacent wells (105–107). It quickly became clear that the 384 well plate format was most suitable for SHERLOCK as it was almost impossible to distinguish positive signal from background using the 96-well plates with DNA1 as target (Figure S6A). Initially we presumed that this was due to poor crRNA design, so RNase A was introduced as a positive control with synthetic DNA 1. RNase A produced a clear signal at high concentrations that faded over time (Figure S6B). This reduction in signal was attributed to a phenomenon called photobleaching (108), which is caused by chemical instability induced by exposure to excessive radiation. Photobleaching can be reduced by limiting the exposure time of the RNA reporter, or by reducing the excitation energy (109). Similar studies have not emphasized the impact of the photobleaching effect in their findings, which makes the hypothesis difficult to confirm.

Regardless it was decided to reduce the measurement time (laser exposure time) from 500 ms to 250 ms in subsequent assays to guard against this eventuality.

With the use of 96 well plates, the signals from all samples reached the same background as the empty wells (air) (Figure S6A-B). Upon observation of the wells afterwards, there was almost no solution left. It was gradually understood that what was previously assumed to be a positive signal after three hours turned out to be an evaporation effect in the wells (110). A comparison of the performance of 96 well plates versus 384 well plates have shown that 384 well plates have significantly lower evaporation rates compared to the 96 well plates (110). Both evaporation and photobleaching were not as prominent in when using the 384-well plates for SHERLOCK, thereby confirming previous studies. However, it took 45 minutes to obtain a detectable signal in the positive sample with 384 well plates (Figure S6C). It was therefore concluded that further LwaCas13a reaction optimization was required to achieve faster and more sensitive detection.

We then hypothesized that a greater sensitivity was achieved by using even smaller wells. The 1536 well plate format showed both the highest S/N and background subtracted fluorescence (Figure 3.1), thereby confirming the hypothesis and previous studies. However, smaller wells also mean lower reaction volumes, and the end signal is more sensitive to changes in the reaction composition. Tiny adjustments in the reaction have an effect on the detected background signal (Figure 3.5B-C). For the use of SHERLOCK on clinical SARS-CoV-2 samples, the 1536 well plates allow several samples to be tested per round when automizing the assay. Significantly, the results demonstrated that optimal sensitivity in fluorescence reading is highly dependent on plate type, and that the 1536 well plate is suitable and sensitive for SHERLOCK.

4.3   Filter and mirror optimisation significantly improved fluoresence readings

Initial filter selection, excitation, and emission (570/10, 600/10nm) interestingly resulted in poor S/N ratios which contradicted the initial thought of that these settings should fit the RNA reporter properties (abs max.596nm, emission max.613nm, IDT). A hypothesis was that the close wavelength shift causes an overlap in energy from the excitation to the emission. The phenomenon is called Stokes shift suggested by the physicist George Gabriel Stokes (111), and

represents the change in wavelength between excited and emitted light due to loss of energy on emitted photons (112). A lowering of the excitation filter to give greater energy-separation, did not show an immediate effect on fluorescence signal detected, but a slightly higher S/N ratio confirming previous assumptions (Figure S8A-B).

Our results correspond with the theory that a greater separation can be achieved between excitation and emission wavelengths by blocking unwanted wavelengths from passing through the filter to the detector, using a dichroic mirror (D590) (112). Although the excitation maximum for the RNA reporter lies at 596 nm, this was the closest mirror available on the market that could potentially filter most of unwanted wavelengths from the RNA reporter emission signal. Further, correct z-focus calibration is crucial for fluorescent readings for each plate format, excluding areas representing air or plastic of the plate (Figure S8). Together, these results demonstrate the importance of appropriate equipment, and adjustment of optical parameters to establish a successful SHERLOCK assay as diagnostic tool for nucleic acid detection.

4.4 pH and ion concentrations impact the LwaCas13a reaction

Gootenberg *et al*., showed that the collateral cleavage activity of LwaCas13a orthologue PsmCas13b was highly dependent on reaction conditions, including pH, buffer, buffer concentration and ion concentration (42). We therefore hypothesized that that buffer composition can affect LwaCas13a collateral cleavage activity. Our results confirm this hypothesis, showing that the fluorescence signal varies in each buffer condition tested (Figure 3.2). The results suggest that LwaCas13a is most active at pH 6.5 in 40 mM MES and 9 mM $MgCl_2$. Moreover, subsequent results in this thesis indicate that LwaCas13a activity is activated faster at pH 7.0, but the collateral activity is maintained at pH 6.5 and so increases over time (Figure 3.4). Similar studies using LwaCas13a have demonstrated that the enzyme exhibits strong collateral activity in other buffer conditions (36,40,42,79), including a pH range of 6,8-7,3 in 40 mM Tris-HCl or HEPES, using 6-9 mM $MgCl_2$. The results are similar to homeostatic cytoplasmic pH conditions in bacterial cells which varies around 7.0 (102). It was decided to use pH 7.0 in all subsequent assays using LwaCas13a for SHERLOCK nucleic acid detection as one of the most important goals was fast detection.

Gootenberg *et al*., also suggest that Cas13b orthologues have different ion preferences for collateral cleavage by demonstrating the addition of various divalent ions for the Cas13b nucleic acid detection of a synthetic ssRNA (42). We therefore hypothesized that LwaCas13a function could be enhanced by other ion preferences. A MES and HEPES buffer was tested in the LwaCas13a collateral reaction as neither strongly complexes with metal ions (113), like Mg^{2+} (except MES with Fe^{3+}, and TAPS with Fe^{3+} Cu^{2+} and Cr^{3+}) which is desirable for enzyme activity assays reactions where chelating of ions can inhibit enzyme activity. Results revealed that only the presence Mg^{2+} cooperates with the LwaCas13a collateral cleavage reaction, thereby rejecting the hypothesis (Figure 3.2B). Previous studies of the type V effector Cas12a showed a divalent metal dependency for nuclease activity by increasing affinity to the associated crRNA, where Mg^{2+} is coordinated in the crRNA structure (114,115). The exact mechanism of Mg^{2+} in the LwaCas13a-crRNA system is not yet established, but several SHERLOCK studies includes the addition of Mg^{2+} to the collateral cleavage reaction giving the impression of that Mg^{2+} is important for collateral cleavage reaction (36,40,42,81). Conversely, too much Mg^{2+} gives a clear inhibitory effect on the LwaCas13a reaction (Figure 3.2B), resulting in weaker fluorescent signal when added at 12 mM or more.

Our results build on the exciting evidence of that the LwaCas13 nuclease activation is tightly controlled and show that the presence of Mg^{2+} is important for activity (72,74,78). As hypothesized, correct buffer composition is essential for optimal LwaCas13a collateral activity, the enzyme is active in both HEPES and MES buffers, in a pH range of 6.5-7.5 using 6-12 mM salt.

4.5   SHERLOCK was inhibited when using novel T7 promoters

LwaCas13a is an RNA targeting enzyme (72,79). As such T7 transcription is essential for the LwaCas13a collateral cleavage reaction converting RPA dsDNA amplicons to targetable RNA. Improvements in T7 transcription were therefore attempted. The introduction of alternative T7 promoters in the RPA forward primers was also explored as a potential enhancing factor for SHERLOCK. Research by Paul et al., showed that four mutant T7 promoter sequences resulted in higher transcription levels (101). The two most significant mutant sequences were integrated into separate forward primers for amplification of synthetic DNA 1. No increase in signal from the collateral cleavage reaction of synthetic DNA 1 with mutant T7 promoters was observed

compared to the original T7 promoter (Figure 3.3B), thereby rejection the hypothesis. It is not clear why the promoters did not work on the specific RNA polymerase used in this experiment. In general, there is not much information about the RNA polymerases used in Paul et al., nor about the T7 RNA polymerase used in this experiment other than it derives from a *E.coli* strain (101). They may have different promoter binding specificity but unfortunately there is no data from similar studies to support this claim. Together our results reveal no improvement of T7-transcription in SHERLOCK when changing T7 promoter sequence (101). We conclude that the T7 promoter sequence is likely highly specific to the exact transcription enzyme and that the original promoter should be used in SHERLOCK.

4.6 Background signals from the RPA reaction lowers assay sensitivity

Initial hypotheses centered on the potential for poor rates of amplification of the target, the presence of interfering reagents or RNases causing unspecific cleavage of the RNA reporter was further addressed. The non-sequence specific RNase activity of LwaCas13a is only activated upon target recognition and binding between crRNA in crRNA-LwaCas13a duplex and the associated target sequence (36,42,72). In order to attempt to identify the origin of our background signal several experiments were conducted using negative controls for RPA and LwaCas13a nucleic acid detection.

The experiments confirmed that LwaCas13a activity is dependent on the presence of associated crRNA (Figure 3.5A). Surprisingly, a signal was also detected using water as the input for the LwaCas13a reaction, which contradicted with literature that describes target activation dependency. From experiments done by Myhrvold et al., it was observed background variations in the LwaCas13a detection step (81). They describe that this might be due to high GC content in the spacer region, polyUs stretches or secondary structures in the crRNA which influences the crRNA performance. They also observed crRNA activity in the absence of target, indicating that this might be the source of some of the background signals (Figure 3.5A).

The signal could also potentially be due to contamination of reagents or water, and this hypothesis was further investigated. As mentioned by the TwistDx, the RPA reaction generates a vast number of amplicons within minutes (84). They further describe that when using RPA products as input to subsequent reactions, amplicon contamination of equipment, surfaces and

reagents can lead to false positive samples if products are not carefully treated (85). Recommendations included careful disinfection of all equipment, surfaces and instruments were subsequently initiated to prevent amplicon contamination in further experiments (85,93,116). New aliquots of each reagent were also made including a new water source. A comparison of the signal generated from negative controls before and after decontamination showed that background signal did not originate from the water source (Figure 3.6) as previously assumed but is generated by other factors in the RPA or LwaCas13a reaction.

At this point it became clear that the RPA reaction can cause some background noise in general as previously mentioned. This signal generation is described by the kit producer as primer noise, emerging as a common problem when using RPA (83,85). How the spurious products from RPA led to collateral activity in the LwaCas13a reactions is not understood. In conclusion, the SHERLOCK assay needs to be further optimized, to minimize the significant impact of background noise in the RPA reaction on assay sensitivity.

4.6.1 *Orf1ab* gives lowest background signal

Since the target in this thesis was genetic detection of SARS-CoV-2, two synthetic sequences mimicking areas within SARS-CoV-2 orf1b and orf1ab were created besides the initially used synthetic DNA 1 (36) to validate the crRNAs and RPA primer design. SHERLOCK could detect all concentrations represented by each synthetic target, indication successful primer (original primer sets) and crRNA design (Figure 3.4). At this time, we were unaware that the RPA reaction has a significant propensity for promiscuous priming in the absence of the target of interest (section 4.6) so a negative, water only, control for RPA was not included. To account for the potential of a background signal an empirically determined background was used for this SHERLOCK assay using the original orf1ab-primer set. That is to say the background signal was subtracted from the fluorescent signal. This metric mostly showed a detectable signal which faded over time because of an increasing background (Figure 3.4).

When trying SHERLOCK on a SARS-CoV-2 positive RNA extract (Figure 3.11), we included a water only input as negative RT-RPA control to make a subtractable background in collateral cleavage reaction. It appeared that the orf1ab target was most promising for the detection of SARS-CoV-2 using SHERLOCK. Our result is in line previously study by Luica et al., which

used the three targets for a Cas12a based SARS-CoV-2 detection including similar orf1b and orf1ab targets, and obtained highest sensitivity when using orf1ab (100).

Together, the results demonstrated the various primers and targets produce different levels of background signal and that this significantly reduces the assay sensitivity. To conclude, fluorescence signals need to take account of any RPA background signals and these vary for each primer condition and RPA reaction time (85). We decided to optimize RPA reaction as the background signal turned out to have a significant impact on the assay sensitivity.

4.7 RPA primers have a significant impact on SHERLOCK sensitivity

As described in Kellner et al., (36), both RPA primers and crRNA design must be optimized to achieve maximal sensitivity. Longer RT-RPA reaction times were shown not to increase assay sensitivity (Figure 3.7B, Figure S10). The results are consistent with the literature, which indicates that a 10-30 minutes RPA reaction time is sufficient (36,42,93). Further, the formulation in the RPA reaction contains a relatively high adenosine tri-phosphate (ATP)-burning recombinase that consumes all energy within 25-30 minutes of reaction (85). The kit manufacturer also specifies that this can be affected by both primer and target complexity.

The next experiment with various reverse transcriptase concentration in RPA indicates that sensitivity is dependent on the high efficiency of the recombinase and less so on the reverse transcriptase (Figure 3.7C) (85). To minimize the amount of reverse transcriptase used in each reaction, it was decided to use the lowest amount showing acceptable sensitivity, which was 1 µL per four reactions. Interestingly, RPA primer combinations had the highest impact on sensitivity (Figure 3.7A, Figure 3.12), thus primer combinations were put in focus.

To achieve single molecule detection in as short time as possible, the RPA kit producer recommends a careful primer screen including three screening steps (85). Because of the specificity within the crRNA sequences, a few primers pairs can be screened to achieve desirable sensitivity (36). Further, Gootenberg et al., managed to reach single molecule sensitivity using SHERLOCK only by the design of two primer sets giving amplicon sizes between 100-200 bp (40). A primer screen on orf1ab did not show a small but not satisfactory increase in assay sensitivity compared to the RT-qPCR analysis of SARS-CoV-2 *E*-gene target

(Figure 3.9, Figure TS4-6). The results suggest that a more accurate primer screen must be repeated for this targets thereby contradicting previous findings (40,42,81). These results demonstrate that assay sensitivity is highly dependent on primer design and that primer screens potensially could increase SHERLOCK sensitivity. Further, the target sequence itself and in combination with associated primers could be a limiting factor for the sensitivity of SHERLOCK. We therefore investigated if novel targets could increase assay sensitivity.

4.8   Novel targtes increase SHERLOCK sensitivity

Alternative nucleic acid sequences should be considered to achieve high sensitivity and specificity in the SHERLOCK assay, and maximize the advantages of this detection technology compared to other diagnostic techniques such as RT-qPCR (85). Recent publications of the SARS-CoV-2 transcriptome have shown that there is a specifically high transcriptional activity at the 3' un-translated region (17,25). Genes have been shown as upregulated and further analysis has shown that the gene expression pattern evolves during infection (17). Among others, genes involved in the expression of the viral nucleocapsid (N-genes) are positioned in these highly expressed regions, and guides targeting both areas are widely used to identify SARS-CoV-2 (32,37,40,93,94).

To identify new target sequences with higher sensitivity, multiple sequence alignments of SARS-CoV-2 genomes was done by Jon K. Lærdahl, research scientist and bioinformatician at MIK, OUH to identify genomically stable regions. From this analysis, two new target sequences were chosen withing the N-gene region of the SARS-CoV-2 (Figure 3.8C, Table S1, Appendix P conserved segment 1 and 2). One of the novel targets, MSA_T1 showed higher sensitivity for the detection of SARS-CoV-2, compared to the original target (*orf1ab*). However, the MSA_T1 target did not manage to detect all positive SARS-CoV-2 samples found positive by RT-qPCR (Figure 3.8A). Whether MSA_T1 is a better target due to high expression as previous studies indicate, or because the site is more genomically stable than orf1ab is uncertain.

When using the MSA_T1 target for SARS-CoV-2 detection, resulted in an increased target sensitivity and significant signals in a shorter time period of 30 minutes. This result complements the findings in Kellner et al., and of Gootenberg et al., that only a few primer pairs are needed for a screen to obtain high assay sensitivity (36,40). The result demonstrate that the choice of target sequence is important for SHERLOCK sensitivity, and that

bioinformatics analyzes must be prioritized to optimize the method. Further results also confirm that target choice in combination with optimal primers increase SHERLOCK assay sensitivity (Figure 3.10). The results in this study also demonstrate that primer optimization is most important as is crRNA design and the selection of a target sequence in achieving sufficient assay sensitivity (36,40,42).

In conclusion, the use of a novel target did not provide satisfactory sensitivity in targeting SARS-CoV-2 compared to RT-qPCR analysis. The MSA_T1 target looks more promising for the detection of SARS-CoV-2 than *orf1ab* which can potentially achieve single molecule detection combined with efficient RPA primers. In further SHERLOCK experiments, this target must be tested for SARS-CoV-2 detection.

PART III SHERLOCK on clinical SARS-CoV-2 samples

4.9   RNA extraction methods impact SHERLOCK preformance

RT-qPCR is the most widely used method for detecting SARS-CoV-2, and it was therefore interesting to compare analytical results from a RT-qPCR detection of SARS-CoV-2 *E-gene* with a SHERLOCK detection of the orf1ab gene. A blind test was conducted on five clinical SARS-CoV-2 samples showed that SHERLOCK did not manage to identify and distinguish positive and negative SARS-CoV-2 samples using *orf1ab* as target (Figure 3.12). This assay failure could have several explanations. First, these samples were collected from a department at OUH that does not routinely perform SARS-CoV-2 testing. Sample handling including the RNA extraction method may have been of poor quality. Secondly, the sensitivity of the two pot SHERLOCK may be too low.

In contrast to these initial results on clinical samples, we were able to detect true positives in other samples collected from a different department that routinely preforms SARS-CoV-2 diagnostics. Hence it is unlikely that assay sensitivity was an issue. On the other hand, the viral load is initially higher (lower Ct values) in these second batch of samples, which could be a contributor to the significant signals detected after 20 minutes reaction (Figure 3.13A). The results fit with previous studies where (RT-)RPA reaction has given detectable signals after

only 20 minutes of incubation (36,40,42,81). This experiment further show that the assay sensitivity is highest after 10-25 minutes, due to an increased background over time.

Conclusively, the results demonstrate that the way clinical specimens are handled affects the SHERLOCK assay sensitivity and this should be considered during the establishment of a diagnostic platform. Further, a SHERLOCK detection and nano-bead extraction of SARS-CoV-2 would be interesting to combine (98).

PART IV Final validation of the SHERLOCK platform

4.10 SHERLOCK maintained high specificity

The SHERLCOK platform utilizes the specific property of the LwaCas13 enzyme that can distinguish between single nucleotide mismatches. As mentioned in Kellner et al., (36), LwaCas13a activation should only occur if there are less than two mismatches between the crRNA and the target sequence in the crRNA: the LwaCas13a duplex (40,72,79). When defining a threshold for detection (Appendix O), the SHERLOCK method showed high specificity (95%) for the detection of SARS-CoV-2 orf1ab with one false positive. Results fits the theory, and are comparable with previous studies using SHERLOCK and DETECTR to detect SARS-CoV-2, resembling high specificity (40,72,89). In conclusion, this study shows that SHERLOCK maintained high assay sensitivity, comparable to RT-qPCR.

4.11 SHERLOCK sensitivity must be optimized

A high sensitivity and rapid detection are essential in diagnostic labs for massive screening and for point-of-care diagnostics, especially when treating conditions such as acute infections. The key behind SHERLOCKs high sensitivity is the inclusion of a pre-amplification step combined with the specific collateral cleavage activity of LwaCas13a. In this study, the SHERLOCK method had a LOD on the *orf1ab* target equal to $8,5*10^4$ copies/µL (142 aM) when testing a dilution series of a SARS-CoV-2 RNA extract (Figure 3.11). This result however was obtained before method optimization and does not represent the final sensitivity of the assay. Moreover, the RNA extract was quantified with Nanodrop spectrophotometer, which cannot distinguish the amount of actual of SARS-CoV-2 nucleic acids from other absorbing sequences in the

clinical sample. Furthermore, the extraction method used to collect SARS-CoV-2 RNA may be of low quality as previously describes as the sample was collected from same department as the 5 sample from the blind test. Compared to other studies with SHERLOCK, this sensitivity is sufficiently lower (36,40). SHERLOCK managed to detect SARS-CoV-2 samples with Ct-values from RT-qPCR up to of 31 of the SARS-CoV-2 *E-gene*. (Figure 3.14B). Compared to the SARS-CoV-2 samples verified by RT-qPCR, the SHERLOCK method showed 86% sensitivity after one hour of detection by a defined threshold (Appendix O). The RT-qPCR SARS-CoV-2 detection uses 4-5 µL inputs of RNA extract (31,32) compared to only 2 µL of sample input used for RT-RPA, which may be a reason for the lower sensitivity. It would be interesting to test larger sample input volumes to see if the sensitivity would increase in SHERLOCK.

The SHERLOCK assay sensitivity in this thesis may be limited to an inefficient RPA reaction due to inefficient priming, crRNAs design, overlapping primers or targeting unknown regions of secondary structure (36,40,81), which leads to poor detection limits compared to RT-qPCR (Figure 3.14). Moreover, the results demonstrate that a lower sample input can reduce the sensitivity of the method. As previously observed, the novel target, MSA_T1, showed higher sensitivity compared to orf1ab for SARS-CoV-2 detection (Figure 3.8A, Figure 3.10A-B), and should be further validated as a potential target for SARS-CoV-2 diagnostic. Conclusively, the SHERLOCK sensitivity must be optimized to reach same sensitivity levels as the RT-qPCR diagnostic approach.

4.12 A Comparison of CRISPR-Cas molecular nucleic acid detection methods and RT-qPCR.

An advantage of SHERLOCK is its rapid nature combined with high sensitivity due to the pre-amplification step. Compared to well-established detections methods like RT-qPCR, the SHERLOCK platform has shown levels of sensitivity reaching attomolar (aM) and even single molecule detection (36,40,42,81,89). In this study, the two-pot SHERLOCK platform was selected for detecting SARS-CoV-2 as it is easier to optimize and has shown higher sensitivity, compared to the one-pot assay. When including the RPA reaction in one pot with LwaCas13a nucleic acid detection, the assay time is sufficiently reduced (36,117). Further, one-pot SHERLOCK also decreases the risk of contamination, which can be a problem when transferring RPA products to the LwaCas13a reaction. However, the viscosity of the RPA

mixture makes a one pot reaction assay less sensitive and robust. A one-pot assay can also be challenging to optimize due to several enzymatic reactions and components in a single reaction. The two pot SHERLOCK is suitable when detection is desirable handling low copy numbers from difficult sample matrixes such as blood, or body fluids (36). Although optimization is easier with a two-pot assay, significant time was spent optimizing fluorescence readings using a plate reader as demonstrated in this thesis. Moreover, the resulting method still suffered from a nonspecific signal underlined by the efficiency of the RPA reaction causing background noise to override real positive signals over time (Figure 3.13D) (85). It is difficult to compare the background signal generated in this SHERLOCK assay to other publication only describe their measurements as background subtracted and do not specify their background levels.

Scientists have explored how to eliminate potential nucleases in the SHERLOCK assay by developing an additional step called "Heating Unextracted Diagnostic Samples to Obliterate Nucleases" (HUDSON), using an additional heating step to the diagnostic samples prior to RPA reaction in SHERLOCK (81). This might make SHERLOCK more sensitive, thus makes the platform more robust for rough sample matrixes and complex targets. HUDSON however increases protocol complexity by requiring higher reaction temperatures, which makes the method less attractive in fields and for point of care diagnostics.

The lateral flow strip method greatly simplifies SARS-CoV-2 SHERLOCK detection due to the independence of advanced instruments, enabling mobile test stations for rapid field friendly diagnostics. (36,42,93). This might be an idea in future disease monitoring by creating test platforms in local medical centers. At the same time, the test capacity decreases compared to fluorescence measurements, due to difficulties in transferring large amounts of data from the visualization on the flow strips. With a view to establishing a platform for disease monitoring of SARS-CoV-2, test capacity is an important factor. This makes the fluorescence-based SHERLOCK assay more attractive and comparable to RT-qPCR test capacity (14) than the lateral flow strips.

LAMP (88) is widely used as a pre-amplification step when detecting SARS-CoV-2 using SHERLOCK or the DETECTR platform (37,89,92,118). The LAMP technique in combination with Cas detection has shown comparable sensitivity to RT-qPCR-based SARS-CoV-2 tests with a detection limit of 10-100 copies / reaction reached within 30 minutes of amplification (89). Broughton et al., showed a 95% positive and 100% negative predictive agreement between

real time RT-PCR and a RT-LAMP based Cas12 DETECTR detection assay, which are higher percentages than observed between SHERLOCK and RT-qPCR (Figure 3.14) (118). Many labs choose to work with the LAMP-technique, due the commercial limited availability of the RPA kit. Moreover, the LAMP technique overcomes the difficulties of viscousness reaction of a one pot-RPA reaction, thereby maintaining rapid detection with high sensitivity levels (93). The restrictions with LAMP however are the high operational temperatures needed as for HUDSON, in combined with instrumental requirement, making the technique less attractive for field deployable diagnostics (88). On the other hand, as mentioned in Kellner et al., (36), the high temperature demand may reduce non-specific effects. However, the LAMP technique has also shown a nonspecific signal patterns (94) as for RPA shown in previous experiments in this thesis (Figure 3.11). When running one pot-LAMP reactions, the Cas enzymes also need thermostability, besides the polymerases (37,92). This might seem achievable when considering diagnostic purposes for rapid SARS-CoV-2 detection as it requires low-cost instruments and reagents. However, LAMP suffers from its methodically complexity, requiring extensive primer design and both primers and multiple crRNAs must be screened to achieve good amplification (88,119).

Another great advantage of the SHERLOCK platform is its ability to detect any bacterial pathogen or virus, just by implementing specific spacer sequences in the crRNAs complementary to the target of interest (36,40). Further, by choosing Cas13 enzymes, there are no requirements for specific PAM sequences flanking the target, as Cas12 enzymes need for activation of cleavage (41). This makes SHERLOCK more versatile compared to DETECTR and HOLMES which utilizes Cas12 enzymes (41,87). On the other hand, the DETECTR and HOLMES platforms does not need T7 transcription as Cas12 enzymes are DNA specific which gives the platform reduced complexity.

4.13 Conclusion and future perspectives

Given the global health issue caused by the ongoing global pandemic (SARS-CoV-2) that pervades today's society, rapid and robust infection detection is important in reducing virus spread. A wider range of diagnostic platforms can help strengthen the health care system for subsequent global health crisis but also in general concerning patients with severe acute infections.

The purpose of this thesis was to establish a CRISPR-Cas13 based platform at the University hospital in Oslo as a rapid and sensitive diagnostic tool for SARS-CoV-2 detection This thesis demonstrates the challenges of establishing such a tool with results indicating that the currently established platform is not as sensitive as the RT-qPCR method (Figure 3.14B). Instrumental, and reaction condition optimization has shown to be important to achieve high sensitivity in SHERLOCK when using fluorescence-based monitoring (Figure 3.1). This thesis along with previous finding elucidates the potential of SHERLOCK (36,40,42,81,117). Within one hour, we obtained significant detectable signal from SARS-CoV-2 samples equal to a Ct value of 33,2 when using the novel MSA_T1 sequence as target (Figure 3.10A-B). SHERLOCK managed to detect 60/72 SARS-CoV-2 samples with *orf1ab* as target resulting in 86% positive 95% negative predictive agreement with RT-qPCR analysis of the SARS-CoV-2 *E-gene*. The road to a full-fledged SHERLOCK establishment at OUH may be shorter, but there is still a lot of data that needs to be produced including a sequence analysis of biproducts generated by RPA as these additional reactions have demonstrated a great influence the SHERLOCK assay. In conclusion, the SHERLOCK platform stands as a promising tool for the detection of virus or bacteria in future diagnostics, with the potential to reach higher sensitivity than currently used diagnostic methods like RT-qPCR.

What remains a problem is that anti-microbial genes who are detected, does not always derive from the actual pathogenic species that cause infection. Another problem with molecular diagnostic tests is that they cannot determine if the foreign nucleic acids originated from active or dead viruses or bacteria. Further, there is uncertainty that the clinical samples taken come from the actual site of infection. The ultimate goal would be a platform compatible for personalized medicine, with accurate disease diagnostics including individualized treatment strategies at point of care. The development of a system that could rapidly process sequence data directly from a clinical sample would be the perfect diagnostic tool.

5 Reference list

1. Opota O, Croxatto A, Prod'hom G, Greub G. Blood culture-based diagnosis of bacteraemia: State of the art. Vol. 21, Clinical Microbiology and Infection. Elsevier; 2015. p. 313–22.
2. Murray PR, Masur H. Current approaches to the diagnosis of bacterial and fungal bloodstream infections in the intensive care unit. Crit Care Med. 2012 Dec;40(12):3277–82. Available from: /pmc/articles/PMC4201853/?report=abstract
3. Franco-Duarte R, Černáková L, Kadam S, Kaushik KS, Salehi B, Bevilacqua A, et al. Advances in chemical and biological methods to identify microorganisms—from past to present. Vol. 7, Microorganisms. MDPI AG; 2019. p. 130. Available from: /pmc/articles/PMC6560418/?report=abstract
4. Higuchi R, Fockler C, Dollinger G, Watson R. Kinetic PCR analysis: Real-time monitoring of DNA amplification reactions. Bio/Technology. 1993;11(9):1026–30. Available from: https://pubmed.ncbi.nlm.nih.gov/7764001/
5. Dingle TC, Butler-Wu SM. MALDI-TOF mass spectrometry for microorganism identification. Vol. 33, Clinics in Laboratory Medicine. Clin Lab Med; 2013. p. 589–609. Available from: https://pubmed.ncbi.nlm.nih.gov/23931840/
6. Fan SL, Miller NS, Lee J, Remick DG. Diagnosing sepsis – The role of laboratory medicine. Vol. 460, Clinica Chimica Acta. Elsevier B.V.; 2016. p. 203–10. Available from: /pmc/articles/PMC4980259/?report=abstract
7. Buszewski B, Rogowska A, Pomastowski P, Złoch M, Railean-Plugaru V. Identification of Microorganisms by Modern Analytical Techniques. J AOAC Int [Internet]. 2017 Nov 1 [cited 2020 Dec 1];100(6):1607–23. Available from: https://academic.oup.com/jaoac/article/100/6/1607-1623/5654264
8. World Health Organization W. Antimicrobial resistance [Internet]. [cited 2020 Dec 1]. Available from: https://www.who.int/health-topics/antimicrobial-resistance
9. Previsdomini M, Gini M, Cerutti B, Dolina M, Perren A. Predictors of positive blood cultures in critically ill patients: A retrospective evaluation. Croat Med J [Internet]. 2012 Feb [cited 2020 Dec 1];53(1):30–9. Available from: /pmc/articles/PMC3284177/?report=abstract
10. Van Vught LAV, Klouwenberg PMCK, Spitoni C, Scicluna BP, Wiewel MA, Horn J, et al. Incidence, risk factors, and attributable mortality of secondary infections in the intensive care unit after admission for sepsis. JAMA - J Am Med Assoc. 2016 Apr 12;315(14):1469–79.
11. Schwenzer KJ, Gist A, Durbin CG. Can bacteremia be predicted in surgical intensive care unit patients? Intensive Care Med [Internet]. 1994 Jul [cited 2020 Dec 6];20(6):425–30. Available from: https://link.springer.com/article/10.1007/BF01710653
12. U.S Food and Drug Administration. Coronavirus Disease 2019 Testing Basics. 2020;(October). Available from: www.fda.gov
13. Johns Hopkins University & Medicine. COVID-19 Map [Internet]. Johns Hopkins Coronavirus Resource Center. 2020 [cited 2020 Dec 1]. Available from: https://coronavirus.jhu.edu/map.html
14. Helsedirektoratet. Testkapasitet for Covid-19 sykdom [Internet]. 2020 Apr [cited 2020 Nov 27]. Available from: https://www.helsedirektoratet.no/rapporter/testkapasitet-for-covid-19-sykdom/Testkapasitet - status i tjenesten, identifisering av flaskehalser og potensialet for økt testkapasitet i fremtiden.pdf/_/attachment/inline/19a154a3-4b88-41f2-b065-42be469ecbee:8
15. World Health Organization W. Coronavirus - Symptoms [Internet]. 2020. Available from: https://www.who.int/health-topics/coronavirus#tab=tab_3
16. Burrell CJ, Howard CR, Murphy FA. Coronaviruses. In: Fenner and White's Medical Virology [Internet]. Elsevier; 2017 [cited 2020 Dec 6]. p. 437–46. Available from: https://linkinghub.elsevier.com/retrieve/pii/B978012375156000031X
17. Blanco-Melo D, Nilsson-Payant BE, Liu WC, Uhl S, Hoagland D, Møller R, et al. Imbalanced Host Response to SARS-CoV-2 Drives Development of COVID-19. Cell. 2020 May 28;181(5):1036-1045.e9.
18. Alagaili AN, Briese T, Mishra N, Kapoor V, Sameroff SC, de Wit E, et al. Middle east respiratory syndrome coronavirus infection in dromedary camels in Saudi Arabia. MBio. 2014;5(2):1–6.
19. World Health Organization W. Severe Acute Respiratory Syndrome (SARS) [Internet]. World Health Organization. Available from: https://www.who.int/health-topics/severe-acute-respiratory-syndrome#tab=tab_1
20. Zhou P, Yang X Lou, Wang XG, Hu B, Zhang L, Zhang W, et al. A pneumonia outbreak associated with a new coronavirus of probable bat origin. Nature [Internet]. 2020;579(7798):270–3. Available from: http://dx.doi.org/10.1038/s41586-020-2012-7
21. Cui J, Li F, Shi ZL. Origin and evolution of pathogenic coronaviruses. Nat Rev Microbiol [Internet]. 2019;17(3):181–92. Available from: http://dx.doi.org/10.1038/s41579-018-0118-9
22. Forni D, Cagliani R, Clerici M, Sironi M. Molecular Evolution of Human Coronavirus Genomes

[Internet]. Vol. 25, Trends in Microbiology. Elsevier Ltd; 2017 [cited 2020 Nov 15]. p. 35–48. Available from: /pmc/articles/PMC7111218/?report=abstract

23. Lu R, Zhao X, Li J, Niu P, Yang B, Wu H, et al. Genomic characterisation and epidemiology of 2019 novel coronavirus: implications for virus origins and receptor binding. Lancet [Internet]. 2020 Feb 22 [cited 2020 Nov 15];395(10224):565–74. Available from: http://dx.doi.org/10.1016/S0140-6736(20)30251-8

24. Su S, Wong G, Shi W, Liu J, Lai ACK, Zhou J, et al. Epidemiology, Genetic Recombination, and Pathogenesis of Coronaviruses [Internet]. Vol. 24, Trends in Microbiology. Elsevier Ltd; 2016 [cited 2020 Dec 5]. p. 490–502. Available from: /pmc/articles/PMC7125511/?report=abstract

25. Kim D, Lee JY, Yang JS, Kim JW, Kim VN, Chang H. The Architecture of SARS-CoV-2 Transcriptome. Cell. 2020 May 14;181(4):914-921.e10.

26. Toms D, Li J, Cai H. Evaluation of WHO listed COVID-19 qPCR primers and probe in silico with 375 SERS-CoV-2 full genome sequences. medRxiv [Internet]. 2020 Apr 28 [cited 2020 Nov 15];2020.04.22.20075697. Available from: https://doi.org/10.1101/2020.04.22.20075697

27. National Institute of Health. Testing for SARS-CoV-2 Infection [Internet]. 2020. Available from: https://www.covid19treatmentguidelines.nih.gov/overview/sars-cov-2-testing

28. Heid CA, Stevens J, Livak KJ, Williams PM. Real time quantitative PCR. Genome Res [Internet]. 1996 [cited 2020 Dec 1];6(10):986–94. Available from: https://pubmed.ncbi.nlm.nih.gov/8908518/

29. Corman VM, Landt O, Kaiser M, Molenkamp R, Meijer A, Chu DKW, et al. Detection of 2019 novel coronavirus (2019-nCoV) by real-time RT-PCR. Eurosurveillance [Internet]. 2020 Jan 23 [cited 2020 Nov 15];25(3). Available from: /pmc/articles/PMC6988269/?report=abstract

30. Kudo E, Id BI, Id CBFV, Id PL, Id LW, Tokuyama M, et al. Detection of SARS-CoV-2 RNA by multiplex RT- qPCR. PLOS Biol [Internet]. 2020;1–9. Available from: http://dx.doi.org/10.1371/journal.pbio.3000867

31. Chu DKW, Pan Y, Cheng SMS, Hui KPY, Krishnan P, Liu Y. Molecular Diagnosis of a Novel Coronavirus (2019-nCoV) Causing an Outbreak of Pneumonia. 2020;555:549–55.

32. World Health Organization W. Summary of available protocols for SARS-CoV-2 diagnostics [Internet]. 2020. Available from: https://www.who.int/docs/default-source/coronaviruse/whoinhouseassays.pdf

33. Park M, Won J, Choi BY, Lee CJ. Optimization of primer sets and detection protocols for SARS-CoV-2 of coronavirus disease 2019 (COVID-19) using PCR and real-time PCR. Exp Mol Med [Internet]. 2020;52(6):963–77. Available from: http://dx.doi.org/10.1038/s12276-020-0452-7

34. Sampson VB. Laboratory Testing Methods for Novel Severe Acute Respiratory. 2020;8(June):1–11.

35. Burbelo PD, Iadarola MJ, Chaturvedi A. Emerging technologies for the detection of viral infections [Internet]. Vol. 14, Future Virology. Future Medicine Ltd.; 2019 [cited 2020 Dec 1]. p. 39–49. Available from: /pmc/articles/PMC6956246/?report=abstract

36. Kellner MJ, Koob JG, Gootenberg JS, Abudayyeh OO, Zhang F. SHERLOCK: nucleic acid detection with CRISPR nucleases. Nat Protoc [Internet]. 2019;14(10):2986–3012. Available from: http://dx.doi.org/10.1038/s41596-019-0210-2

37. Joung J, Ladha A, Saito M, Segel M, Bruneau R, Huang M, et al. Point-of-care testing for COVID-19 using SHERLOCK diagnostics. medRxiv Prepr Serv Heal Sci. 2020;

38. The Nobel Committee for Chemistry. The Nobel Prize in Chemistry 2020 - Popular information [Internet]. 2020 [cited 2020 Dec 2]. Available from: https://www.nobelprize.org/prizes/chemistry/2020/popular-information/

39. Jinek M, Chylinski K, Fonfara I, Hauer M, Doudna JA, Charpentier E. A programmable dual-RNA-guided DNA endonuclease in adaptive bacterial immunity. Science (80-) [Internet]. 2012 Aug 17 [cited 2020 Nov 23];337(6096):816–21. Available from: http://science.sciencemag.org/

40. Gootenberg JS, Abudayyeh OO, Lee JW, Essletzbichler P, Dy AJ, Joung J, et al. Nucleic acid detection with CRISPR-Cas13a/C2c2. Science [Internet]. 2017 Apr 28;356(6336):438–42. Available from: https://www.sciencemag.org/lookup/doi/10.1126/science.aam9321

41. Chen JS, Ma E, Harrington LB, Da Costa M, Tian X, Palefsky JM, et al. CRISPR-Cas12a target binding unleashes indiscriminate single-stranded DNase activity. Science (80-) [Internet]. 2018 Apr 27 [cited 2020 Nov 10];360(6387):436–9. Available from: https://pubmed.ncbi.nlm.nih.gov/29449511/

42. Gootenberg JS, Abudayyeh OO, Kellner MJ, Joung J, Collins JJ, Zhang F. Multiplexed and portable nucleic acid detection platform with Cas13, Cas12a and Csm6. Science (80-). 2018;360(6387):439–44.

43. Jansen R, Van Embden JDA, Gaastra W, Schouls LM. Identification of genes that are associated with DNA repeats in prokaryotes. Mol Microbiol [Internet]. 2002 Mar 1 [cited 2020 Nov 15];43(6):1565–75. Available from: https://onlinelibrary.wiley.com/doi/full/10.1046/j.1365-2958.2002.02839.x

44. Ishino Y, Shinagawa H, Makino K, Amemura M, Nakatura A. Nucleotide sequence of the iap gene, responsible for alkaline phosphatase isoenzyme conversion in Escherichia coli, and identification of the gene product. J Bacteriol [Internet]. 1987 Dec 1 [cited 2020 Dec 6];169(12):5429–33. Available from:

http://jb.asm.org/

45. Makarova KS, Wolf YI, Koonin E V. Comparative genomics of defense systems in archaea and bacteria. Nucleic Acids Res [Internet]. 2013 Apr [cited 2020 Nov 16];41(8):4360–77. Available from: https://pubmed.ncbi.nlm.nih.gov/23470997/

46. Mojica FJM, Ferrer C, Juez G, Rodríguez-Valera F. Long stretches of short tandem repeats are present in the largest replicons of the Archaea Haloferax mediterranei and Haloferax volcanii and could be involved in replicon partitioning. Mol Microbiol [Internet]. 1995 [cited 2020 Nov 16];17(1):85–93. Available from: https://pubmed.ncbi.nlm.nih.gov/7476211/

47. Horvath P, Barrangou R. CRISPR/Cas, the immune system of Bacteria and Archaea [Internet]. Science American Association for the Advancement of Science; Jan 8, 2010 p. 167–70. Available from: http://science.sciencemag.org/

48. Bolotin A, Quinquis B, Sorokin A, Dusko Ehrlich S. Clustered regularly interspaced short palindrome repeats (CRISPRs) have spacers of extrachromosomal origin. Microbiology [Internet]. 2005 Aug 1 [cited 2020 Dec 6];151(8):2551–61. Available from: https://www.microbiologyresearch.org/content/journal/micro/10.1099/mic.0.28048-0

49. Makarova KS, Grishin N V., Shabalina SA, Wolf YI, Koonin E V. A putative RNA-interference-based immune system in prokaryotes: Computational analysis of the predicted enzymatic machinery, functional analogies with eukaryotic RNAi, and hypothetical mechanisms of action [Internet]. Vol. 1, Biology Direct. Biol Direct; 2006 [cited 2020 Nov 16]. Available from: https://pubmed.ncbi.nlm.nih.gov/16545108/

50. Grissa I, Vergnaud G, Pourcel C. The CRISPRdb database and tools to display CRISPRs and to generate dictionaries of spacers and repeats. BMC Bioinformatics [Internet]. 2007 May 23 [cited 2020 Nov 16];8. Available from: https://pubmed.ncbi.nlm.nih.gov/17521438/

51. Mojica FJM, Díez-Villaseñor C, Soria E, Juez G. Biological significance of a family of regularly spaced repeats in the genomes of Archaea, Bacteria and mitochondria [Internet]. Vol. 36, Molecular Microbiology. Mol Microbiol; 2000 [cited 2020 Nov 16]. p. 244–6. Available from: https://pubmed.ncbi.nlm.nih.gov/10760181/

52. Mojica FJM, Díez-Villaseñor C, García-Martínez J, Soria E. Intervening sequences of regularly spaced prokaryotic repeats derive from foreign genetic elements. J Mol Evol [Internet]. 2005 Feb [cited 2020 Dec 6];60(2):174–82. Available from: https://link.springer.com/article/10.1007/s00239-004-0046-3

53. Lillestøl RK, Redder P, Garrett RA, Brügger K. A putative viral defence mechanism in archaeal cells. Archaea [Internet]. 2006 [cited 2020 Nov 16];2(1):59–72. Available from: /pmc/articles/PMC2685585/?report=abstract

54. Haft DH, Selengut J, Mongodin EF, Nelson KE. A Guild of 45 CRISPR-Associated (Cas) Protein Families and Multiple CRISPR/Cas Subtypes Exist in Prokaryotic Genomes. Eisen JA, editor. PLoS Comput Biol [Internet]. 2005 Nov 11 [cited 2020 Nov 16];1(6):e60. Available from: https://dx.plos.org/10.1371/journal.pcbi.0010060

55. Pourcel C, Salvignol G, Vergnaud G. CRISPR elements in Yersinia pestis acquire new repeats by preferential uptake of bacteriophage DNA, and provide additional tools for evolutionary studies. Microbiology [Internet]. 2005;151(3):653–63. Available from: https://www.microbiologyresearch.org/content/journal/micro/10.1099/mic.0.27437-0

56. Barrangou R, Fremaux C, Deveau H, Richards M, Boyaval P, Moineau S, et al. CRISPR provides acquired resistance against viruses in prokaryotes. Science (80-) [Internet]. 2007 Mar 23 [cited 2020 Nov 16];315(5819):1709–12. Available from: https://pubmed.ncbi.nlm.nih.gov/17379808/

57. Deveau H, Barrangou R, Garneau JE, Labonté J, Fremaux C, Boyaval P, et al. Phage Response to CRISPR-Encoded Resistance in Streptococcus thermophilus. J Bacteriol [Internet]. 2008 [cited 2020 Dec 6];190(4):1390–400. Available from: http://www.ncbi.nlm.nih.gov/gorf/gorf.html

58. Horvath P, Romero DA, Coûté-Monvoisin AC, Richards M, Deveau H, Moineau S, et al. Diversity, activity, and evolution of CRISPR loci in Streptococcus thermophilus. J Bacteriol [Internet]. 2008 Feb [cited 2020 Dec 6];190(4):1401–12. Available from: /pmc/articles/PMC2238196/?report=abstract

59. Brouns SJJ, Jore MM, Lundgren M, Westra ER, Slijkhuis RJH, Snijders APL, et al. Small CRISPR RNAs guide antiviral defense in prokaryotes. Science (80-) [Internet]. 2008 Aug 15 [cited 2020 Nov 16];321(5891):960–4. Available from: https://science.sciencemag.org/content/321/5891/960

60. Marraffini LA, Sontheimer EJ. CRISPR interference: RNA-directed adaptive immunity in bacteria and archaea [Internet]. Vol. 11, Nature Reviews Genetics. NIH Public Access; 2010 [cited 2020 Dec 6]. p. 181–90. Available from: /pmc/articles/PMC2928866/?report=abstract

61. Deveau H, Garneau JE, Moineau S. CRISPR/Cas system and its role in phage-bacteria interactions [Internet]. Vol. 64, Annual Review of Microbiology. Annu Rev Microbiol; 2010 [cited 2020 Nov 23]. p. 475–93. Available from: https://pubmed.ncbi.nlm.nih.gov/20528693/

62. Jiang F, Doudna JA. CRISPR-Cas9 Structures and Mechanisms [Internet]. Vol. 46, Annual Review of

Biophysics. Annual Reviews Inc.; 2017 [cited 2020 Dec 7]. p. 505–29. Available from: https://doi.org/10.1146/annurev-biophys-

63. Kunin V, Sorek R, Hugenholtz P. Evolutionary conservation of sequence and secondary structures in CRISPR repeats. Genome Biol [Internet]. 2007 Apr 18 [cited 2020 Nov 16];8(4). Available from: https://pubmed.ncbi.nlm.nih.gov/17442114/

64. Mojica FJM, Díez-Villaseñor C, García-Martínez J, Almendros C. Short motif sequences determine the targets of the prokaryotic CRISPR defence system. Microbiology [Internet]. 2009 [cited 2020 Nov 16];155(3):733–40. Available from: https://pubmed.ncbi.nlm.nih.gov/19246744/

65. Doudna Lab. CRISPR Systems [Internet]. 2020. Available from: https://doudnalab.org/research_areas/crispr-systems/

66. Shmakov S, Smargon A, Scott D, Cox D, Pyzocha N, Yan W, et al. Diversity and evolution of class 2 CRISPR-Cas systems. Nat Rev Microbiol [Internet]. 2017;15(3):169–82. Available from: https://www.nature.com/articles/nrmicro.2016.184

67. Konermann S, Lotfy P, Brideau NJ, Oki J, Shokhirev MN, Hsu PD. Transcriptome Engineering with RNA-Targeting Type VI-D CRISPR Effectors. Cell. 2018 Apr 19;173(3):665-676.e14.

68. Yan WX, Chong S, Zhang H, Makarova KS, Koonin E V., Cheng DR, et al. Cas13d Is a Compact RNA-Targeting Type VI CRISPR Effector Positively Modulated by a WYL-Domain-Containing Accessory Protein. Mol Cell. 2018 Apr 19;70(2):327-339.e5.

69. Makarova KS, Koonin E V. Annotation and classification of CRISPR-Cas systems. Methods Mol Biol [Internet]. 2015 [cited 2020 Nov 16];1311:47–75. Available from: /pmc/articles/PMC5901762/?report=abstract

70. Shmakov S, Abudayyeh OO, Makarova KS, Wolf YI, Jonathan S, Semenova E, et al. Discovery and functional characterization of diverse Class 2 CRISPR-Cas systems. Mol Cell. 2015;60(3):385–97.

71. Karginov F V., Hannon GJ. The CRISPR System: Small RNA-Guided Defense in Bacteria and Archaea. Vol. 37, Molecular Cell. Cell Press; 2010. p. 7–19.

72. Abudayyeh OO, Gootenberg JS, Konermann S et al. C2c2 is a single-component programmable RNA-guided RNA-targeting CRISPR effector. 2016;353(6299):1–23. Available from: https://www.ncbi.nlm.nih.gov/pmc/articles/PMC5706658/pdf/nihms920681.pdf

73. Smargon AA, Cox DBT, Pyzocha NK, Zheng K, Slaymaker IM, Gootenberg JS, et al. Cas13b Is a Type VI-B CRISPR-Associated RNA-Guided RNase Differentially Regulated by Accessory Proteins Csx27 and Csx28. Mol Cell [Internet]. 2017 Feb 16 [cited 2020 Nov 16];65(4):618-630.e7. Available from: https://pubmed.ncbi.nlm.nih.gov/28065598/

74. Liu L, Li X, Ma J, Li Z, You L, Wang J, et al. The Molecular Architecture for RNA-Guided RNA Cleavage by Cas13a. Cell [Internet]. 2017;170(4):714-726.e10. Available from: http://dx.doi.org/10.1016/j.cell.2017.06.050

75. Zetsche B, Gootenberg JS, Abudayyeh OO, Slaymaker IM, Makarova KS, Essletzbichler P, et al. Cpf1 Is a Single RNA-Guided Endonuclease of a Class 2 CRISPR-Cas System. Cell [Internet]. 2015 Oct 22 [cited 2020 Nov 23];163(3):759–71. Available from: http://dx.doi.org/10.1016/j.cell.2015.09.038http://dx.doi.org/10.1016/j.cell.2015.09.038

76. Anders C, Niewoehner O, Duerst A, Jinek M. Structural basis of PAM-dependent target DNA recognition by the Cas9 endonuclease. Nature [Internet]. 2015;513(7519):569–73. Available from: http://dx.doi.org/10.1038/nature13579%0Apapers3://publication/doi/10.1038/nature13579

77. Zhang B, Ye Y, Ye W, Perčulija V, Jiang H, Chen Y, et al. Two HEPN domains dictate CRISPR RNA maturation and target cleavage in Cas13d. Nat Commun [Internet]. 2019;10(1). Available from: https://www.nature.com/articles/s41467-019-10507-3

78. O'Connell MR. Molecular Mechanisms of RNA Targeting by Cas13-containing Type VI CRISPR–Cas Systems. J Mol Biol [Internet]. 2019;431(1):66–87. Available from: https://doi.org/10.1016/j.jmb.2018.06.029

79. Abudayyeh OO, Gootenberg JS, Essletzbichler P, Han S, Joung J, Belanto JJ, et al. RNA targeting with CRISPR-Cas13. Nature [Internet]. 2017 Oct 12 [cited 2020 Oct 30];550(7675):280–4. Available from: /pmc/articles/PMC5706658/?report=abstract

80. Murugan K, Seetharam AS, Severin AJ, Sashital DG. CRISPR-Cas12a has widespread off-target and dsDNA-nicking effects [Internet]. Vol. 295, Journal of Biological Chemistry. American Society for Biochemistry and Molecular Biology Inc.; 2020 [cited 2020 Nov 16]. p. 5538–53. Available from: http://www.jbc.org/

81. Myhrvold C, Freije CA, Gootenberg JS, Abudayyeh OO, Metsky HC, Durbin AF, et al. Field-deployable viral diagnostics using CRISPR-Cas13. Science (80-). 2018;360(6387):444–8.

82. Abudayyeh OO, Gootenberg JS. Cas13 — Zhang Lab [Internet]. [cited 2020 Nov 13]. Available from: https://zlab.bio/cas13

83. Piepenburg O, Williams CH, Stemple DL, Armes NA. DNA detection using recombination proteins.

PLoS Biol. 2006;4(7):1115–21.

84. TwistDx^TM. RPA. The versatile PCR replacement [Internet]. Available from: https://www.twistdx.co.uk/en/rpa

85. TwistDx^TM Limited. TwistAmp® DNA Amplification Kits Assay Design Manual. 2018 [cited 2020 Nov 1];1–32. Available from: https://www.twistdx.co.uk/docs/default-source/RPA-assay-design/twistamp-assay-design-manual-v2-5.pdf?sfvrsn=29

86. Addgene. Finding nucleic acids with SHERLOCK and DETECTR [Internet]. Addgene blog. 2020. Available from: https://blog.addgene.org/finding-nucleic-acids-with-sherlock-and-detectr?_ga=2.33281854.1855698696.1595795714-1796050122.1589894122

87. Li SY, Cheng QX, Li XY, Zhang ZL, Gao S, Cao RB, et al. CRISPR-Cas12a-assisted nucleic acid detection [Internet]. Vol. 4, Cell Discovery. Nature Publishing Groups; 2018 [cited 2020 Nov 10]. Available from: https://pubmed.ncbi.nlm.nih.gov/29707234/

88. Notomi T, Okayama H, Masubuchi H, Yonekawa T, Watanabe K, Amino N, et al. Loop-mediated isothermal amplification of DNA. Nucleic Acids Res [Internet]. 2000 [cited 2020 Nov 5];28(12):e63. Available from: /pmc/articles/PMC102748/?report=abstract

89. Broughton JP, Deng X, Yu G, Fasching CL, Servellita V, Singh J, et al. CRISPR–Cas12-based detection of SARS-CoV-2. Nat Biotechnol [Internet]. 2020;38(7):870–4. Available from: http://dx.doi.org/10.1038/s41587-020-0513-4

90. Schermer B, Fabretti F, Damagnez M, Di Cristanziano V, Heger E, Arjune S, et al. Rapid SARS-CoV-2 testing in primary material based on a novel multiplex RT-LAMP assay. PLoS One [Internet]. 2020;15(11 November):1–26. Available from: https://www.medrxiv.org/content/10.1101/2020.06.18.20130377v1.full.pdf

91. Tanner N. Optimized Integration of New England Biolabs ® Loop-mediated Isothermal Amplification (LAMP) Reagents with Axxin ISO Instruments. 2019.

92. Li L, Li S, Wang J. CRISPR-Cas12b-assisted nucleic acid detection platform. bioRxiv [Internet]. 2018 Jul 6 [cited 2020 Nov 10];362889. Available from: https://doi.org/10.1101/362889

93. Zhang F, Abudayyeh OO, Gootenberg JS, Sciences C, Mathers L. A protocol for detection of COVID-19 using CRISPR diagnostics. Bioarchive. 2020;1–8.

94. Joung J, Ladha A, Saito M, Kim N-G, Woolley AE, Segel M, et al. Detection of SARS-CoV-2 with SHERLOCK One-Pot Testing, supplementary appendix. N Engl J Med. 2020;383(15):1492–4.

95. Ambion by life technologies(TM). MEGAscript ® Kit - Phenol : chloroform purification [Internet]. 2012 [cited 2020 Nov 1]. p. 11–2. Available from: http://tools.thermofisher.com/content/sfs/manuals/1330M_G.pdf

96. Thermo Fisher Scientific. The Basics: RNA Isolation [Internet]. Thermo Fisher Scientific. [cited 2020 Dec 3]. Available from: https://www.thermofisher.com/no/en/home/references/ambion-tech-support/rna-isolation/general-articles/the-basics-rna-isolation.html

97. Chomczynski P, Sacchi N. The single-step method of RNA isolation by acid guanidinium thiocyanate-phenol-chloroform extraction: Twenty-something years on. Nat Protoc. 2006 Jul;1(2):581–5.

98. NTNU- Norwegian University of Science and Technology. Norwegian COVID-19 test to be used in India and Denmark. Partner.sciencenorway.no [Internet]. 2020 Sep [cited 2020 Nov 27]; Available from: https://partner.sciencenorway.no/covid19-epidemic-health/norwegian-covid-19-test-to-be-used-in-india-and-denmark/1747475

99. QIAGEN. QIAquick® Gel Extraction Kit. 2018;23–4. Available from: https://www.qiagen.com/cn/resources/download.aspx?id=a72e2c07-7816-436f-b920-98a0ede5159a&lang=en

100. Lucia C, Federico P-B, Alejandra GC. An ultrasensitive, rapid, and portable coronavirus SARS-CoV-2 sequence detection method based on CRISPR-Cas12. bioRxiv [Internet]. 2020 Mar 2 [cited 2020 Nov 3];2020.02.29.971127. Available from: https://doi.org/10.1101/2020.02.29.971127

101. Paul S, Stang A, Lennartz K, Tenbusch M, Überla K. Selection of a T7 promoter mutant with enhanced in vitro activity by a novel multi-copy bead display approach for in vitro evolution. Nucleic Acids Res. 2013;41(1):1–11.

102. Zilberstein D, Agmon V, Schuldiner S, Padan E. Escherichia coli intracellular pH, membrane potential, and cell growth. J Bacteriol [Internet]. 1984;158(1):246–52. Available from: https://www.ncbi.nlm.nih.gov/pmc/articles/PMC215405/pdf/jbacter00233-0254.pdf

103. Armbruster DA, Pry T. Limit of Blank, Limit of Detection and Limit of Quantitation. Vol. 29, Clin Biochem Rev. 2008.

104. Takara Bio USA Inc. Guide-it ^TM sgRNA In Vitro Transcription and Screening Systems User Manual. 2017;(0):9. Available from: takarabio.com

105. Promega Biotech AB. Which Plates Should I Choose for Fluorescence and Luminescence Measurements? Promega Biotech AB [Internet]. [cited 2020 Nov 27]; Available from:

       https://no.promega.com/Resources/PubHub/which-plates-to-choose-for-fluorescence-and-luminescence-measurements/

106. PerkinElmer Inc. Microplates For Fluorescence Assays | Lab Products & Services | PerkinElmer [Internet]. PerkinElmer. [cited 2020 Nov 14]. Available from: https://www.perkinelmer.com/no/lab-products-and-services/application-support-knowledgebase/microplates/fluorescence-plates.html#Microplatesforfluorescenceassays-Autofluorescence

107. Berthold Technologies GmbH & Co.KG. MINIMISING CROSSTALK [Internet]. Berthold Technologies mbH & Co.KG - Magazine. 2020. Available from: https://www.berthold.com/en/bioanalytic/knowledge/magazine/minimising-crosstalk/

108. ThermoFisher Scientific. Photobleaching Principles [Internet]. Thermo Fisher Scientific - NO. [cited 2020 Nov 27]. Available from: https://www.thermofisher.com/no/en/home/life-science/cell-analysis/cell-analysis-learning-center/molecular-probes-school-of-fluorescence/fluorescence-basics/fluorescence-fundamentals/photobleaching-principles.html

109. Yan M. How to Minimize Photobleaching - Enzo Life Sciences, Inc. [Internet]. Enzo Life Sciences, Inc. 2018 [cited 2020 Nov 27]. Available from: https://www.enzolifesciences.com/science-center/technotes/2018/december/how-to-minimize-photobleaching/

110. Shen Z, Scholz WK, Nanda SKW, Whittlinger KO, Chen S, Sullivan BM. Nunc 384-Well Plate Design and Performance Evaluation - Cole-Parmer scientific experts [Internet]. Coleparmer.com. 2019 [cited 2020 Nov 14]. Available from: https://www.coleparmer.com/tech-article/nunc-384-well-plate-design-and-performance

111. Stokes GG. On the Change of Refrangibility of Light. Philos Trans R Soc London [Internet]. 1852 [cited 2020 Nov 13];142:463–562. Available from: https://www.jstor.org/stable/108550?seq=1#metadata_info_tab_contents

112. Ockenga W. Fluorescence in Microscopy [Internet]. Tutorial. Philipps University Marburg, Institute of Cytobiology and Cytopathology, Germany; 2011 [cited 2020 Nov 26]. Available from: https://www.leica-microsystems.com/science-lab/fluorescence-in-microscopy/

113. Ferreira CMH, Pinto ISS, Soares E V., Soares HMVM. (Un)suitability of the use of pH buffers in biological, biochemical and environmental studies and their interaction with metal ions-a review. RSC Adv [Internet]. 2015;5(39):30989–1003. Available from: http://dx.doi.org/10.1039/C4RA15453C

114. Fonfara I, Richter H, BratoviÄ M, Le Rhun A, Charpentier E. The CRISPR-associated DNA-cleaving enzyme Cpf1 also processes precursor CRISPR RNA. Nature. 2016;532(7600):517–21.

115. Dong D, Ren K, Qiu X, Zheng J, Guo M, Guan X, et al. The crystal structure of Cpf1 in complex with CRISPR RNA. Nature [Internet]. 2016 Apr 28 [cited 2020 Oct 29];532(7600):522–6. Available from: https://www.nature.com/articles/nature17944

116. World Health Organization W. Dos and Don'ts for molecular testing [Internet]. World Health Organization. World Health Organization; 2018 [cited 2020 Oct 30]. Available from: http://www.who.int/malaria/areas/diagnosis/molecular-testing-dos-donts/en/

117. Joung J, Ladha A, Saito M, Kim N-G, Woolley AE, Segel M, et al. Detection of SARS-CoV-2 with SHERLOCK One-Pot Testing. N Engl J Med [Internet]. 2020 Oct 8 [cited 2020 Nov 5];383(15):1492–4. Available from: https://www.nejm.org/doi/full/10.1056/NEJMc2026172

118. Broughton JP, Deng W, Fasching CL, Singh J, Chiu CY, Chen JS, et al. A protocol for rapid detection of the 2019 novel coronavirus SARS-CoV-2 using CRISPR diagnostics: SARS-CoV-2 DETECTR [Internet]. Bioarchive. 2020 [cited 2020 Nov 3]. Available from: https://www.synthego.com/publications/a-protocol-for-rapid-detection-of-the-2019-novel-coronavirus-sars-cov-2-using-crispr-diagnostics-sars-cov-2-detectr

119. Kashir J, Yaqinuddin A. Loop mediated isothermal amplification (LAMP) assays as a rapid diagnostic for COVID-19. Med Hypotheses [Internet]. 2020;141(March):109786. Available from: https://doi.org/10.1016/j.mehy.2020.109786

Table of contents – Appendix

Appendix A. Materials

All laboratory equipment, chemicals, kits, molecular markers, solutions, buffers, and gels used in the experimental part in this thesis are listed in tables below (Table A1-6).

Table A1 Lab equipment used in the experimental part in this thesis including product names, respective manufacturers, and catalogue numbers.

EQUIPMENT	MODEL	MANUFACTURER
SPECTROPHOTOMETERS	NanoDrop™ One/One^c Microvolume UV-Vis	Thermo Fisher scientific
	Qubit®2.0 Fluorometer	Invitrogen™
CENTRIFUGES	Avanti®Centrifuge J-26XP	Beckman Coultier™
	Eppendorf Centrifuge 5418 R	Eppendorf
	Spectrafuge Mini Centrifuge C1301-230V	Labnet International Inc.
	Microcentrifuge, MiniStar silverline	VWR™
	MEGA Star 1.6R Centrifuge	VWR™
INCUBATORS	Peltier Thermal cycler (PTC-200)	MJ research
	Thermal cycler 2720	Applied Biosystems
	Innova™4230 Refrigerated incubator shaker	New Brunswick Scientific
	Block Heater SBH130D	Stuart®
STERILE HOODS	Zafe 82 1200	Zystm A/S
	Safe 2020, Class II Biological Safety Cabinet	Thermofisher Scientific
GEL ELECTROPHORESIS CHAMBERS	Min Gel tank	Invitrogen™
	Mini-PROTEAN® II Electrophoresis	BIO-RAD
	GIBCO-BRL Horizon®58 Horizontal Gel Electrophoresis System	Life Technologies ™
OTHER		
Plate reader	Victor ® Nivo™ Multimode Plate Reader	PerkinElmer

96-well plate	Non-sterile polystyrene plate, black with transparent bottom 655096	GREINER bio-one
384-well plate	SensoPlate™ F-bottom, glass bottom, black, sterile, 781892	GREINER bio-one
1536-well plate	Standard polystyrene microplates, Clear bottom well plate, flat bottom, non-treated 734-1198	Corning Life Science
1536-well plate	Standard polystyrene microplates, Standard well plate, flat bottom, non-treated 734-4125	Corning Life Science
FPCL column	HiTrap® SP HP column 1mL	GE Healthcare Life science
FPLC system	ÄKTA™ Explorer	GE Healthcare Life science
Gel imager	Molecular imager ® ChemiDoc XRS + System	BIO-RAD
Gel visualizer	Safe Imager™ 2.0 Blue-Light Transilluminator, 10507584	Invitrogen™
Tape Station	TapeStation System, 4150	Agilent
Vortexer	Vortex mixer MELB 1719	MERCK® eurolab
Mixer	Stuart™ Gyro-rocker SSL3	Merck®
pH electrode	pH Microelectrode, Platinum Diaphragm, 97041-878	VWR
pH meter	pH, ORP and ISE Benchtop Meter Lab 845, 285206810	SI analytics
Magnet	DynaMag™ -2 Magnet	Thermo Fisher scientific
Weight	BP 4100 weighing scale	Sartorius
Sonication Instrument	Vibra Cell ™	Sonics and materials Inc.
Power supply	Electrophoresis power supply EPS 60	Amersham Pharmacia biotech
Tape Station RNA screen tape	High Sensitivity RNA Screen Tape, 5067-5579	Agilent Technologies
Gentle mixer	Rock'n Roller L-201	LABINCO

Table A2 Chemicals used in the experimental part in this thesis including concentration/purity, catalogue number and manufacturer.

CHEMICAL	CONCENTRATION /PURITY	CATALOGUE NUMBER	MANUFACTURER
Ampicillin	100 mg/mL	NA	OUH
Isopropyl beta-D-1-thiogalactopyranoside (IPTG)	1 mol/L	NA	OUH
1,4-Dithiothreitol DTT	1 mol /L	NA	NA
Strep-Tactin® Superflow Plus	NA	30004	Qiagen
SUMO protease	1 U/µL	12588018	Thermo Fisher Scientific
DEPC-Treated Water	NA	AM9916	Thermo Fisher Scientific
NP-40 IGEPAL CA-630	NA	I8898	Sigma Aldrich
S4-(2-hydroxyethyl)-1-piperazineethanesulfonic acid (HEPES) pH 7	1 mol/L	NA	OUH
Tris(hydroxymethyl)methylamino-propane sulfonic acid (TAPS)	≥99,5%	T5131	Sigma Aldrich
2-(N-morpholino)-ethane sulfonic acid (MES)	≥99,5%	M2933	Sigma Aldrich
Ethylenediaminetetraacetic acid (EDTA)	0,5 mol/L	NA	OUH
Gel Loading Buffer II (Denaturing PAGE)	NA	AM8546G	Invitrogen™
550 nt RNA	3,7 mg/mL	NA	OUH
SYBR™ Safe DNA Gel Stain (in BMSO*)	10,000x	S33102	Invitrogen™
UltraPure™ Agarose	NA	16500100	Invitrogen™
RNaseZap™	NA	AM9782	Invitrogen™
Sodium chloride (NaCl)	5 mol/L	NA	OUH
Calcium chloride (CaCl$_2$)	3 mol/L	NA	OUH
Magnesium chloride (MgCl$_2$)	3 mol/L	NA	OUH
Potassium chloride (KCl)	3 mol/L	NA	OUH
Tween®20	NA	P2287	Sigma Aldrich
2-Propanol	≥99.5%	I9516	Merck
Sodium Hypochlorite solution	10-15%	42044	Sigma Aldrich
x50 Tris-acetate-EDTA (TAE) buffer	NA	NA	OUH
Tris-HCl pH 7.5	1 mol/L	NA	OUH

Tris-HCl pH 8.0	1 mol/L	NA	OUH
Ultra pure ™ Agarose	≥99%	16500500	Invitrogen™
Ultrapure™ DNase/RNase-Free Distilled Water	500 mL	10977049	Thermo Fisher Scientific
Acid-Phenol: Chloroform, pH 4.5 (with IAA, 125:24:1)	≥99%	AM9720	Thermo Fisher Scientific
Chloroform	≥99%	288306	Sigma-Aldrich
Gel loading buffer (Orange 6x)	6x	B7022S	BioLabs®
Glycerol	60 %	NA	OUH
20x Bolt™ MES SDS Running Buffer	20x	B0002	Invitrogen™
Ribonucleotide tri-phosphate solution mix (rNTP solution mix)	50 µmol	N0466L	BioLabs®
RNase inhibitor (murine)	40,000 U/mL	M0314S	BioLabs®
NxGen T7 RNA polymerase	50,000 U/mL, ≥99% (SDS page purity)	30223-2	Lucigen
UREA	≥98%	U5378	Sigma Aldrich
Ammonium persulphate (APS)	10 %	NA	OUH
N,N,N´,N´- tetra-methylerhylene-diamine TEMED	≥99%	T7024	Sigma Aldrich
Sequence-specific reporter for LwaCas13a (/5TEX615/T*A*rArUG *C*/3IAbRQSp/)	1 µmol	224615684	IDT®
40% Polyacrylamide (19:1)	≥99,9%	1610144	BIO-RAD
SuperScript™ VI reverse transcriptase	200 U/µL	18090010	Invitrogen™
10X Bolt™ Sample Reducing Agent	10x	B0009	Invitrogen™
4X Bolt™ LDS Sample Buffer	4x	B0008	Invitrogen™
Tris-Borate-EDTA (TBE)			OUH
High Sensitivity RNA Screen Tape Sample Buffer	NA	5067-5580	Agilent Technologies
High Sensitivity RNA Screen Tape Ladder	NA	5067-5581	Agilent Technologies

Magnetic nano-particle mix (NTNU_MAG_V2)	NA	NA	NTNU
Lysis buffer (NTNU_MAG_V2)	NA	NA	NTNU
Bolt Bis-Tris Plus 1mm x 10 well (gradient 4-12%)	NA	NW04120BOX	Invitrogen™

Table A3 Molecular markers used in the experimental part in this thesis including concentration/purity, catalogue number and manufacturer.

MOLECULAR MARKER	CATHALOGUE NUMBER	MANUFACTURER
BIO-RAD Precision Plus Protein™ dual color standard, NA	1610374	BIO-RAD
Quick-load Purple 100 bp DNA Ladder, 50 µg/mL	NO553G	BioLabs®
Quick load purple low molecular weight DNA ladder, 50 µg/ml	N0557S	BioLabs®

Table A4. Kits used in the experimental part in this thesis including kit product, catalogue number and manufacturer.

KIT	CATHALOGUE NUMBER	MANUFACTURER
QIAquick Gel extraction Kit	28706	QIAGEN
MEGA script™ T7 Transcription Kit	AM1334	Thermo Fisher Scientific
Qubit™ Protein Assay Kit	Q33212	Invitrogen™
HiScribe T7 Quick High Yield RNA Synthesis Kit	E2050S	BioLabs®
TwistAmp Basic kit	TABAS03KIT	TwistDx® Inc
BIOTAQ™ PCR Kit	BIO-21071	Bioline
Qubit™ dsDNA HS Assay Kit	Q32851	Invitrogen™

Table A4 Buffers, solutions, and gels used in the experimental part in this thesis including recipe

BUFFER/SOLUTION /GEL	RECIPE
Luria-Bertani (LB)-ampicillin (1L)	10 g NaCl, 10 g tryptone, 5 g yeast extract, 100 mg/mL ampicillin, dH$_2$O to a volume of 1 L
Terrific Broth (TB) media	12 g/L tryptone, 24 g/L yeast extract, 9,4 g/L K2HPO4, 2,2 g/L KH2PO4, 100 µg /mL, sigma, 100 µg/mL ampicillin
Lysis buffer	20 mM Tris-HCl pH 8.0, 500 mM NaCl, 1 mM DTT
SUMO protease cleavage solution	20 mM Tris-HCl pH 8, 500 mM NaCl 1 mM DTT, 0.15% Igepal (NP-40), 50 Units of SUMO protease (1U/µL)
Protein storage buffer	600mM NaCl, 20 mM Tris-HCl pH 7.5, 5% glycerol, 2mM DTT
0,5 Tris-HCl and ethylenediaminetetraacetic acid (TE) buffer	5mM Tris-HCL pH 7,5-8, 0,5mM EDTA
Buffer A	200mM NaCl, 20mM Tris-HCl (pH 7.5, 1M), 5% Glycerol (50%(wt/vol), 1mM DTT
Buffer B	1 M NaCl, 20mM Tris-HCl (pH 7.5, 1M), 5% Glycerol (50%(wt/vol), 1mM DTT
Cossamie Blue staining solution	40% methanol, 10% acetic acid, 0,1 % Cossamie Blue
Destaining solution	40% methanol, 10% acetic acid, 4% Glycerol
2 % agarose	1 g agarose, 1xTAE
6% polyacrylamide	6% Polyacrylamide (19:1), 6g UREA, 1x TBE, 8% APS*, 5 µL TEMED** to 12 mL Milliq water
LB-ampicillin gel	20 g Agar, 10 g NaCl, 10 g tryptone, 5 g yeast extract, 100 mg/mL ampicillin, dH$_2$O to a volume of 1 L

Table A6 Software and online resources. Special softwares used in the experimental part of this thesis

SOFTWARE/ONLINE RESOURCES	SUPPLIER	APPLICATION
Image LabTM Software	Bio-Rad	Visualization of protein product on gel, and nuclease test of protein extract
Tape Station systems	Agilent	An automated electrophoresis solution, for visualization and quantification of crRNA *in vitro* transcription products
Biorender online illustration tool	https://biorender.com/	To create illustrations, flow charts and figures
Image Lab^{TM} Software	Bio-Rad	Visualization of protein product on gel, and nuclease test of protein extract

Protparam	https://www.expasy.org/	Finding the extinction coefficient and molecular weight for LwaCas13a quantification	
Uniprot	https://www.uniprot.org/	Used to find accession number of U2PSH1 for LwaCas13a by typing the plasmid amino acid sequence (section 2.1.4)	

Appendix B. Sequences, primers, and crRNAs used in this study

Table S1: List of primer sequences and synthetic targets (ssDNA oligomers) used in this study for PCR and/or (RT-)RPA. For each primer/target; name, sequence and source and applications are noted. Bold sequences indicate the T7 promoter used for T7-RNA transcription in the LwaCas13a nucleic acid reaction. Pink marks represent the PFS in the target. The oligomers were ordered as lyophilized materials and dissolved in 0,5 x TE buffer, pH 8. 10 µM stocks of each ssDNA oligomer was made by dilution with 10 mM Tris in nuclease free water. *these are only sequences representing target areas in a reference genome and not real material used in this assay.

Description	Primer name/ID	Sequence 5'→3'	Source
Synthetic DNA 1 template *	Synthetic DNA1 template/24024	GGCCAGTGAATTCGAGCTCGGTACCCGGGG ATCCTCTAGAAATATGGATTACTTGGTAGA ACAGCAATCTACTCGACCTGCAGGCATGCA AGCTTGGCGTAATCATGGTCATAGCTGTTT CCTGTGTTTATCCGCTCACAATTCCACACAA CATACGAGCCGGAAGCATAAAG	Kellner et al.,(36)
Synthetic DNA 1 RT-RPA forward original primer	DNA1 original forward primer/24025F	**AATTCTAATACGACTCACTATAGGG**ATCC TCTAGAAATATGGATTACTTGGTAGAACAG	Kellner et al.,(36)
Synthetic DNA 1 RT-RPA forward primer T7_1	24127F	**TAATACGACTCACAATCGCGGAG**ATCCTC TAGAAATATGGATTACTTGGTAGAACAG	Paul et al., (101)
Synthetic DNA 1 RT-RPA forward primer T7_2	24128F	**TAATACGACTCACTCCGGCAATC**ATCCTC TAGAAATATGGATTACTTGGTAGAACAG	Paul et al., (101)
Synthetic DNA 1 RT-RPA reverse original primer	DNA1 original reverse primer/24026R	GATAAACACAGGAAACAGCTATGACCATG ATTACG	Kellner et al.,(36)
Synthetic SARS-CoV-2_T2 (orf1b)	Synthetic orf1b target /24136	CAATGGGGTTTTACAGGTAACCTACAAAGC AACCATGATCTGTATTGTCAAGTCCATGGT AATGCACATGTAGCTAGTTGTGATGCAATC ATGACTAGGTGTCTAGCTGTCCACGAGTGC TTTGTTAAGCG	Lucia et al., (100)
SARS-CoV-2 orf1b RT-RPA original forward primer	Orf1b original forward primer/24134F	**GAAATTAATACGACTCACTATAGGG**CAAT GGGGTTTTACAGGTAACCTACAAAGCAACC	GenBank: MN908947.3
SARS-CoV-2 orf1b RT-RPA original reverse primer	Orf1b original reverse primer/24135R	CGCTTAACAAAGCACTCGTGGACAGCTAGA CAC	GenBank: MN908947.3
Synthetic SARS-CoV-2_T3 (orf1ab)	Synthetic orf1ab target /24140	CCCTGTGGGTTTTACACTTAAAAACACAGT CTGTACCGTCTGCGGTATGTGGAAAGGTTA TGGCTGTAGTTGTGATCAACTCCGCGAACC CATGCTTCAGTCAGCTGATGCACAATCGTT	Lucia et al., (100)
SARS-CoV-2 orf1ab RT-RPA original forward primer	Orf1ab original forward primer/24138F	**GAAATTAATACGACTCACTATAGGG**CCCT GTGGGTTTTACACTTAAAAACACAGTCT	GenBank: MN908947.3
SARS-CoV-2 orf1ab RT-RPA original reverse primer	Orf1ab original reverse primer/24139R	AACGATTGTGCATCAGCTGACTGAAGCATG GG	GenBank: MN908947.3

SARS-CoV-2 orf1ab RT-RPA new forward primer	Orf1ab new forward primer/24275F	**GAAATTAATACGACTCACTATAGGG**TTTTACACTTAAAAACACAGTCTGTACCG	GenBank: MN908947.3
SARS-CoV-2 orf1ab RT-RPA new reverse primer	Orf1ab new reverse primer/24276R	AAGCATGGGTTCGCGGAGTTGATCACAACT	GenBank: MN908947.3
*SARS-CoV-2 MSA_T1 target sequence	MSA_T1	GCCAACAACAACAAGGCCAAACTGTCACTAAGAAATCTGCTGCTGAGGCTTCTAAGAAGCCTCGGCA<mark>A</mark>AAACGTACTGCCACTAAAGCATACAATGTAACACAAGCTTT	Jon K. Lærdahl, research scientist and bioinformatician at MIK, OUH
SARS-CoV-2 MSA_T1 RPA Forward primer	MSA_T1-F/24271F	**GAAATTAATACGACTCACTATAGGG**CAAGGTTTACCCAATAATACTGCGTCTTGG	GenBank: MN908947.3
SARS-CoV-2 MSA_T1 RT-RPA Reverse primer	MSA_T1-R/24272R	TGGAACGCCTTGTCCTCGAGGGAATTTAAG	GenBank: MN908947.3
*SARS-CoV-2 MSA_T2 target sequence	MSA_T2	CGATCAAAACAACGTCGGCCCCAAGGTTTACCCAATAATACTGCGTCTTGGTTCACCGCTCTCACTCAACATGGCAAGGAAG<mark>A</mark>CCTTAAATTCCCTCGAGGACAAGGCGTTCCAATTAACACCAATAGCAGTCCA	Jon K. Lærdahl, research scientist and bioinformatician at MIK, OUH
SARS-CoV-2 MSA_T2 RT-RPA forward primer	MSA_T2-F/24273F	**GAAATTAATACGACTCACTATAGGG**CAACAACAACAAGGCCAAACTGTCACTAAG	GenBank: MN908947.3
SARS-CoV-2 MSA_T2 RT-RPA reverse primer	MSA_T2-R/24274R	TACATTGTATGCTTTAGTGGCAGTACGTTT	GenBank: MN908947.3

Table S2: List of ssDNA *in vitro* transcription templates for crRNAs, and pre synthesized crRNAs used in this study. Bold font indicates a T7 promoter sequence for *in vitro* transcription of ssDNA crRNA templates, and corresponding *in vitro* transcription-primer (3G-T7). The RNA oligomers were ordered as lyophilized material and dissolved in 0,5 x TE buffer, pH 7,5.

Description	Primer name/ID	Sequence 5'→3'	Source
Synthetic DNA 1 LwaCas13a DNA1-crRNA ssDNA oligo	DNA1-crRNA	CTCGACCTGCAGGCATGCAAGCTTGGCGGTTTTAGTCCCCTTCGTTTTTGGGGTAGTCTAAAT**CCCTATAGTGAGTCGTATTAATTTC**	Kellner et al.,(36)
SARS-CoV-2 orf1b-crRNA ssDNA oligo	Orf1b-crRNA	CTGTATTGTCAAGTCCATGGTAATGCACGTTTTAGTCCCCTTCGTTTTTGGGGTAGTCTAAAT**CCCTATAGTGAGTCGTATTAATTTC**	Kellner et al.,(36) & Lucia et al., (100)
SARS-CoV-2 orf1ab-crRNA ssDNA oligo	Orf1ab-crRNA	CTGCGGTATGTGGAAAGGTTATGGCTGTGTTTTAGTCCCCTTCGTTTTTGGGGTAGTCTAAAT**CCCTATAGTGAGTCGTATTAATTTC**	Kellner et al.,(36) & Lucia et al., (100)
3G-T7 *In vitro* transcription primer	T7-3G	**GAAATTAATACGACTCACTATAGGG**	Kellner et al.,(36)
SARS-CoV-2 orf1ab_2 crRNA	Orf1ab2-crRNA	GAUUUAGACUACCCCAAAAACGAAGGGGACUAAAACACAGCCAUAACCUUUCCACAUACCGCAG	Kellner et al.,(36) & Lucia et al., (100)
SARS-CoV-2 MSA_T1 crRNA	MSA_T1-crRNA	GAUUUAGACUACCCCAAAAACGAAGGGGACUAAAACCUUCCUUGCCAUGUUGAGUGAGAGCGGU	Jon K. Lærdahl, research scientist and bioinformatician at MIK, OUH.
SARS-CoV-2 MSA_T2 crRNA	MSA_T2-crRNA	GAUUUAGACUACCCCAAAAACGAAGGGGACUAAAACUGCCGAGGCUUCUUAGAAGCCUCAGCAG	Jon K. Lærdahl, research scientist and bioinformatician at MIK, OUH
SARS-CoV-2 MSA_T2 crRNA	MSA_T2-crRNA	GAUUUAGACUACCCCAAAAACGAAGGGGACUAAAACUGCCGAGGCUUCUUAGAAGCCUCAGCAG	Jon K. Lærdahl, research scientist and bioinformatician at MIK, OUH

Table S3. PRIMARY RIMER SCREEN ASSAY on SARS-CoV-2 *orf1ab*. Bold sequence represents the T7 promoter overhang on the forward primers. Gray marks represent the RT-RPA primer set used as basis for designing primary primer candidate for the primary primer screen. For each primer: name, sequence and length (nt) and primer source are noted. All primers were ordered as lyophilized materials and dissolved in 0,5 x TE buffer, pH 8. 10 µM stocks of each primer was made by dilution with 10 mM Tris in nuclease free water.

Description	Primer name/ID	Sequence 5'→3'	Length (nt)	Source
nCOV-ORF1ab- RT-RPA Forward primer	Orf1ab original forward primer/24138F	**GAAATTAATACGACTCACTATAG GG**CCCTGTGGGTTTTACACTTAAA AACACAGTCT	32 + T7 overhang	Kellner et al.,(36) & Lucia et al., (100)
nCOV-ORF1ab- RT-RPA Reverse primer	Orf1ab new reverse primer/24276R	AAGCATGGGTTCGCGGAGTTGATC ACAACT	30	Kellner et al.,(36) & Lucia et al., (100)
nCoV-ORF1ab- RT-RPA Forward primer 1	orf1ab-F1/24391F	**GAAATTAATACGACTCACTATAG GG**TGGGTTTTACACTTAAAAACAC AGTCTGTA	30 + T7 overhang	GenBank MN908947.3
nCoV-ORF1ab- RT-RPA Forward primer 2	orf1ab-F2/24392F	**GAAATTAATACGACTCACTATAG GG**TGTGCTAATGACCCTGTGGGTT TTACACTT	30 + T7 overhang	GenBank MN908947.3
nCoV-ORF1ab- RT-RPA Forward primer 3	orf1ab-F3/24393F	**GAAATTAATACGACTCACTATAG GG**CTACAACTTGTGCTAATGACCC TGTGGGTT	30 + T7 overhang	GenBank MN908947.3
nCoV-ORF1ab- RT-RPA Forward primer 4	orf1ab-F4/24394F	**GAAATTAATACGACTCACTATAG GG**TACAAATACCTACAACTTGTGC TAATGACC	30 + T7 overhang	GenBank MN908947.3
nCoV-ORF1ab- RT-RPA Forward primer 5	orf1ab-F5/24395F	**GAAATTAATACGACTCACTATAG GG**TAAGTATGTACAAATACCTACA ACTTGTGC	30 + T7 overhang	GenBank MN908947.3
nCoV-ORF1ab- RT-RPA Revers primer 1	orf1ab-R1/24396R	CGGAGTTGATCACAACTACAGCCA TAACCT	30	GenBank MN908947.3
nCoV-ORF1ab- RT-RPA Revers primer 2	orf1ab-R2/24397R	TCGCGGAGTTGATCACAACTACAG CCATAA	30	GenBank MN908947.3
nCoV-ORF1ab- RT-RPA Revers primer 3	orf1ab-R3/24398R	AGCATGGGTTCGCGGAGTTGATCA CAACTA	30	GenBank MN908947.3
nCoV-ORF1ab- RT-RPA Revers primer 4	orf1ab-R4/24399R	CTGACTGAAGCATGGGTTCGCGGA GTTGAT	30	GenBank MN908947.3
nCoV-ORF1ab- RT-RPA Revers primer 5	orf1ab-R5/24400R	GTGCATCAGCTGACTGAAGCATGG GTTCGC	30	GenBank MN908947.3

Table S4. SECONDARY PRIMER SCREEN ASSAY on SARS-CoV-2 *orf1ab*. Bold sequence represents the T7 promoter overhang on the forward primers. For each primer: name, sequence, length (nt) and primer source are noted.

Description	Primer name/ID	Sequence 5'→3'	Length (nt)	Source
nCoV-ORF1ab- RT-RPA Forward primer a	orf1ab-Fa/24471F	**GAAATTAATACGACTCACTATAGG G**TACCTACAACTTGTGCTAATGACC CTGTGG	30 + T7 overhang	GenBank MN908947.3
nCoV-ORF1ab- RT-RPA Forward primer b	orf1ab-Fb/24472F	**GAAATTAATACGACTCACTATAGG G**AATACCTACAACTTGTGCTAATGA CCCTGT	30 + T7 overhang	GenBank MN908947.3
nCoV-ORF1ab- RT-RPA Forward primer c	orf1ab-Fc/24473F	**GAAATTAATACGACTCACTATAGG G**CAAATACCTACAACTTGTGCTAAT GACCCT	30 + T7 overhang	GenBank MN908947.3

nCoV-ORF1ab- RT-RPA Forward primer d	orf1ab-Fd/24474F	**GAAATTAATACGACTCACTATAGG G**CCTACAACTTGTGCTAATGACCCT GTGGGT	30 + T7 overhang	GenBank MN908947.3
nCoV-ORF1ab- RT-RPA Forward primer a	orf1ab-Ra/24475R	GGTTCGCGGAGTTGATCACAACTAC AGCCA	30	GenBank MN908947.3
nCoV-ORF1ab- RT-RPA Revers primer b	orf1ab-Rb/24476R	ATGGGTTCGCGGAGTTGATCACAAC TACAG	30	GenBank MN908947.3
nCoV-ORF1ab- RT-RPA Revers primer c	orf1ab-Rc/24477R	GCATGGGTTCGCGGAGTTGATCACA ACTAC	30	GenBank MN908947.3
nCoV-ORF1ab- RT-RPA Revers primer d	orf1ab-Rd/24478R	GAAGCATGGGTTCGCGGAGTTGATC ACAAC	30	GenBank MN908947.3

Table S5. PRIMARY PRIMER SCREEN ASSAY for SARS-CoV-2 MSA_T1. Bold sequence represents the T7 promoter overhang on the forward primers. Gray marks represent the RT-RPA primer set used as basis for designing primary primer candidate for the primary primer screen. For each primer; name, sequence and length (nt) and primer source are noted.

Description	Primer name/ID	Sequence 5'→3'	Length (nt)	Source
MSA_T1 RT-RPA forward primer	MSA_T1-F/24271F	**GAAATTAATACGACTCACTATAGGG** CAAGGTTTACCCAATAATACTGCGTCT TGG	30 + T7 overhang	Jon K. Lærdahl, research scientist and bioinformatician at MIK, OUH
MSA_T1 RT-RPA revers primer	MSA_T1-R/24272R	TGGAACGCCTTGTCCTCGAGGGAATTT AAG	30	Jon K. Lærdahl, research scientist and bioinformatician at MIK, OUH
MSA_T1 RT-RPA forward primer 1	MSA_T1-F1/24479F	**GAAATTAATACGACTCACTATAGGG** ATAATACTGCGTCTTGGTTCACCGCTC TCA	30 + T7 overhang	GenBank MN908947.3
MSA_T1 RT-RPA forward primer 2	MSA_T1-F2/24480F	**GAAATTAATACGACTCACTATAGGG** TTACCCAATAATACTGCGTCTTGGTTC ACC	31	GenBank MN908947.3
MSA_T1 RT-RPA forward primer 3	MSA_T1-F3/24481F	**GAAATTAATACGACTCACTATAGGG** ACGTCGGCCCCAAGGTTTACCCAATA ATAC	30 + T7 overhang	GenBank MN908947.3
MSA_T1 RT-RPA forward primer 4	MSA_T1-F4/24482F	**GAAATTAATACGACTCACTATAGGG** ATCAAAACAACGTCGGCCCCAAGGTT TACC	30 + T7 overhang	GenBank MN908947.3
MSA_T1 RT-RPA revers primer 1	MSA_T1-R1/24483R	GTCCTCGAGGGAATTTAAGGTCTTCCT TGC	30 + T7 overhang	GenBank MN908947.3
MSA_T1 RT-RPA revers primer 2	MSA_T1-R2/24484R	ACGCCTTGTCCTCGAGGGAATTTAAGG TCT	30	GenBank MN908947.3
MSA_T1 RT-RPA revers primer 3	MSA_T1-R3/24485R	GTTAATTGGAACGCCTTGTCCTCGAGG GAA	30	GenBank MN908947.3
MSA_T1 RT-RPA revers primer 4	MSA_T1-R4/24486R	GTCATCTGGACTGCTATTGGTGTTAAT TGG	30	GenBank MN908947.3

```
F5      TAAGTATGTACAAATACCTACAACTTGTGC →
F4            TACAAATACCTACAACTTGTGCTAATGACC →
Fc         CAAATACCTACAACTTGTGCTAATGACCCT →
Fb       AATACCTACAACTTGTGCTAATGACCCTGT →
Fa      TACCTACAACTTGTGCTAATGACCCTGTGG →
Fd     CCTACAACTTGTGCTAATGACCCTGTGGGT →
F3     CTACAACTTGTGCTAATGACCCTGTGGGTT →
F2       TGTGCTAATGACCCTGTGGGTTTTACACTT →
24138F        CCCTGTGGGTTTTACACTTAAAAACACAGTCT →
F1              TGGGTTTTACACTTAAAAACACAGTCTGTA →

5'GGTAAGTATGTACAAATACCTACAACTTGTGCTAATGACCCTGTGGGTTTTACACTTAAAAACACAGTCTGTACCGTCTGCGGTATG
3'CCATTCATACATGTTTATGGATGTTGAACACGATTACTGGGACACCCAAAATGTGAATTTTTGTGTCAGACATGGCAGACGCCATAC

5'TGGAAAGGTTATGGCTGTAGTTGTGATCAACTCCGCGAACCCATGCTTCAGTCAGCTGATGCACAATCGTTTTTA
3'ACCTTTCCAATACCGACATCAACACTAGTTGAGGCGCTTGGGTACGAAGTCAGTCGACTACGTGTTAGCAAAAAT
        ← TCCAATACCGACATCAACACTAGTTGAGGC                                R1
          ← AATACCGACATCAACACTAGTTGAGGCGCT                              R2
        ← ACCGACATCAACACTAGTTGAGGCGCTTGG                                Ra
           ← GACATCAACACTAGTTGAGGCGCTTGGGTA                             Rb
            ← CATCAACACTAGTTGAGGCGCTTGGGTACG                            Rc
             ← ATCAACACTAGTTGAGGCGCTTGGGTACGA                           R3
                ← TCAACACTAGTTGAGGCGCTTGGGTACGAA                        24276R
            ← CAACACTAGTTGAGGCGCTTGGGTACGAAG                            Rd
               ← TAGTTGAGGCGCTTGGGTACGAAGTCAGTC                         R4
                  ← CGCTTGGGTACGAAGTCAGTCGACTACGTG                      R5
```

Figure TS4. Illustration of the primers used in the primer screen of SARS-CoV-2 orf1ab target. Gray areas indicate the primer pair used as basis for designing new primers in the screen. Underline indicates the target area for associated crRNA. Blue sequences indicate a part of the SARS-CoV-2 genome (Genbank: MN908947.3) converted to dsDNA. Forward primers are represented without T7 promoter.

```
MSA_T1-F5 TGGGGCGCGATCAAAACAACGTCGGCCCCA →
MSA_T1-F4         ATCAAAACAACGTCGGCCCCAAGGTTTACC →
MSA_T1-F3        ACGTCGGCCCCAAGGTTTACCCAATAATAC →
RT-RPA MSA_T1_F      CAAGGTTTACCCAATAATATACTGCGTCTTGG →
MSA_T1-F2            TTACCCAATAATACTGCGTCTTGGTTCACC →
MSA_T1-F1               ATAATACTGCGTCTTGGTTCACCGCTCTCA →
    5'AGTGGGGCGCGATCAAAACAACGTCGGCCCCAAGGTTTACCCAATAATACTGCGTCTTGGTTCACCGCTCTCACTCAACAT
    3'TCACCCCGCGCTAGTTTTGTTGCAGCCGGGGTTCCAAATGGGTTATTATGACGCAGAACCAAGTGGCGAGAGTGAGTTGTA

    GGCAAGGAAGACCTTAAATTCCCTCGAGGACAAGGCGTTCCAATTAACACCAATAGCAGTCCAGATGACCAAATTGGCTA-3'
  ← CCGTTCCTTCTGGAATTTAAGGGAGCTCCTGTTCCGCAAGGTTAATTGTGGTTATCGTCAGGTCTACTGGTTTAACCGAT-5'
    ← CGTTCCTTCTGGAATTTAAGGGAGCTCCTG                                MSA_T1-R1
       ← TCTGGAATTTAAGGGAGCTCCTGTTCCGCA                             MSA_T1-R2
          ← AAGGGAGCTCCTGTTCCGCAAGGTTAATTG                          MSA_T1-R3
           ← CTGTTCCGCAAGGTTAATTGTGGTTATCGTC                        RT-RPA MSA_T1-R
              ← CAAGGTTAATTGTGGTTATCGTCAGGTCTA                      MSA_T1-R4
                 ← GTTATCGTCAGGTCTACTGGTTTAACCGAT   MSA_T1-R5
```

Figure TS5. Illustration of the primers used in the primer screen of SARS-CoV-2 MSA_T1 target. Gray areas indicate the primer pair used as basis for designing new primers in the screen. Underline indicates the target area for associated crRNA. Blue sequences indicate a part of the SARS-CoV-2 genome (Genbank: MN908947.3) converted to dsDNA. Forward primers are represented without T7 promoter.

Table S6. PRIMARY PRIMER SCREEN ASSAY for SARS-CoV-2 MSA_T2. Bold sequence represents the T7 promoter overhang on the forward primers. Gray marks represent the RT-RPA primer set used as basis for designing primary primer candidate for the primary primer screen. For each primer; name, sequence and length (nt) and primer source are noted.

Description	Primer name/ID	Sequence 5→3'	Length (nt)	Source
MSA_T2 RT-RPA forward primer	MSA_T2-F/24273F	**GAAATTAATACGACTCACTAT AGGG**CAACAACAACAAGGCCA AACTGTCACTAAG	30 + T7 overhang	Jon K. Lærdahl, research scientist and bioinformatician at MIK, OUH.
MSA_T2 RT-RPA reverse primer	MSA_T2-R/24274R	TACATTGTATGCTTTAGTGGCA GTACGTTT	30 nt	Jon K. Lærdahl, research scientist and bioinformatician at MIK, OUH
MSA_T2 RT-RPA forward primer 1	MSA_T2-F1/24487 F1	**GAAATTAATACGACTCACTAT AGGG**CAAACTGTCACTAAGAA ATCTGCTGCTGAG	30 + T7 overhang	GenBank MN908947
MSA_T2 RT-RPA forward primer 2	MSA_T2-F2/24488 F2	**GAAATTAATACGACTCACTAT AGGG**AAGGCCAAACTGTCACT AAGAAATCTGCTG	30 + T7 overhang	GenBank MN908947
MSA_T2 RT-RPA forward primer 3	MSA_T2-F3/24489 F3	**GAAATTAATACGACTCACTAT AGGG**AATGTCTGGTAAAGGCC AACAACAACAAGG	30 + T7 overhang	GenBank MN908947
MSA_T2 RT-RPA forward primer 4	MSA_T2-F4/24490 F4	**GAAATTAATACGACTCACTAT AGGG**CTTGAGAGCAAAATGTC TGGTAAAGGCCAA	30 + T7 overhang	GenBank MN908947
MSA_T2 RT-RPA revers primer 1	MSA_T2-R1/24491 R1	TATGCTTTAGTGGCAGTACGTT TTTGCCGA	30	GenBank MN908947
MSA_T2 RT-RPA revers primer 2	MSA_T2-R2/24492 R2	ATTGTATGCTTTAGTGGCAGTA CGTTTTTG	30	GenBank MN908947
MSA_T2 RT-RPA revers primer 3	MSA_T2-R3/24493 R3	TGCCGAAAGCTTGTGTTACATT GTATGCTT	30	GenBank MN908947
MSA_T2 RT-RPA revers primer 4	MSA_T2-R4/24494 R4	ACCACGTCTGCCGAAAGCTTGT GTTACATT	30	GenBank MN908947

```
MSA_T2-F4               CTTGAGAGCAAAATGTCTGGTAAAGGCCAA
MSA_T2-F3                      AATGTCTGGTAAAGGCCAACAACAACAAGG
RT-RPA MSA_T2-F                      CAACAACAACAAGGCCAAACTGTCACTAAG
MSA_T2-F2                                   AAGGCCAAACTGTCACTAAGAAATCTGCTG
MSA_T2-F1                                      CAAACTGTCACTAAGAAATCTGCTGCTGAG
           5'-CTTGACAGATTGAACCAGCTTGAGAGCAAAATGTCTGGTAAAGGCCAACAACAACAAGGCCAAACTGTCACTAAGAAATCTGCTGCTGAG
           3'-GAACTGTCTAACTTGGTCGAACTCTCGTTTTACAGACCATTTCCGGTTGTTGTTGTTCCGGTTTGACAGTGATTCTTTAGACGACGACTC

           GCTTCTAAGAAGCCTCGGCAAAAACGTACTGCCACTAAAGCATACAATGTAACACAAGCTTTCGGCAGACGTGGTCCAGAAC-3'
           CGAAGATTCTTCGGAGCCGTTTTTGCATGACGGTGATTTCGTATGTTACATTGTGTTCGAAAGCCGTCTGCACCAGGTCTTG-5'
                     AGCCGTTTTTGCATGACGGTGATTTCGTAT                       MSA_T2-R1
                       GTTTTTGCATGACGGTGATTTCGTATGTTA                     MSA_T2-R2
                       TTTGCATGACGGTGATTTCGTATGTTACAT                     RT-RPA MSA_T2_R
                           TTCGTATGTTACATTGTGTTCGAAAGCCGT                 MSA_T2-R3
                            TTACATTGTGTTCGAAAGCCGTCTGCACCA                MSA_T2-R4
```

Figure TS6. Illustration of the primers used in the primer screen of SARS-CoV-2 MSA_T2 target. Gray areas indicate the primer pair used as basis for designing new primers in the screen. Underline indicates the target area for associated crRNA. Blue sequences indicate a part of the SARS-CoV-2 genome (Genbank: MN908947.3) converted to dsDNA. Forward primers are represented without T7 promoter.

Appendix C. Plasmid used in this study
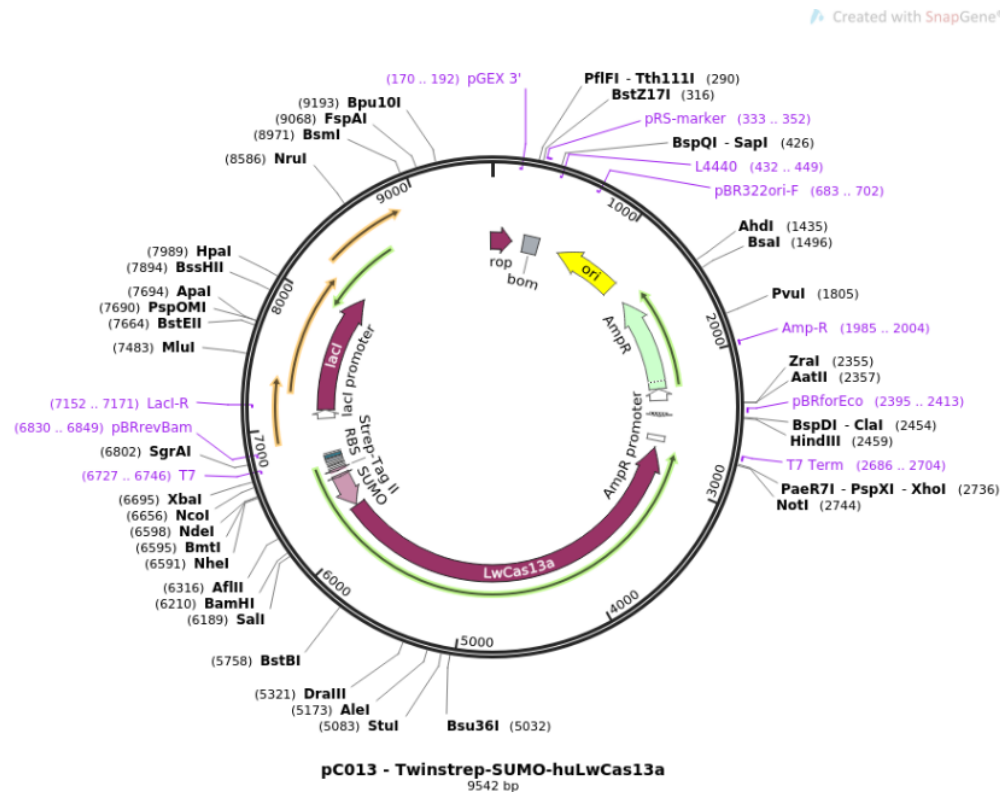
Figure S1. Plasmid map for twinstrep-SUMO-huLwCas13a. The plasmid was collected from Addgene https://www.addgene.org/90097/¨.

Appendix D. SDS page -protein expression and purification

To confirm successful protein expression and purification, samples collected along the protein purification were visualized with SDS-PAGE. Samples taken from protein extraction using a SUMO tag, was loaded at 10 µL with 2 µL 10x Bolt sample-reducing agent, 5 µL 4xBolt LDS sample buffer and 3 µL ultrapure water to a total loading volume of 20 µL. 3µL of sample fractions collected from FPLC, 6µL column applied protein sample and flow-through were loaded with same amount of 10x Bolt sample-reducing agent and 4xBolt LDS sample buffer but to 10 µL or 7 µL ultrapure water respectively. The samples migrated for 1h with a 140 V current, using 1x MES as running buffer. The gel was stained for 1h with Cossamie brilliant blue protein staining solution on a moving stand and washed with a de-staining solution. The gels were visualized using a ChemiDoc XRS+ System, with a white background plate.
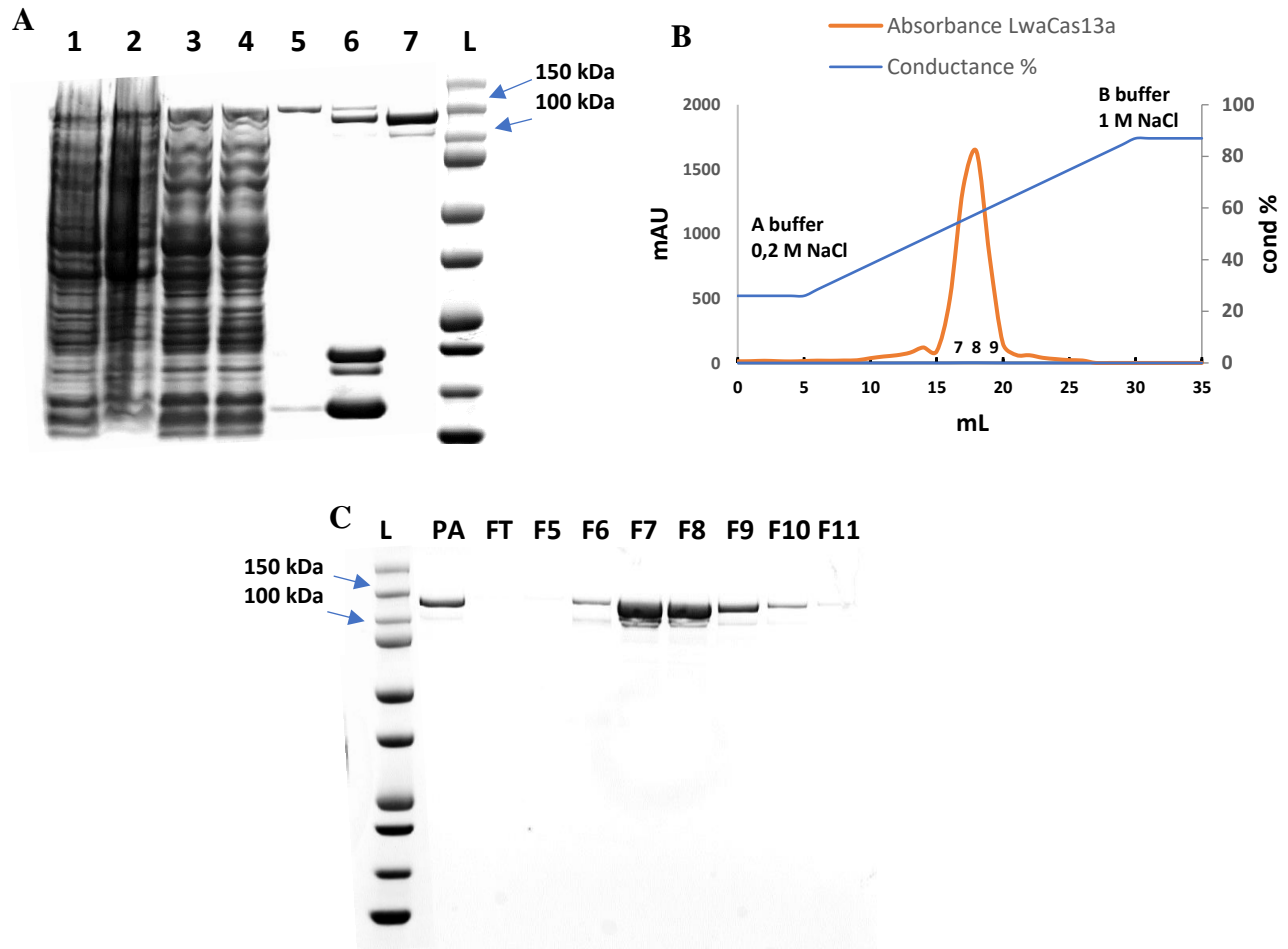
Figure S2. Purification of LwaCas13a. The protein purification process of LwaCas13a correspondingly to step 9-18 in Kellner *et al*., 2019 visualized on two Coomassie blue stained SDS-PAGE 4-12% gradient gel including fractions taken along the process (section 2.2.1). The expected size of LwaCas13a is 138,5 kDa. The fractions in **(A)** shows fractions taken during SUMO-protease purification and are: 1, cell lysate; 2,cell pellet after clearing of lysate; 3, cleared cell lysate; 4, flow through following Strep-Tactin batch binding; 5, Strep-Tactin bound to SUMO-Protein; 6, wash of resin after SUMO-protease cleavage (non-SUMO cutted products); 7, eluted fraction post SUMO-protease cleavage; L, Precision Plus Protein Dual Color ladder. **(B)** Elution profile of LwaCas13a (orange) using Äkta explorer FPLC system and a 1 mL SP HP cation exchange column. The protein was eluted from a NaCl concentration of 200 mM to 1 M using buffer A and B. Pooled fractions (7,8,9) used for SHERLOCK is noted. Blue line shows the salt profile (conductance %) and orange profile represents milli arbitrary units (mAU). **(C)** shows protein containing fractions taken from the cation exchanger chromatography with HPLC SP HP. The fractions in are: L, Precision Plus Protein™ Dual Color ladder; PA, column applied protein sample; FT, flow through (FT); F5, fraction 5; F6, fraction 6; F7, fraction 7; F8, fraction 8; F9, fraction 9; F10, fraction 10; F11, fraction 11.

Appendix E. Magnetic nano-bead purification protocol for crRNA

A lysis buffer and nano-bead mix (20 µL magnetic nano-bead stock, 380 isopropanol, pr sample) where provided by the Magnar Bjørås group at NTNU, and a 50 µL elution buffer of nuclease free water and 1% Tween-20 was used.

Protocol:
1. Pipette out 200 µL lysis buffer (pr.sample-tube or well if using a well-plate)
2. Add 100 µL Sample mix (pipetting/vortexing), leave at room temperature for 5 minutes.
3. Resuspend magnetic bead-mix. Vortex thoroughly to resuspend all beads.
4. Add 400 µL Bead-mix to each sample/lysis tube, mix(pipetting/vortexing)
5. Keep the beads in solution for 10 minutes by mixing/shaking
6. Remove supernatant using a magnet
7. Wash the beads in 400 µL Isopropanol, mix 2 minutes
8. Remove supernatant using a magnet
9. Wash the beads in 400 µL 80% EtOH, mix 2 minutes
10. Remove supernatant using a magnet
11. Wash the beads in 400 µL 80% EtOH, mix 2 minutes
12. Remove supernatant using a magnet
13. Dry the beads for 10 min in room temperature, NB! Important that the beads are dried completely.
14. Resuspend the beads in 50 µL elution buffer, mix 5 min
15. Collect the supernatant using a magnet for qPCR.

Appendix F. Nuclease test on purified LwaCas13a batch

A nuclease test on the purified LwaCas13a protein extract was executed, using a 550 nt RNA sequence (3,7 µg/µL) as target. Figure Y shows a 6% polyacrylamide gel the bands resulting on a incubation
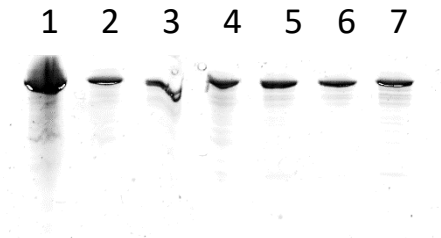
Figure S3: Nuclease activity test of LwaCas13a extract. Results from a SDS-PAGE on a SYBRsafe stained, 7% polyacrylamide gel including a negative nondigested 550 nt RNA (5,55µg) control sequence (1); 5µL Cas13a nucleic acid detection master mix (9mM MgCl2, 20mM HEPES pH 7.0) with 550 nt RNA(0,55 µg) sequence incubated at 37°C for 20 minutes(2), 40minutes(3) and 1 hour (4); and 5µL LwaCas13a nucleic acid detection master mix (9mM MgCl2, 20mM HEPES pH 7.0) including LwaCas13a and 550 nt RNA (0,55 µg) sequence incubated at 37°C for 20 minutes(5), 40minutes(6) and 1 hour (7).

Appendix G. PCR of synthetic sequences and *in vitro* transcription of crRNAs
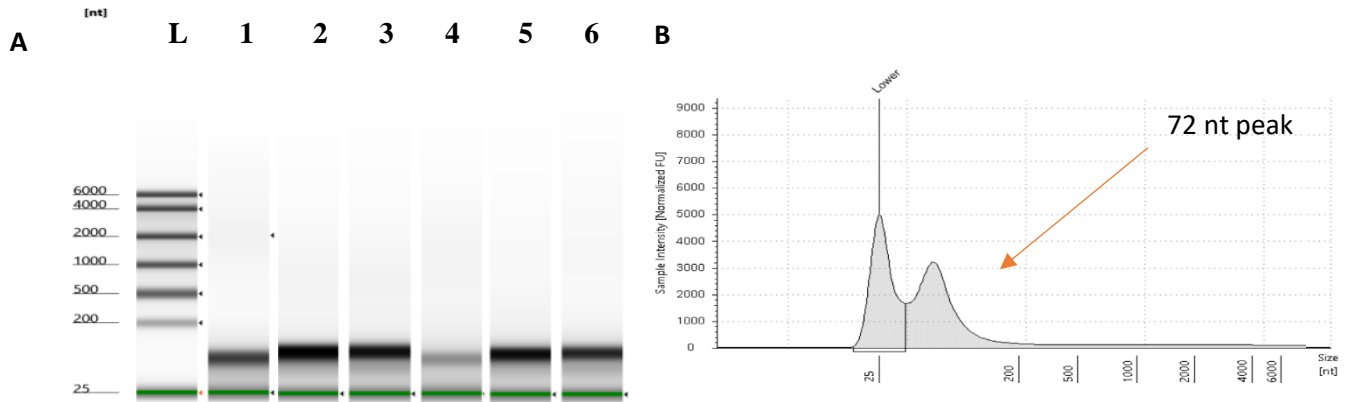
Figure S4: Visualization of *in vitro* transcribed crRNA products using Tape Station. crRNA products post phenol: chloroform or magnetic nano-bead purification visualized with Tape Station system (BIO-RAD). A) a digital gel picture including: L, RNA Screen Tape ladder(**reagents**); 1, phenol: chloroform purified synthetic DNA 1 crRNA; 2, phenol: chloroform purified synthetic SARS-CoV-2 orf1b-crRNA; 3, phenol: chloroform purified synthetic SARS-CoV-2 orf1ab-crRNA; 4, magnetic nano-beads purified synthetic DNA 1 crRNA; 5, magnetic nano-beads purified synthetic SARS-CoV-2 orf1b-crRNA; 6, magnetic nano-beads purified synthetic SARS-CoV-2 orf1ab-crRNA. B) a digital graph showing sample intensity of orf1ab-crRNA product by phenol: chloroform purification with an intensity peak at 72 nt.
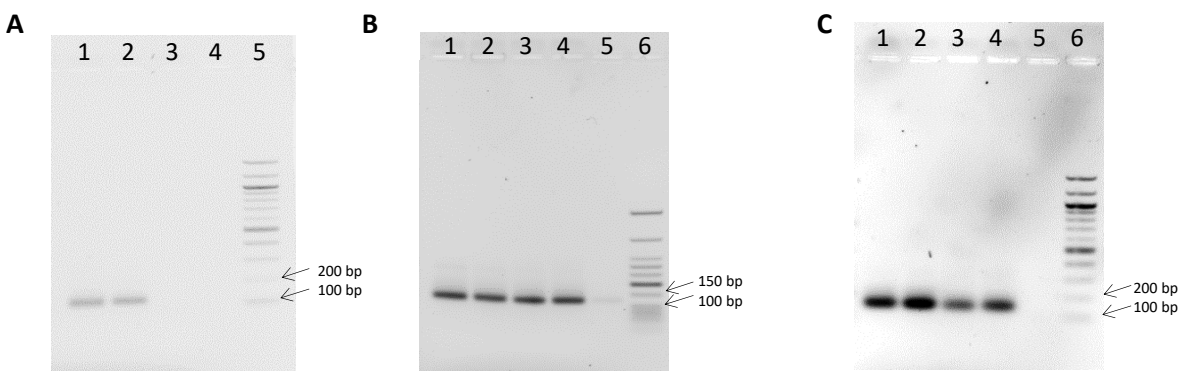
Figure S5. Visualization of the PCR products of synthetic sequences on 2% agarose gels, stained with CYBR-Safe. **A)** Synthetic DNA 1 PCR product (24025F, 24026R) loaded in well 1 and 2. Quick load purple100bp DNA ladder was used as standard (well 5). **B)** PCR product of synthetic DNA 1 with two new T7 promoters 24127F (well 1,2) and 24128F (well 3,4). Quick load purple low molecular weight DNA ladder was used as standard (well 6). **C)** Synthetic SARS-CoV-2 targets T2 (*orf1b*) in well 1 and 2, and T3 (*orf1ab*) in well 3 and 4. Quick load purple100bp DNA ladder was used as standard (well 6)

Appendix H. Trial experiments excluding RPA from SHERLOCK
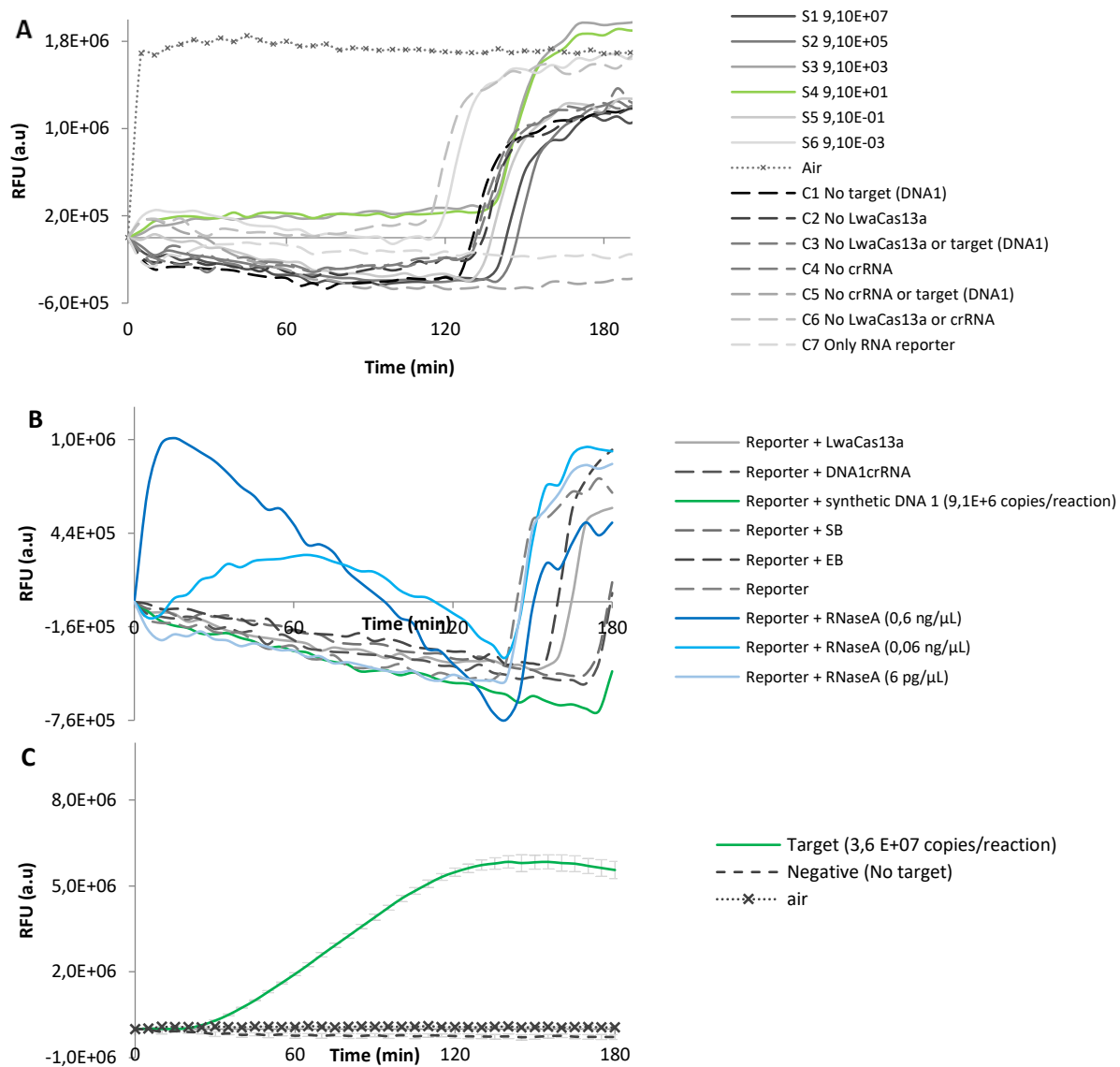
Figure S6. Trial LwaCas13a nucleic acid detection experiments on 96- or 384 well plates. Three LwaCas13a nucleic acid detection assays conducted on synthetic DNA 1 at various concentrations, or RNase A as positive controls. Values are represented in relative fluorescent units (± SD in **C**), over three hours of LwaCas13a nucleic acid detection reaction. The synthetic DNA1-crRNA was used as guide for LwaCas13a. Buffer conditions includes 20 mM HEPES pH 7, with 9 mM $MgCl_2$ **(A)** A dilution series of synthetic DNA 1 PCR product as positive controls (S), and seven negative controls (C) with various components included in the LwaCas13a reaction. A 96 well plate was used for fluorescent monitoring. **(B)** A dilution series of RNase A as positive control besides a PCR product of synthetic DNA 1. Negative controls included LwaCas13a reactions excluding one or more reaction components or adding protein storage buffer (SB) or QIAquick gel extraction elution buffer (EB). A 96 well plate was used for fluorescent monitoring. **(C)** LwaCas13a detection of a synthetic DNA 1 PCR product using a 384 well plate for fluorescent readings. A negative control without target was used for fluorescent monitoring.

Appendix I. Optimization of VICTOR Nivo fluorescence monitoring

A

	-2,25	-1,125	0	1,125	2,25
-2,25	310736	266881	434971	358740	220121
-1,125	266374	421362	582283	506814	417873
0	371301	464317	561902	506141	412174
1,125	382179	388780	452251	394244	345369
2,25	339012	468028	477001	423873	130163

B

	-2,5	-1,25	0	1,25	2,5
-2,5	60994	33644	36248	43688	44814
-1,25	45011	99493	117017	58763	61693
0	56409	152367	558173	97495	72813
1,25	49412	49139	66089	48352	49642
2,5	54340	40006	50028	31401	41041

Figure S7: Area scan. Endpoint area scan (mm) on fluorescent intensity on a black 96 and 384 well plate, using default settings on all other parameters.

A) 96 well plate area scan on a positive control containing RNase A (0,6 ng/µL)

B) 384 well plate area scan on a positive control containing RNase A (0,6 ng/µL)
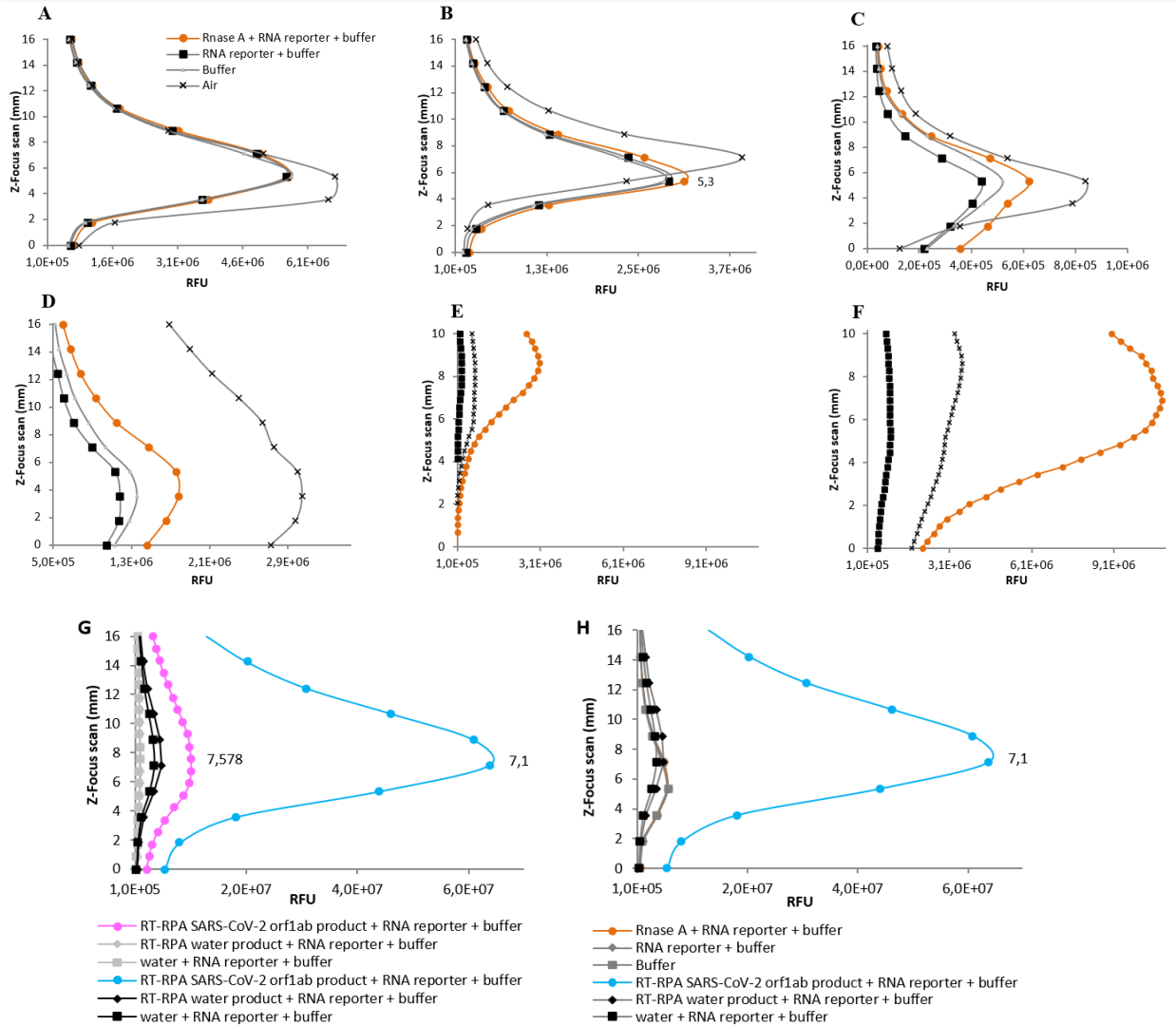
Figure S8: Z-focus scans. Endpoint z-focus scan with 10-20 scan points from 0 mm to 10-16 mm, showing relative fluorescent intensity (RFU) on black 96-, 384-, and 1536 well plates, with excitation filter 570/10 or 530/30, emission filter 600/10 nm, a measurement time to 500ms or 250ms, and excitation and emission spot size 0.5 mm or 1.0 mm and 1.0 mm or 2.0 mm respectively, with a 50/50 general or D590 dichroic mirror. Default settings on all other parameters including: Top measurement in x,y plane (0,0). A positive control containing RNase A (0,6 ng/µL, orange), and negative controls containing water, or water in a master mix (black) excluding the fluorescent RNA. For **G-H**; A RT-RPA product of SARS-CoV-2 *ORFab1* of positive clinical sample (Table S8 , U10) was used as positive control along with RT-RPA + water and water only input as negative controls in the Cas13a detection assay.

    A. A 96 well plate z-focus scan using excitation filter 570/10, a 500ms measurement time, and excitation and emission spot size 0.5 mm and 1.0 mm respectively. n=1

    B. A 96 well plate z-focus scan using excitation filter 530/30, a 500ms measurement time, and excitation and emission spot size 0.5 mm and 1.0 mm respectively. n=1

    C. A 384 well plate z-focus scan using excitation filter 530/30, a 250ms measurement time, and excitation and emission spot size 0.5 mm and 1.0 mm respectively. n=3

    D. A 384 well plate z-focus scan using excitation filter 530/30, a 250ms measurement time, and excitation and emission spot size 1.0 mm and 2.0 mm respectively. n=3

E. A 1536 well plate z-focus scan using excitation filter 530/30, a 250ms measurement time, and excitation and emission spot size 0.5 mm and 1.0 mm respectively. n=3

F. A 1536 well plate z-focus scan using excitation filter 530/30, a 250ms measurement time, and excitation and emission spot size 1.0 mm and 2.0 mm respectively. n=3

G. Comparison of original general 50/50 (pink) and new dichroic mirror D590 (blue) on a black 1536 round, nontransparent bottom, well-plate. Parameters used; excitation and emission filters 530/30, and 610/10 nm; excitation and emission spot sizes 1.0 mm and 2.0 mm respectively; measurement time and direction, 250 ms and top direction. n=3

H. Comparison of the original and new optical settings and plate formats used to detect florescent signal in the plate reader. The original scan includes the RNase A positive control (0,6 ng/µL) n=1, and the final z-scan includes the RT-RPA product of SARS-CoV-2 *orf1ab* from a clinical sample (Table S8, U10), n=3. Excitation filter was adjusted from 570/10 to 530/30, excitation and emission spot sizes from 0.5 mm, 1.0 mm to 1.0 mm, 2.0 mm respectively, a measurement time from 500 ms to 250 ms, and a z-focus to 7,1 mm. A black 96 round transparent bottom, well plate was changed with a black 1536 round non-transparent bottom, well plate for fluorescent monitoring in the LwaCas13a detection assay.

Appendix J. Buffer optimization on LwaCas13a collateral cleavage activity
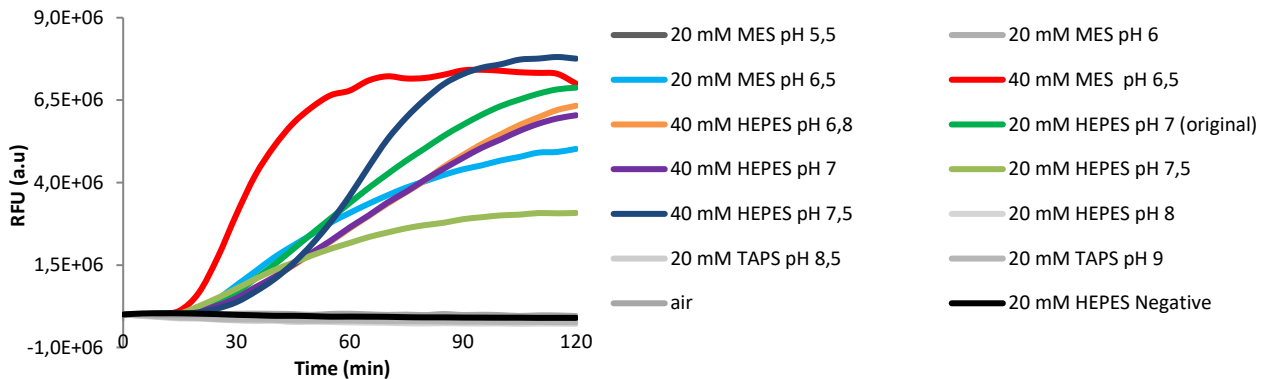
Figure S9: LwaCas13a buffer optimization. Reaction kinetics showing relative fluorescent signal in means of Cas13a collateral cleavage over two-three hours targeting synthetic DNA 1 PCR products (1,53-2E+7 copies/reaction). DNA1-crRNA was used as guide for LwaCas13a. Procedure was done according to section 2.2.6.2. Different buffers were tested: 40 mM MES, 40 mM TAPS or 20mM HEPES was used as LwaCas13a reaction buffer to get a pH range from 5,5 to 9,0. A black 384-well plate with round transparent bottom was used for fluorescent readouts. A black 1536-well plate with round transparent bottom was used for fluorescent readouts. Optical parameters including excitation and emission spot sizes, 1.0/2.0 mm; Z-focus, 7,1 mm; measurement time/direction, 250 ms/top; dichroic mirror, general (50/50); excitation/emission filter, 530/30 and 600/10 nm. n=3

Appendix K. LwaCas13a nucleic acid detection on synthetic sequences
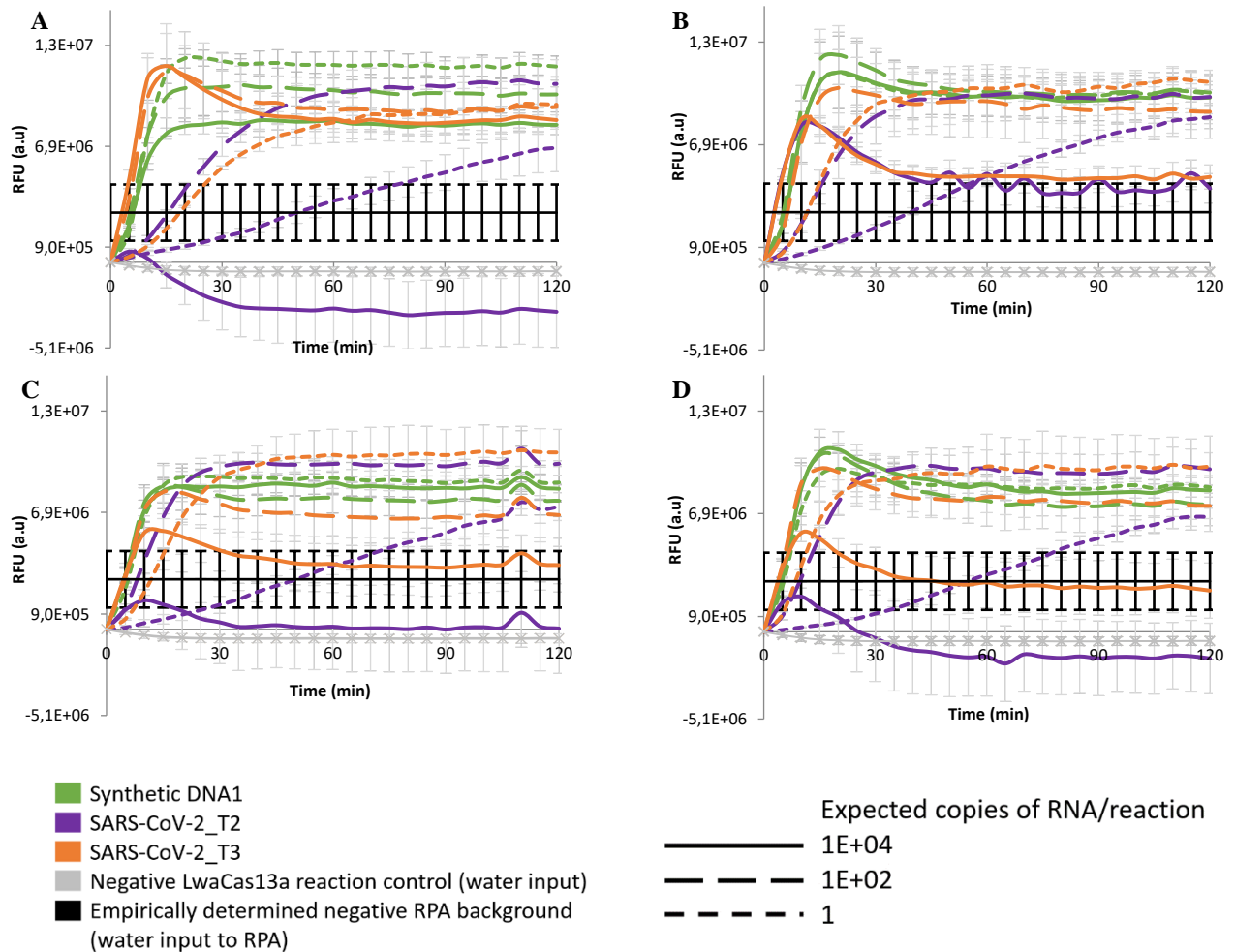
**Figure S10: Kinetics from LwaCas13a detection of synthetic- DNA 1, SARS-CoV-2_T2 and T3 PCR products.** Samples were detected with a **A)** 5, **B)** 10, **C)**15 or **D)** 30-min RPA incubation followed by two hours of LwaCas13a reaction. orf1b-and orf1ab-original primers was used to detect the synthetic SARS-CoV-2 targets orf1b (purple), orf1ab (orange), and DNA1-primer set was used to detect synthetic DNA1 PCR product (green). Each graph represent the detected collateral cleavage activity for a given input concentration of synthetic DNA 1, SARS-CoV-2_T2 and SARS-CoV-2_T3 in E+04 , 1,0E+02, and 1 copies / reaction. Graphs indicate mean ± SD of relative fluorescence measured from three technical replicates. Associated DNA1-crRNA, orf1ab-crRNA and orf1b-crRNA was used as guides for Cas13a targeting each RPA product, respectively. Black line indicates an empirical threshold calculated as described in section 2.2.9.1. A negative water only input to LwaCas13a reaction was used as negative control. 9mM Mg^{2+} were used in the Cas13a reaction buffer combined with either 40 mM MES pH 6,5 or 20 mM HEPES pH 7,0. A black 1536-well plate with round transparent bottom was used for fluorescent readouts. Optical parameters include excitation and emission spot sizes, 1.0/2.0 mm; Z-focus, 6,9 mm; measurement time/direction, 250 ms/top; dichroic mirror, general (50/50); excitation/emission filter, 530/30 and 600/10 nm.

Appendix L. Optimization of background signal in SHERLOCK
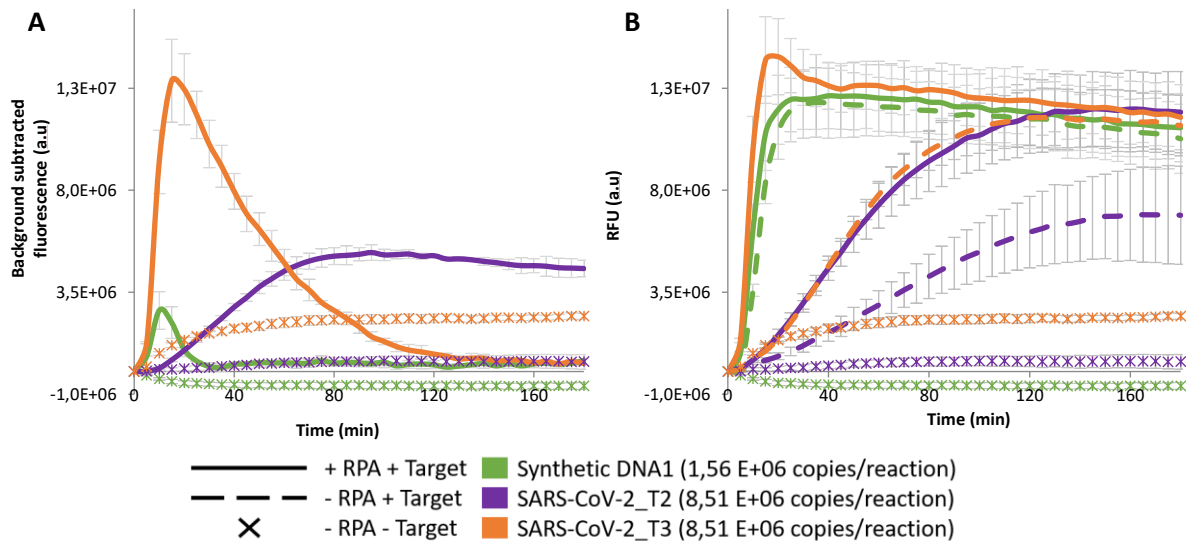
Figure S11. SHERLOCK on a SARS-CoV-2 RNA extract. LwaCas13a reaction kinetics over three hours represented as **A)** background subtracted fluorescent signal in means ± SD or **B)** fluorescent signal in means ± SD, on a positive SARS-CoV-2 extract targeting *orf1b* (purple) or *orf1ab* (orange) and synthetic DNA 1 PCR product (green). A negative water only input to RPA reaction (stripes) and a negative water only input to Cas13a reaction (cross) are included for each target. n=3

Appendix M. Optimization of targets in SHERLOCK
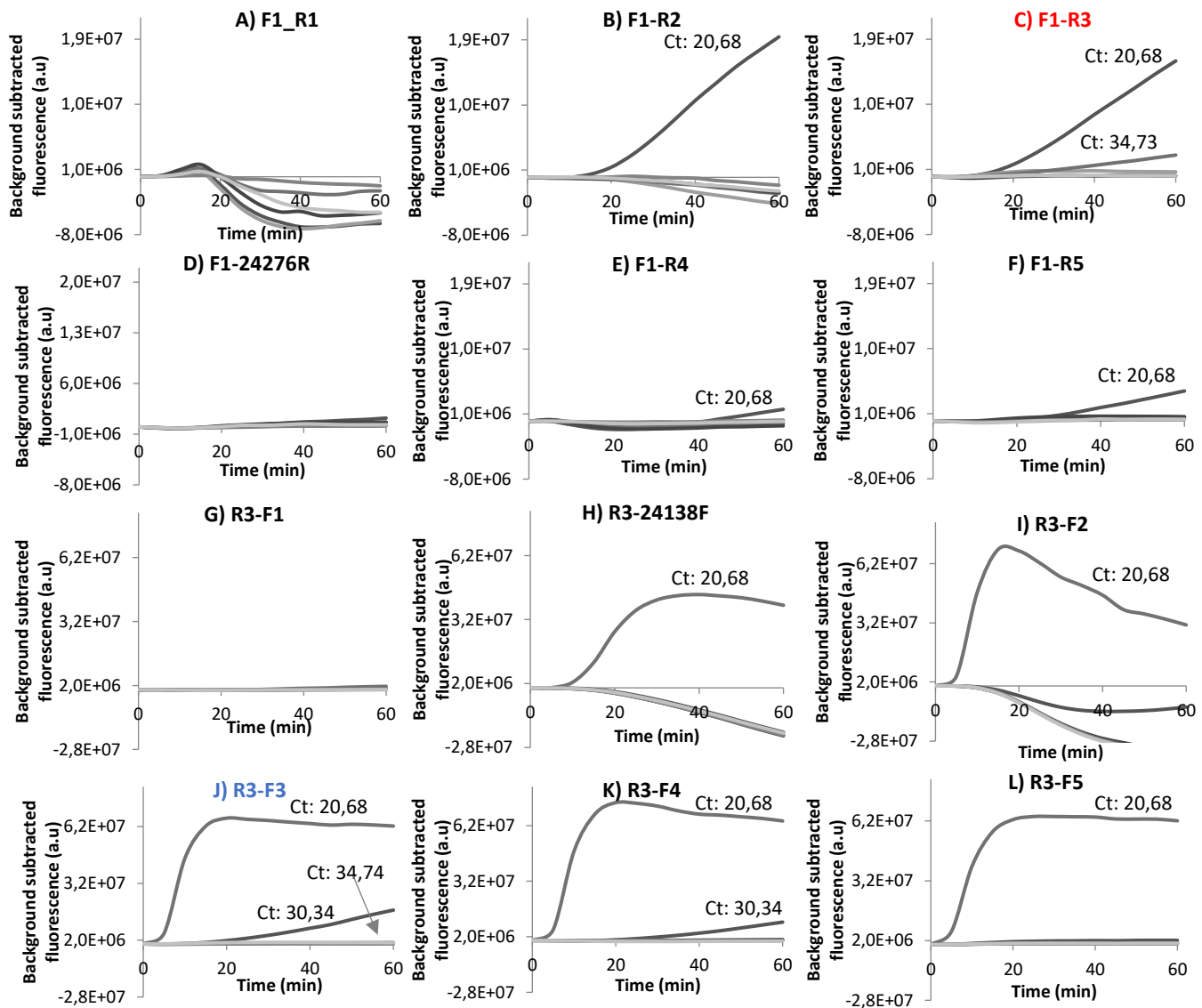
Figure S12. Primary primer screen for detection of SARS-CoV-2 detection of orf1ab using SHERLOCK. A primary primer screen on for *orf1ab* in SARS-CoV-2 was executed using five clinical SARS-CoV-2 samples as targets. Samples were detected with a 30-minute RT-RPA incubation followed by 60 minutes of LwaCas13a nucleic acid detection. Graphs represents background subtracted fluorescence (a.u) in means ± SD after 60 minutes of SHERLOCK-Cas13a collateral reaction from four technical replicates of each sample. Ct-values of 20,68, 30,34, 34,79, 35,59 and 37,58 were registered for the five samples using RT-qPCR of *E-gene* in SARS-CoV-2 (done by employees at OUS. First, combinations of orf1ab-F1 primer with orf1ab- R1, R2, R3, R4 or R5 primers were tested in the RT-RPA reaction (A-F). The most sensitive reverse primer from reverse screen, orf1ab-R3 (C ,red) were combined with forward primers F1, F2, F3, F4 and F5 in RT-RPA (G-L). The resulting, most sensitive primer pair is noted in blue (J). Associated orf1ab_2-crRNA was used as guide for Cas13a. A black 1536-well plate with round non-transparent bottom was used for fluorescent readouts. Optical parameters include excitation and emission spot sizes, 1.0/2.0 mm; Z-focus, 6,9 mm; measurement time/direction, 250 ms/top; dichroic mirror, D590; excitation/emission filter, 530/30 and 600/10 nm.
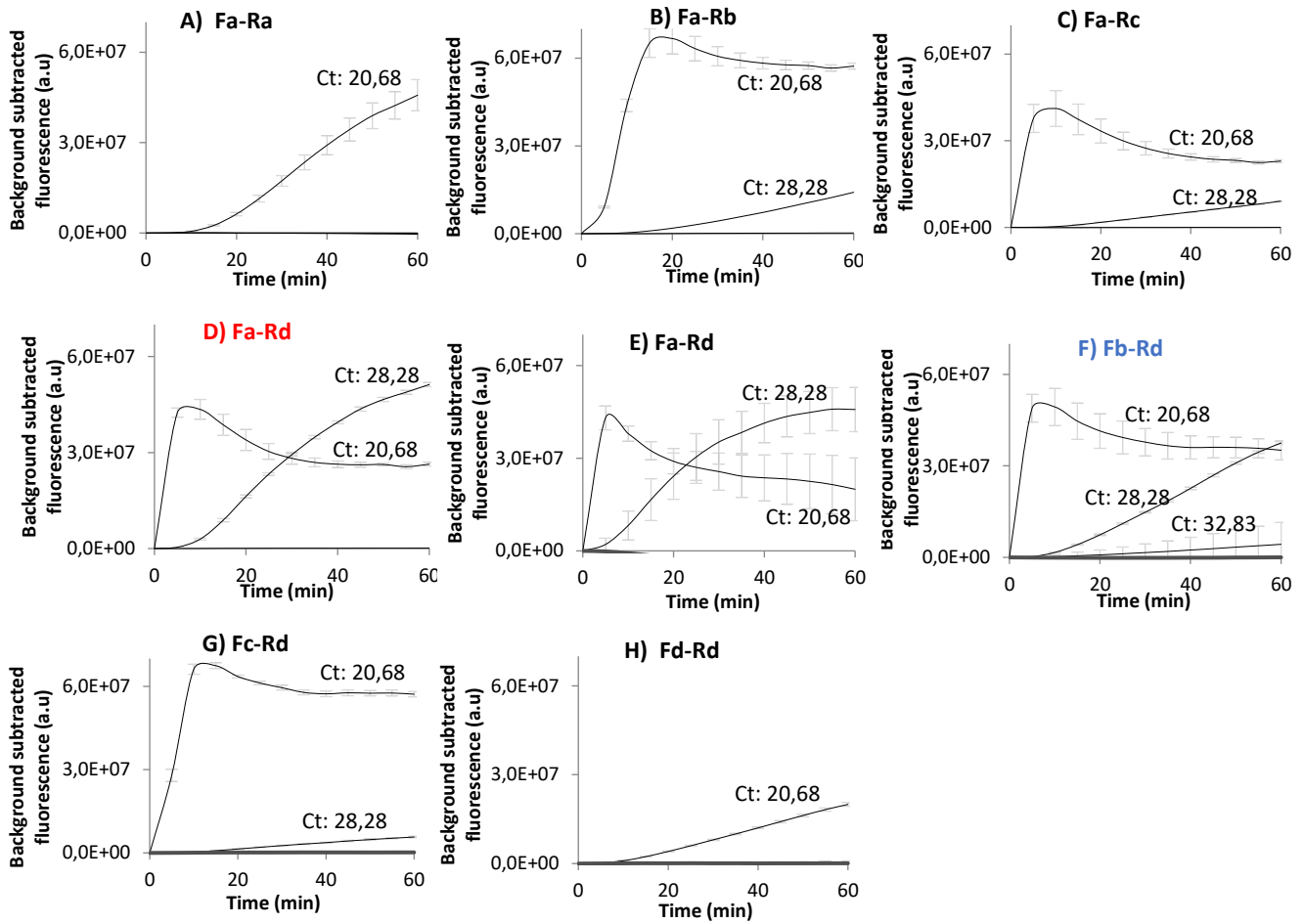
Figure S13. Secondary primer screen for detection of SARS-CoV-2 detection of o1ab using SHERLOCK. A secondary primer screen on for *orf1ab* in SARS-CoV-2 was executed using three clinical SARS-CoV-2 samples as target. Samples were detected with a 30-minute RT-RPA incubation followed by 60 minutes of LwaCas13a nucleic acid detection. Graphs represents background subtracted fluorescence (a.u) in means ± SD after 60 minutes of SHERLOCK-Cas13a collateral reaction from four technical replicates of each sample. Ct-values of 20,68, 28,28, and 32,83 were registered for the three samples using RT-qPCR of *E-gene* in SARS-CoV-2 (done by employees at OUS. First, combinations of orf1ab-Fa primer with orf1ab- Ra, Rb, Rc or Rd were tested in the RT-RPA reaction (A-D). The most sensitive reverse primer from reverse screen, orf1ab-Ra (D ,red) were combined with forward primers Fa, Fb, Fc and Fd in RT-RPA (E-H). The resulting, most sensitive primer pair is noted in blue (F). Associated orf1ab_2-crRNA was used as guide for Cas13a. A black 1536-well plate with round non-transparent bottom was used for fluorescent readouts. Optical parameters include excitation and emission spot sizes, 1.0/2.0 mm; Z-focus, 6,9 mm; measurement time/direction, 250 ms/top; dichroic mirror, D590; excitation/emission filter, 530/30 and 600/10 nm.

Appendix N. Clinical samples used in this study

Table S7. Four positive or negative clinical SARS-CoV-2 samples (RNA extracts) collected from Rikshospitalet (OUH) with Ct values registered from a RT-qPCR analysis of the *E-gene*. Sample name and registration number is also represented. Samples were used to test assay sensitivity and to find primers suitable for low copy number samples. Samples were stored at -80°C.

Sample name:	Ct-values from a RT-qPCR analysis of the SARS-CoV-2 *E-gene:*
R1	31.4 & 28.2
R2	34.2 & 31.6
R3	-
R4	-
R5	Positive control -

Table S8. Ten positive clinical SARS-CoV-2 samples (RNA extracts) collected from the university hospital in Oslo with Ct values <25, registered from an RT-qPCR analysis of the *E-gene*. Sample name and registration number is also represented. Samples was used as positive controls in the SHERLOCK assay. Samples were stored at -80°C.

Sample name:	Ct-value from a RT-qPCR analysis of the SARS-CoV-2 *E-gene:*
U1	<25
U2	<25
U3	<25
U4	<25
U5	<25
U6	<25
U7	<25
U8	<25
U9	<25
U10	<25

Table S9. Negative SARS-CoV-2 samples (RNA/DNA extracts) collected from the university hospital in Oslo with corresponding Ct values registered from an RT-qPCR analysis of A-*genes*. Sample name and registration number is also represented. Samples were used in a specificity test of the SHERLOCK assay. Samples were stored at -80°C. Red Ct -values indicates detectable samples, with resulting fluorescent values over a threshold: 2,0E+6 background subtracted fluorescence after 60 minutes of LwaCas13a nucleic acid detection

Sample name:	Ct-value from a RT-qPCR analysis of Non-SARS-CoV-2-*genes*:
Inf-B	18,2
hMPV	36,63
Inf-A	20,64
Inf-B	36,28
Para1	36,51
hMPV	36,33
Para3	34,79
RSV-B	35,82
EV-D68	28,41
Inf-B	36,38
RSV-B	35
Rhino	29,39
Inf-A	36
RSV-A	36,4
Para2	35,57
EV-D68	37,43
Rhino	35,29
hMPV	18,86
EV-D68	20,65

Table S10. 72 Positive (P) and three negative (N) clinical SARS-CoV-2 samples (RNA extracts) collected from the university hospital in Oslo with corresponding Ct values registered from an RT-qPCR analysis of the *E-gene*. Sample name and registration number is also represented. Samples were used in a sensitivity test of the SHERLOCK assay. Samples were stored at -80°C. Red Ct -values indicates detectable samples, with resulting fluorescent values over a threshold: 2,0E+6 background subtracted fluorescence after 60 minutes of LwaCas13a nucleic acid detection of *orf1ab*.

Sample name:	Ct-value from a RT-qPCR analysis of the SARS-CoV-2 *E-gene:*	Sample name:	Ct-value from a RT-qPCR analysis of the SARS-CoV-2 *E-gene:*
P1	15,51	P39	25,42
P2	15,61	P40	25,56
P3	16,57	P41	25,68
P4	17,04	P42	25,75
P5	17,11	P43	25,91
P6	17,38	P44	25,96
P7	17,48	P45	26,76
P8	17,51	P46	26,76
P9	17,52	P47	26,83
P10	17,55	P48	26,91
P11	17,79	P49	26,91
P12	18,46	P50	27,3
P13	18,89	P51	27,71
P14	18,97	P52	28,28
P15	19,01	P53	28,72
P16	20,58	P54	29,17
P17	20,63	P55	29,77
P18	20,68	P56	30,09
P19	20,76	P57	30,34
P20	20,84	P58	30,73
P21	21,29	P59	31,96
P22	21,56	P60	32,41
P23	21,6	P61	32,61
P24	21,72	P62	32,83
P25	21,72	P63	33,1
P26	21,97	P64	34,1
P27	22,02	P65	34,28
P28	22,13	P66	34,78
P29	22,5	P67	34,92
P30	22,61	P68	34,94
P31	22,66	P69	35,59
P32	22,73	P70	36,72
P33	23,08	P71	37,58
P34	23,4	P72	38,29
P35	23,44	N1	-
P36	23,66	N2	-
P37	24,33	N3	-
P38	24,82		

Table S11. Positive (P) clinical SARS-CoV-2 samples (RNA extracts) collected from the university hospital in Oslo with corresponding Ct values registered from an RT-qPCR analysis of the *E-gene*. Sample name and registration number is also represented. Samples were in the primer screens for MSA_T1 and MSA_T2, stored at -80°C.

Sample name:	Ct-value from a RT-qPCR analysis of the SARS-CoV-2 *E-gene:*
P18	20,68
P74	24,70
P75	27,69
P76	30,45
P77	33,20

Appendix O. SHERLOCK sensitivity and specificity

Table S12. Validation of SHERLOCK sensitivity and specificity A signaling threshold was set to verify assay specificity and sensitivity. Samples in table S9 and S10 was used calculate sensitivity and specificity, and results are marked in yellow.

LwaCas13a collateral cleavage reaction (min)	30	60
Threshold (background subtracted fluorescence (a.u)	2,00E+06	2,00E+06
True positives (TP)	72	72
False positives (FP)	0	1
False negatives (FN)	14	12
True negatives (TN)	19	19
Sensitivity	0,84	0,86
Specificity	1	0,95

Equations used to calculate 1) specificity and 2) sensitivity

    (1) Specificity formula: $TN / (TN + FP)$

    (2) Sensitivity formula: $TP / (TP + FN)$

Percent of positive SARS-CoV-2 samples detected after 60 minutes of LwaCas13a detection: 60/72 ~ 83%

Percent of negative SARS-CoV-2 samples detected: 1/19 ~ 5%

Appendix P. Detection of highly conserved segments of the SARS-CoV-2 genome

NB: The work in this appendix was exclusively done and written by Jon K. Lærdahl, research scientist and bioinformatician at MIK, OUH.

The SARS-CoV-2 RNA reference genome was generated by performing deep meta-transcriptomic sequencing of bronchoalveolar lavage fluid from a 41-year-old man who was hospitalized at the Central Hospital of Wuhan on Dec 26th, 2019 (1). The patient was employed at an indoor seafood market in Wuhan. The reference sequence has 29,903 nucleotides (nt). It was submitted to GenBank on Jan 5th, 2020 and given GenBank reference identifier MN908947. RNA genomic sequences are, by convention, presented in public databases as the corresponding DNA sequences, and this convention was also used in this analysis.

```
>MN908947.3 Severe acute respiratory syndrome coronavirus 2 isolate Wuhan-Hu-1, complete genome
ATTAAAGGTTTATACCTTCCCAGGTAACAAACCAACCAACTTTCGATCTCTTGTAGATCTGTTCTCTAAA
CGAACTTTAAAATCTGTGTGGCTGTCACTCGGCTGCATGCTTAGTGCACTCACGCAGTATAATTAATAAC
TAATTACTGTCGTTGACAGGACACGAGTAACTCGTCTATCTTCTGCAGGCTGCTTACGGTTTCGTCCGTG
.
..
```

```
. . .
GATCGAGTGTACAGTGAACAATGCTAGGGAGAGCTGCCTATATGGAAGAGCCCTAATGTGTAAAATTAAT
TTTAGTAGTGCTATCCCCATGTGATTTTAATAGCTTCTTAGGAGAATGACAAAAAAAAAAAAAAAAAAAA
AAAAAAAAAAAAA
```

The SARS-CoV-2 viral genome has 5'- and 3'-untranslated terminal sequences of 265 nt and 229 nt, respectively, typical for betacoronaviruses (1). The *ORF1ab* gene is more than 21,000 nt in length and located at the 5' end. It comprises 16 predicted non-structural proteins. *ORF1ab* is followed by the so-called *Spike* (*S*) gene of 3,822 nt and a number of shorter, partially overlapping genes at the 3' end of the genome (1).

Since January 2020, a large, and accelerating, number of SARS-CoV-2 viral genomes have been sequenced and submitted to databases. It is common practice in biology to make sequence data available in the open-access International Nucleotide Sequence Database Collaboration (INSDC) databases, such as GenBank maintained by the National Center for Biotechnology Information (NCBI) or the European Nucleotide Archive (ENA) from the European Bioinformatics Institute (EBI). For example, the SARS-CoV-2 viral genome was submitted to the NCBI GenBank on Jan 5th, 2020, it became accessible in GenBank on Jan 12th and in ENA on Jan 13th.

Unlike other parts of biology, there appears to be a culture, or common practice, in SARS-CoV-2 research, to submit to a different database, GISAID. This practice seems to be adopted from influenza virus research, for which GISAID was constructed. GISAID is a public-private partnership between the German government and the nonprofit organization Friends of GISAID. It is hosted by the German government. Unlike the sequence data submitted to the INSDC databases, GISAID's database access agreement ensures that contributors keep their intellectual property rights to the data. This is problematic for fully open research, and is being heavily discussed, but GISAID was, and is still, the best resource for SARS-CoV-2 genomic data. As an example, there were 932 SARS-CoV-2 sequences available in the NCBI databases on April 16th, not all full-length genomic sequences, and 9370 sequences, nearly all full-length genomes, in GISAID at April 17th. Although not stated anywhere, as there appears to be no communication between the INSDC databases and GISAID, the GISAID sequence with identifier EPI_ISL_402125 appears to be the same SARS-CoV-2 reference viral genome as GenBank's MN908947.3. Both sequences and their annotations, including the submitters, are identical.

The mutation rate of SARS-CoV-2 is not very high compared to other RNA viruses. Based on 7666 viral genomes downloaded from GISAID in late April 2020 van Dorp *et al.* (2) found an estimated mutation rate of 6×10^{-4} nt/genome/year (95% CI: 4×10^{-4} - 7×10^{-4}) underlying the global diversity of SARS-CoV-2. The global SARS-CoV-2 population had, at that time, accumulated moderate diversity. Between any two genomes, the average pairwise difference was 9.6 nt of 29,903 nt, supporting a quite recent Most Recent Common Ancestor (MRCA). The MRCA, which marks to the start of the COVID-19 pandemic, was estimated to have jumped from an animal to human host between Oct 6th, 2019 and Dec 11th 2019 (95% CI) (2). Few, if any, biologically relevant insertions or deletions in the viral genome are found in the GISAID data.

Optimal targets for the SHERLOCK detection of SARS-CoV-2, as for PCR detection, correspond to segments of the viral genome that have acquired no, or as few as possible, mutations. A preliminary, exploratory test was performed with all SARS-CoV-2 sequences available in the NCBI databases on April 9th 2020, 535 sequences. Of these, 460 sequences were full-length genomes. The aligned sequences were downloaded and analyzed with our own Python scripts. We detected 198 segments in the SARS-

CoV-2 genome that were longer than 50 nt and fully conserved (100% identical) in the full 535 sequences dataset.

```
   51  GTGTTTTAATGTCTAATTTAGGCATGCCTTCTTACTGTACTGGTTACAGAG  7017 - 7067
   51  TCCACACGCAAGTTGTGGACATGTCAATGACATATGGACAACAGTTTGGTC  5001 - 5051
   52  AGGGAGTCACCTTTTGTTATGATGTCAGCACCACCTGCTCAGTATGAACTTAA  5664 - 5715
   52  CTAGATAAACGCACTACGTGCTTTTCAGTAGCTGCACTTACTAACAATGTTG  14605 - 14656
   53  TTGTGCTAGTGAGTACACTGGTAATTACCAGTGTGGTCACTATAAACATATAA  5731 - 5783
   55  AATGTTTTTATGTCTGAAGCAAAATGTTGGACTGAGACTGACCTTACTAAAGGAC  15811 - 15865
   55  TACAATAAAATTGTTGATGAGCCTGAAGAACATGTCCAAATTCACACAATCGACG  26089 - 26143
   55  TTGCCTGGTTGTGATGGTGGCAGTTTGTATGTAAATAAACATGCATTCCACACAC  19270 - 19324
...
...
  255
AAATCAGCTGGTTTTCCATTTAATAAATGGGGTAAGGCTAGACTTTATTATGATTCAATGAGTTATGAGGATCAAGATGCACTTTTCGCATATACAAAACGTAATGTCATCCCTACTATAACTCAAATGAATCTTAAGTATGCCATTAGTG
CAAAGAATAGAGCTCGCACCGTAGCTGGTGTCTCTATCTGTAGTACTATGACCAATAGACAGTTTCATCAAAAATTATTGAAATCAATAGCCGCCACTAGAGGA  14938 - 15192
  279
AGAAGGCTATGCCTTCGAACATATCGTTTATGGAGATTTTAGTCATAGTCAGTTAGGTGGTTTACATCTACTGATTGGACTAGCTAAACGTTTTAAGGAATCACCTTTTGAATTAGAAGATTTTATTCCTATGGACAGTACAGTTAAAAAC
TATTTCATAACAGATGCGCAAACAGGTTCATCTAAGTGTGTGTGTTCTCGTTATTGATTTATTACTTGATGATTTTGTTGAAATAATAAAATCCCAAGATTTATCTGTAGTTTCTAAGGTTGTCAAAGT  20301 - 20579
  281
TACTGTACTGGTTCTATACCTTGTAGTGTTTGTCTTAGTGGTTTAGATTCTTTAGACACCTATCCTTCTTTAGAAACTATACAAATTACCATTTCATCTTTTAAATGGGATTTAACTGCTTTTGGCTTAGTTGCAGAGTGGTTTTTGGCAT
ATATTCTTTTCACTAGGTTTTTCTATGTACTTGGATTGGCTGCAATCATGCAATTGTTTTTCAGCTATTTTGCAGTACATTTTATTAGTAATTCTTGGCTTATGTGGTTAATAATTAATCTTGTACAAAT  7106 - 7386
  282
GTCCTTTTTATGTCTATGCTAATGGAGGTAAAGGCTTTTGCAAACTACACAATTGGAATTGTGTTAATTGTGATACATTCTGTGCTGGTAGTACATTTATTAGTGATGAAGTTGCGAGAGACTTGTCACTACAGTTTAAAAGACCAATAAAT
CCTACTGACCAGTCTTCTTACATCGTTGATAGTGTTACAGTGAAGAATGGTTCCATCCATCTTTACTTTGATAAAGCTGGTCAAAAGACTTATGAAAGACATTCTCTCTCTCATTTTGTTAACTTAGACAA  7561 - 7842
  283
TGGTACCACATATATCACGTCAACGTCTTACTAAATACACAATGGCAGACCTCGTCTATGCTTTAAGGCATTTTGATGAAGGTAATTGTGACACATTAAAAGAAATACTTGTCACATACAATTGTTGTGATGATGATTATTTCAATAAAAA
GGACTGGTATGATTTTGTAGAAAACCCAGATATATTACGCGTATACGCCAACTTAGGTGAACGTGTACGCCAAGCTTTGTTAAAAACAGTACAATTCTGTGATGCCATGCGAAATGCTGGTATTGTTGGTGT  13769 - 14051
  312
CACAGCAAGTGCACTTGGAAAACTTCAAGATGTGGTCAACCAAAATGCACAAGCTTTAAACACGCTTGTTAAACAACTTAGCTCCAATTTTGGTGCAATTTCAAGTGTTTTAAATGATATCCTTTCACGTCTTGACAAAGTTGAGGCTGAA
GTGCAAATTGATAGGTTGATCACAGGCAGACTTCAAAGTTTGCAGACATATGTGACTCAACAATTAATTAGAGCTGCAGAAATCAGAGCTTCTGCTAATCTTGCTGCTACTAAAATGTCAGAGTGTGTACTTGGACAATCAAAAAGAGTTG
ATTTTTGTGG  24382 - 24693
```

The longest fully conserved segment was 312 nt, started at position 24,382 in the 29,903 nt of MN908947.3 and ended at 24,693.

Since data growth was rapid and most of the SARS-CoV-2 data was submitted to the GISAID database, our next analysis was based on GISAID data (https://www.gisaid.org). The full multiple sequence alignment (MSA) of all available GISAID SARS-CoV-2 sequences were downloaded on May 4th, 2020. This MSA contained 14839 sequences. Each sequence, obviously, contains at each nucleotide position, one of the four DNA (actually RNA) bases A, C, G, and T, but in addition many sequences contains ambiguous base calls (annotated as in https://www.bioinformatics.org/sms/iupac.html). For example, IUPAC nucleotide codes are, obviously, A for adenine and C for guanine, but R for "A or G" (due to an ambiguous base call), Y for "C or T", B for "C or G or T", and so on. N is the code for "any base", a completely ambiguous base call, while a gap character "-", shows a gap in the MSA for a given sequence (row in MSA matrix) in a given column (nt position in matrix).

GISAID had in their MSA with 14839 sequences already removed poor quality viral genomes, defined as containing more than 5% ambiguous base calls (more than 5% N characters), and sequences shorter than 29,000 nt. The downloaded MSA, a large matrix of 14839 sequences (rows) with >29,000 nt (columns) was clearly too large to analyze manually, and Python scripts were generated for this purpose. Only 3382 rows had no characters except "-ACGT", so only this number of viral genomes had no ambiguous base calls. 716 sequences had >1000 N characters, and the largest number was 1494 corresponding to the screening performed by GISAID (5% of 29,903 is 1495). 1987 sequences had characters that were not "-NACGT", that is, ambiguous, but not fully ambiguous (i.e., "N"), but only 26 had more than 3 characters of this type.

While our preliminary analysis on NCBI data from April 9th gave 198 fully conserved segments of >50 nt, our analysis of 14839 GISAID sequences from May 4th resulted in no such fully conserved segments of >50 nt. Some very few conserved segments were 30 to 40 nt, most much shorter. Careful analysis showed that this was to some degree reflecting more diversity in the sequence data, however, there were also many sequences with obvious sequencing errors, mainly wrongly called bases. The GISAID data had been submitted by hundreds of labs around the world, and some of these had clearly not used sufficiently stringent cut-off values for calling bases as ambiguous. Hundreds, if not thousands, of viral

genomes contained called bases that should have been masked as ambiguous given a better, more strict, choice of cut-off threshold. These problems with viral genome data were at the time, and is still, discussed in various online fora, and no obvious solution has yet been found. It is very difficult, if not impossible, to determine from sequences alone if a unique mutation in a single sequence is actually a true mutation or just a rare error due to sequencing and/or genome assembly. The obvious solution is to make the actual sequencing reads available to the public, but this is currently not possible in GISAID.

Due to the very imperfect nature of the sequenced viral genome data, and in order to find segments of the SARS-CoV-2 genome that could be promising as SHERLOCK targets, we tested various approaches and ended up with the following working definition of a "useful SHERLOCK conserved segment":

1. Segments of 50 nt or more that are "nearly identical" to the reference SARS-CoV-2 viral genomic sequence in all GISAID sequences as of May 4 (14839 sequences)
2. "Nearly identical" means that for each column in the segment a maximum of 2 sequences may have an nt not matching the reference sequence. Ambiguous characters (N, Y, W etc.) are not counted
3. Sequences with more than 1% ambiguous characters (3831 sequences) are left of out the analysis as they
   o Possibly have poorer quality overall
   o Are in some few cases not optimally aligned with the reference sequence in the GISAID MSA

This analysis gave a set of 110 "conserved segments", 17 longer than 100 nt.

After discussions with James Booth and a check of previously published data (3,4), it was decided to focus on the region of the SARS-CoV-2 genome between nt 28,000 and the 3' end. The amount of viral RNA in infected cells available for diagnostics appears to be much higher in this region. The above working definition for a "useful SHERLOCK conserved segment" was made slightly more relaxed,

1. Segments of 90 nt or more that are "nearly identical" to the reference SARS-CoV-2 viral genomic sequence in all GISAID sequences as of May 4 (14839 sequences)
2. "Nearly identical" means that for each column in the segment a maximum of 5 sequences may have an nt not matching the reference sequence. Ambiguous characters (N, Y, W etc.) are not counted
3. Sequences with more than 1% ambiguous characters (3831 sequences) are left of out the analysis as they
   o Possibly have poorer quality overall
   o Are in some few cases not optimally aligned with the reference sequence in the GISAID MSA
4. Only segments starting at nt 28,000 or higher are considered

This analysis gave two sequence segments that were highly conserved within the 2,000 3' nucleotides of the viral genome. The numbering of nucleotides is as in the SARS-CoV-2 reference sequence, MN908947.3/EPI_ISL_402125. The sequences are given by:

`>SARS-CoV-2 conserved segment 1: 135 nt long, between nt 28,379 and nt 28,513`
`CGATCAAAACAACGTCGGCCCCAAGGTTTACCCAATAATACTGCGTCTTGGTTCACCGCTCTCACTCAACATGGCAAGGAAGACCTTAAATTCC`
`CTCGAGGACAAGGCGTTCCAATTAACACCAATAGCAGTCCA`

`>SARS-CoV-2 conserved segment 2: 109 nt long, between nt 28,986 and nt 29,094`

GCCAACAACAACAAGGCCAAACTGTCACTAAGAAATCTGCTGCTGAGGCTTCTAAGAAGCCTCGGCAAAAACGTACTGCCACTAAAGCATACAA
TGTAACACAAGCTTT

Mutations that have emerged independently multiple times in a lineage, for example in SARS-CoV-2 in the COVID-19 epidemic, are known as homoplasies. These are likely candidates for adaptation taking place in SARS-CoV-2 to its novel human host. Sites of homoplasies should clearly be avoided as PCR or SHERLOCK targets, as mutations are likely to accumulate here during the course of COVID-19. van Dorp *et al.*(2) found 198 statistically significant homoplasy sites in SARS-CoV-2. None of these are found in the two SARS-CoV-2 conserved segments discussed above.

The two segments described above were the most conserved in the SARS-CoV-2 viral genome, at the 3' end, in early May 2020 and contains no known homoplasy sites. They are thus good candidates for selecting SHERLOCK primers and reporter sequences that will be able to stably detect as much as possible of the SARS-CoV-2 genomic pool, that is, avoiding false negatives. It is, however, also important to avoid false positives. In order to check if the two conserved sequences also have significant similarity to DNA/RNA that is not from SARS-CoV-2, BLAST sequence searching were performed in several databases. None of the sequences corresponding to conserved segment 1 or 2 had any statistically significant hits to the human genome.

SARS-CoV-2, SARS-CoV-1, and some few other bat, and possibly pangolin, viruses are all the known viruses in the sarbocovirus subgenus. Sarbecoviruses are subgroup B of the betacoronavirus genus. MERS coronavirus is in subgroup C, while there are other human and mammalian coronaviruses in subgroup A. Clearly, if sarbecovirus is diagnosed in a patient, this is either SARS-CoV-2, SARS-CoV-1 (not detected in human since 2004), or a third, new coronavirus of bat origin.

A BLAST search (blastn type, nt sequence search) in GenBank (June 19th, 2020) with the first conserved sequence described above (135 nt) (non-default parameters: word size = 7 nt (the smallest, most sensitive available) & E-value cut-off = 0.25, limited to records that exclude SARS-CoV-2 (taxid:2697049)), gave 296 hits. These are all SARS-CoV-1 strains or sarbecoviruses from bats, in addition to some few from pangolin. The top hit, as expected, is bat sarbecovirus RaTG13, the virus with the highest known similarity to SARS-CoV-2 (131 of 135 nt identical). The second-best hit was with bat SARS coronavirus Rf1 (109 of 135 nt identical). The search was repeated, but limited to records excluding sarbecoviruses, and this gave no significant hits. The search procedures were repeated for the second conserved sequence described above (109 nt), and also this time no significant hits were detected outside of sarbecoviruses.

This analysis shows that SHERLOCK based on the sequences in SARS-CoV-2 conserved segments 1 and 2 is expected to be highly specific for SARS-CoV-2,but might theoretically also detect other sarbecoviruses only known from SARS-CoV-1 and from viral samples taken from bats and pangolins.

1.   Wu F, Zhao S, Yu B, Chen YM, Wang W, Song ZG, et al. A new coronavirus associated with human respiratory disease in China. Nature [Internet]. 2020 Mar 12 [cited 2020 Dec 10];579(7798):265–9. Available from: /pmc/articles/PMC7094943/?report=abstract
2.   van Dorp L, Acman M, Richard D, Shaw LP, Ford CE, Ormond L, et al. Emergence of genomic diversity and recurrent mutations in SARS-CoV-2. Infect Genet Evol [Internet]. 2020 Sep 1 [cited 2020 Dec 10];83:104351. Available from: /pmc/articles/PMC7199730/?report=abstract
3.   Blanco-Melo D, Nilsson-Payant BE, Liu WC, Uhl S, Hoagland D, Møller R, et al. Imbalanced Host Response to SARS-CoV-2 Drives Development of COVID-19. Cell. 2020 May 28;181(5):1036-1045.e9.
4.   Kim D, Lee J-Y, Yang J-S, Kim JW, Kim VN, Correspondence HC, et al. The Architecture of SARS-CoV-2 Transcriptome In Brief The SARS-CoV-2 transcriptome and epitranscriptome reveal a complex array of canonical and non-canonical viral transcripts with RNA modifications. ll The Architecture of SARS-CoV-2 Transcriptome. ; Available from: https://doi.org/10.1016/j.cell.2020.04.011